

Aus dem Bereich
Theoretische Medizin und Biowissenschaften
der Medizinischen Fakultät
der Universität des Saarlandes, Homburg/Saar

**The role of nuclear factor κ B
in the radiation-induced bystander response**

Dissertation zur Erlangung des Grades eines Doktors der Naturwissenschaften
der Medizinischen Fakultät
der UNIVERSITÄT DES SAARLANDES
2020

vorgelegt von: Sebastian Diegeler
geb. am: 05.02.1988 in Siegburg

Tag der Promotion: 28.09.2020

Dekan: Prof. Dr. M. D. Menger

1. Berichterstattende: Prof. Dr. J. Engel

2. Berichterstattende: PD Dr. Y. Dzierma

*„Dans la vie, rien n'est à craindre, tout est à comprendre”
(Nothing in life is to be feared, it is only to be understood)*

- Marie Skłodowska Curie

Table of contents

1. Abstract	5
2. Zusammenfassung.....	6
3. Introduction.....	7
3.1. Ionizing radiation.....	8
3.1.1. Dose quantities.....	9
3.1.2. Space radiation.....	9
3.2. Effect of ionizing radiation on biological systems.....	11
3.2.1. Acute radiation effects.....	11
3.2.2. Late radiation effects.....	12
3.3. Cellular radiation response.....	13
3.3.1. DNA damage.....	13
3.3.2. DNA repair.....	14
3.3.3. Cell cycle arrest.....	21
3.4. Cell fates.....	25
3.4.1. Cell death.....	25
3.4.2. Cellular senescence.....	25
3.5. Nuclear factor κ B.....	26
3.5.1. The NF- κ B family.....	26
3.5.2. Canonical NF- κ B signaling pathway.....	27
3.5.3. Non-canonical NF- κ B signaling pathway.....	30
3.5.4. Genotoxic stress-induced NF- κ B activation.....	32
3.6. The radiation-induced bystander effect.....	37
3.6.1. Gap-junctional transfer of RIBE-inducing factors.....	37
3.6.2. Induction of RIBE via secreted soluble factors.....	37
3.6.3. Amplification and propagation of bystander signals.....	38
3.6.4. Cellular consequences of the radiation-induced bystander response.....	39
3.7. Aim of this thesis.....	40
4. Material and Methods.....	41
4.1. Cell culture.....	41
4.1.1. Cell lines.....	41
4.1.2. Cell culture.....	41
4.1.3. Cryoconservation and thawing of cells.....	42
4.2. Treatment conditions.....	42

4.2.1.	Addition of NF- κ B activators and senescence inducers	42
4.2.2.	Irradiation and medium conditioning	43
4.3.	Fluorescence-based assays.....	43
4.3.1.	Immunofluorescence staining	43
4.3.2.	Fluorescence image analysis	46
4.3.3.	Flow cytometry.....	47
4.4.	Cellular senescence	51
4.4.1.	β -galactosidase assay	51
4.5.	Clonogenic survival.....	53
4.5.1.	Colony forming ability assay.....	53
4.5.2.	Linear-quadratic model	54
4.5.3.	Single-hit multi-target model	56
4.6.	Statistics.....	58
5.	Results	59
5.1.	Direct Exposure to X-rays	59
5.1.1.	Cellular survival	59
5.1.2.	Cellular senescence	67
5.1.3.	Apoptosis and cell cycle progression.....	70
5.1.4.	DNA damage.....	74
5.2.	Bystander treatment with conditioned medium	78
5.2.1.	NF- κ B nuclear translocation.....	78
5.2.2.	Cellular survival	80
5.2.3.	Cellular senescence	86
5.2.4.	Apoptosis and cell cycle progression.....	89
5.2.5.	DNA damage.....	93
6.	Discussion	97
6.1.	Scientific approach	97
6.2.	The role of NF- κ B in the cellular radiation response	97
6.2.1.	Survival after exposure to X-rays.....	97
6.2.2.	Premature senescence induction by X-irradiation.....	98
6.2.3.	Apoptosis after exposure to X-rays	100
6.2.4.	Cell cycle arrest after exposure to X-rays.....	101
6.2.5.	X-ray-induced DNA damage	102
6.2.6.	The role of NF- κ B after direct exposure to ionizing radiation	103
6.3.	The role of NF- κ B in the radiation-induced bystander response.....	104

6.3.1.	Activation of NF- κ B in irradiated and bystander cells.....	104
6.3.2.	Survival after treatment with conditioned medium from irradiated cells.....	106
6.3.3.	Senescence induction after treatment with conditioned medium from irradiated cells 108	
6.3.4.	Apoptosis in bystander cells.....	110
6.3.5.	Cell cycle arrest in bystander cells.....	110
6.3.6.	RIBE-induced DNA damage	111
6.3.7.	Summary of the role of NF- κ B in the radiation-induced bystander response.....	114
6.4.	Conclusion	116
6.5.	Outlook.....	116
7.	Abbreviations	117
8.	List of Figures.....	121
9.	List of Tables.....	123
10.	References.....	125
11.	Acknowledgements	143
12.	Curriculum Vitae.....	145

1. Abstract

Radiation-induced bystander effects play a special role in the cellular response to ionizing radiation. Besides direct consequences of radiation exposure such as cell death, cell cycle arrest and deoxyribonucleic acid (DNA) repair, signaling pathways are activated that result in the secretion of different factors for intercellular communication (cytokines, radicals, damage markers and extracellular vesicles). These factors incite multiple effects in nearby non-irradiated target cells (bystander cells), among those are induction of DNA damage as well as further signal transduction. DNA damage in bystander cells can lead to cell death or activation of repair, similar to direct irradiation responses. Continuing activation of signaling pathways leads to further secretion of signaling factors thereby amplifying and promoting the damage signal originating from the irradiated cell. A key molecule in intra- and intercellular signal transduction is the transcription factor nuclear factor κ B (NF- κ B). Target genes of the transcription factor encode proteins that affect intracellular processes like repair and cell cycle progression as well as cytokines that are secreted for intercellular communication. In this work the role of NF- κ B in the radiation-induced bystander response was investigated. To this end, embryonic fibroblasts from wildtype (wt) and NF- κ B essential modulator (NEMO) knock-out (ko) mice were used. In these NEMO ko murine embryonic fibroblasts (MEF), the NF- κ B response is dysfunctional. Direct X-ray exposure of MEF wt cells resulted in reduced survival, induction of premature senescence at high doses, cell cycle arrest in G2/M phase and DNA double strand breaks (DSB) that were partially repaired with time. Furthermore, X-irradiation of MEF wt cells led to nuclear translocation of the NF- κ B subunit p65, indicating activation of NF- κ B. MEF NEMO ko cells show a similarly reduced survival upon X-irradiation, a more sensitive response regarding senescence induction, cell cycle arrest in G2/M phase and DNA DSB induction compared to MEF wt. Bystander MEF cells were incubated with culture medium conditioned by irradiated cells. MEF wt bystander cells show NF- κ B activation, a dose threshold-dependent reduction of cellular survival, induction of premature senescence and induction of DNA DSB, but no changes in cell cycle progression. MEF NEMO ko bystander cells show an increased survival fraction after treatment with conditioned medium and a more sensitive response regarding senescence induction, but no changes in cell cycle progression similar to MEF wt cells. The amount of DNA DSB in MEF NEMO ko bystander cells depends on incubation time and conditioning dose. The survival response of bystander cells has been found to depend on the NF- κ B status of the recipient cells, indicating involvement of NF- κ B in the amplification and transmission of the bystander signal.

2. Zusammenfassung

Strahlen-induzierte *Bystander* Effekte spielen bei der zellulären Reaktion auf ionisierende Strahlung eine besondere Rolle. Neben den direkten Folgen von Strahlenexposition wie Zelltod, Zyklusarrest und Reparatur werden zusätzlich Signalwege aktiviert, an deren Ende verschiedene Faktoren für die interzelluläre Kommunikation ausgeschüttet werden (Zytokine, Radikale, Schadensmarker und extrazelluläre Vesikel). Diese Faktoren lösen in naheliegenden nicht-bestrahlten Zielzellen (*Bystander* Zellen) diverse Effekte aus, unter anderem DNA-Schäden und weitere Signaltransduktions-Prozesse. DNA-Schäden in *Bystander* Zellen können, ähnlich den direkten Strahlenfolgen, zu Zelltod oder Reparatur führen. Anhaltende Aktivierung von Signalwegen führt zu erhöhter Ausschüttung von Signalfaktoren. Dadurch kommt es zu einer Verstärkung und Weiterleitung des Schadenssignals, welches von der bestrahlten Zelle ausgeht. Ein Schlüssel-molekül in intra- und interzellulärer Signaltransduktion ist der Transkriptionsfaktor *nuclear factor κ B* (NF- κ B). Die Zielgene des Transkriptionsfaktors kodieren Proteine, welche intrazelluläre Vorgänge wie Reparatur und Zellzyklusverlauf beeinflussen, sowie Zytokine, die ausgeschüttet werden, um interzelluläre Kommunikation zu ermöglichen. In dieser Arbeit wurde die Rolle von NF- κ B in der strahleninduzierten *Bystander* Antwort untersucht. Dazu wurden embryonale Fibroblasten von wildtyp (wt) und *NF- κ B essential modulator* (NEMO) knock-out (ko) Mäusen verwendet. In diesen NEMO-ko murinen embryonalen Fibroblasten (MEF) ist die NF- κ B-Antwort dysfunktional. Exposition mit Röntgenstrahlung bewirkte in MEF-wt-Zellen eine reduzierte Überlebensfähigkeit, sowie Induktion von früher Seneszenz bei hohen Dosen, Zellzyklusarrest in der G2/M Phase und DNA Doppelstrangbrüche (DSB), welche mit der Zeit teilweise repariert wurden. Des Weiteren führte Röntgenbestrahlung von MEF-wt-Zellen zur einer nukleären Translokation der NF- κ B Untereinheit p65, was eine Aktivierung von NF- κ B erkennen lässt. MEF-NEMO-ko-Zellen zeigten ein ähnlich reduziertes Überleben und eine sensitivere Reaktion bezüglich der Seneszenz-Induktion, des Zellzyklusarrestes und des DNA-DSB-Aufkommens verglichen mit MEF-wt-Zellen. *Bystander*-MEF-Zellen wurden mit Kulturmedium inkubiert, welches von bestrahlten Zellen konditioniert wurde. MEF-wt-*Bystander*-Zellen zeigten NF- κ B Aktivierung, eine Dosis-Schwellenwert-abhängige Reduzierung des Überlebens, das Auftreten von früher Seneszenz und von DNA-DSB, allerdings keine Veränderung der Zellzyklusprogression. MEF-NEMO-ko-*Bystander*-Zellen wiesen eine erhöhte Überlebensfraktion auf, nachdem sie mit konditioniertem Medium behandelt wurden, sowie ein sensitiveres Seneszenz-Auftreten, jedoch – ähnlich den wt-Zellen – keine Veränderung der Zellzyklusprogression. Die Anzahl von DNA-DSB in MEF-NEMO-ko-*Bystander*-Zellen war abhängig von der Inkubationszeit und der Konditionierungsdosis. Die Überlebensantwort von *Bystander*-Zellen hing vom NF- κ B Status der Empfängerzellen ab, was impliziert, dass NF- κ B an der Verstärkung und Übertragung des *Bystander*-Signales beteiligt ist.

3. Introduction

Radiation is not only one of the main limiting factors for human spaceflight, it is also a means to produce energy and to treat disease. The discovery of radioactivity as well as X-rays at the end of the 19th century marked the beginning of radiation research. Soon thereafter X-rays were applied for medical purposes for the first time. In the following decades, advancement of radiation therapy led to more efficient treatment of a multitude of ailments. At the same time, scientists advanced the understanding of the basic concepts of radiation biology.

The discovery of deoxyribonucleic acid (DNA) – and its acceptance as the material of genetic information – led to the concept of radiation-induced DNA damage and repair as the key mechanism for therapeutic success. Later discovered cellular reactions to stress could be applied in radiation treatment. Inflammation was observed in clinic as part of the radiation response and the underlying mechanism was found to be based on the activation of intracellular signal transduction and transcription factors, e.g. the tumor suppressor p53 or nuclear factor κ B (NF- κ B).

The key assumption in radiation therapy of a proportional relationship between applied dose and radiation effect was challenged when Nagasawa and Little discovered non-targeted effects in 1992 (NAGASAWA, LITTLE, 1992). They found that exposure of α -particles to < 1 % of a cell population led to chromosomal aberrations in > 30 % of the cells. Non-targeted effects therefore are effects on structures that were not directly targeted by irradiation.

Since then the mechanisms of these non-targeted effects have been studied in order to understand the cellular behavior after radiation exposure, and for application in tumor therapy. It was found that even low doses of radiation could provoke strong effects in non-targeted cells, as the initial signal can be biologically amplified. Thus the underlying principles of intercellular communication can be surmised to form the basis of these non-targeted effects.

For therapeutic considerations, non-targeted effects originating in the irradiated tumor can affect healthy tissue and vice versa. Immune cells, activated and recruited due to irradiation effects, are part of the non-targeted response.

Nowadays it has been recognized that radiation therapy should implement aspects of immune therapy by applying communicative and non-targeted effects into therapy. Such therapeutic approaches could efficiently eradicate tumors whilst mitigating the burden of radiation injury to healthy tissue. The underlying mechanisms for radiation effects on non-targeted structures remain to be further elucidated.

3.1. Ionizing radiation

Ionizing radiation (IR) describes the transfer of energy with enough power to detach electrons from atoms by pushing them out of their orbitals, a process called ionization. The removal of electrons renders an atom positively charged and can break molecular bonds. In order to regain net neutrality the positively charged ion reacts with surrounding molecules, attracting electrons and forming new bonds.

IR occurs naturally as cosmic radiation or as by-product of radioactive decay, a process in which unstable energy-rich atoms discharge energy in order to approach an energetic equilibrium. The excess energy can be discharged in form of electromagnetic or particle radiation. The most common decay products are α -, β - and γ -radiation. α -particles are naturally occurring helium nuclei, while β -particles are electrons. γ -rays are highly energetic photons and therefore ionizing electromagnetic radiation.

X-rays can be artificially produced in X-ray tubes. The application of a voltage in an X-ray tube accelerates electrons towards a cathode thereby generating excess energy. Upon collision with the atoms of a target, the electrons are stopped and the excess energy is discharged as *bremsstrahlung* in form of electromagnetic radiation. The amplitude and voltage applied in the X-ray tube and the target material determine the intensity and physical properties of the X-rays. Certain energy levels elicit intensity peaks that illustrate the characteristic X-ray spectrum.

Other radiation species, such as heavy ion nuclei, protons or electrons, can be artificially generated in particle accelerators. The application of electromagnetic forces allows the acceleration of positively or negatively charged particles in an electromagnetic field. The energy of the accelerated particle depends on the type of particle generator and the associated acceleration. In a linear accelerator, the electromagnetic field accelerates the particles in a straight line, so the length of the accelerator determines the maximum energy the particle can achieve. By the same principle as an X-ray tube, upon collision of the accelerated particle with a target, highly energetic X-rays are produced. In a cyclic particle accelerator, such as a cyclotron or a synchrotron, the magnetic field bends the direction of the accelerated particle slightly so that the particle can follow a circular path. This permits a greater energy input compared to linear accelerators. For acceleration of heavy ion species atoms are first stripped of electrons and then transported into vacuum tunnels for acceleration.

Depending on the energy and the type of radiation, the distance that a wave or a particle can travel is limited. The range of a particle is also determined by the material they travel through. Each atomic interaction with molecules in a medium such as air or water leads to a transfer of energy to the environment (linear energy transfer, LET). Accelerated protons and heavy ion nuclei interact strongly

with the environment, slowing down during the process, depending on the velocity and the size of the particle, to the point where they stop. Due to this physical property, most energy of those particles is discharged at minimal terminal velocity, a phenomenon called the Bragg-peak.

IR can be categorized in densely and sparsely IR. Protons and ions are densely ionizing and produce a track of ionizations while travelling through matter. Photons and electrons are sparsely IR.

3.1.1. Dose quantities

The energy dose (E) is measured as transferred energy per mass of the irradiated matter, organ or tissue with the unit Gray ($Gy = J/kg$). The energy of accelerated particles is given with the unit electron volt (eV), referring to the kinetic energy that a single electron accumulates when traveling in vacuum through an electric potential difference of one Volt.

Densely IR has a stronger impact on biological systems than sparsely IR. This is quantified by comparing the doses required for inducing a relevant biological endpoint by the radiation quality in question to the dose of a reference radiation, usually X- or γ -rays, resulting in the relative biological effectiveness (RBE) of the examined radiation quality. For radiation protection purposes, simplified dimensionless weighting factors (W) are used, which are based on empiric RBE data. The weighting factor W_R considers different radiation qualities (photons, electrons, myons, protons, charged pions, α -particles, fission fragments, heavy ions, neutrons). The weighting factor W_T considers the radiation sensitivities of different tissues.

The mass-averaged energy dose absorbed by a tissue ($D_{T,R}$) as well as the weighting factors W_R and W_T are used to calculate the effective dose in a tissue: $E_D = \sum_{T,R} W_T \times W_R \times D_{T,R}$. For cosmic radiation the value for a dimensionless radiation quality factor Q_{LET} is set by international convention with regard to the LET in water of an accelerated particle (ICRP, 2007). The absorbed dose and the radiation quality factor are used to calculate the equivalent dose: $H = D \times Q_{LET}$.

The unit of H and E_D is Sievert (Sv). For scientific purposes, X-rays and γ -rays are used as a reference radiation quality with a predefined $Q_{LET} = 1$ (FREY et al., 2017; SIHVER et al., 2015; SOLLAZZO et al., 2016).

3.1.2. Space radiation

While the background radiation on Earth accounts to an average annual dose of 2.1 mSv (in Germany), astronauts travelling outside Earth's atmosphere and magnetic field are exposed to higher doses of IR (BEAUJEAN et al., 2002; BERGER et al., 2013; GUO et al., 2015). This makes extraterrestrial radiation exposure a major health risk for human spaceflight. The most important constituents of space radiation for the radiation risk during space missions are solar particle events

(SPE) and galactic cosmic rays (GCR), originating from the Sun and from outside our solar system, respectively.

SPE are spontaneous eruptions of the Sun correlating to its magnetic activity. Protons are the charged particles primarily ejected in a SPE with energies up to several hundred MeV. Over the time course of a SPE, the dose rate can fluctuate between 0 – 100 *mGy/h* inside a protected vehicle (NORBURY et al., 2016).

The most relevant particles of GCR are nuclei that have an energy ranging from 10 *MeV/n* to 50 *GeV/n* and can penetrate a shielding of tens to hundreds of centimeters of water or aluminium. Due to the low fluence of GCR every cell of an astronaut is traversed by a proton approximately every three days and by a high charge and high energy (HZE) particle once every few months (NORBURY et al., 2016). HZE particle traversals are not random and not statistically independent. Particles on the order of 10^9 traverse the same track through the cell nuclei of tissues simultaneously (NORBURY et al., 2016). The accumulated dose for long term missions to the Mars or on the Moon may exceed the radiation limits set by the National Aeronautics and Space Administration (NASA). The dose limits allow a probability of < 3 % for radiation-induced cancer death (CUCINOTTA et al., 2017).

3.2. Effect of ionizing radiation on biological systems

The biological consequences of radiation exposure relate to the ionization of intracellular molecules. DNA is the most important molecule in a cell regarding the ionization-associated breakage of molecular bonds, since unrepaired DNA damage may result in cell death or mutations that can lead to tumor formation. Loss of integrity of the sugar-phosphate backbone of the DNA can result in the formation of DNA double strand breaks (DSB) that can lead to the death of the cell. The ionization of water molecules (radio-hydrolysis) can produce reactive oxygen species (ROS), which in turn can react with the DNA to form strand breaks or oxidized bases (ROOS, KAINA, 2006).

3.2.1. Acute radiation effects

The death of one cell can prove useful to protect the organism from neoplastic transformation, but the death of large cell populations can ultimately lead to functional disruptions and organ failures. On a systemic level, acute total body exposure to a single dose of IR can cause the so-called acute radiation syndrome (ARS) with symptoms that depend on the received equivalent dose. Doses > 0.5 Gy lead to the prodromal stage of the syndrome, characterized by a rapid onset of nausea and vomiting due to inflammatory stimulation of the caudal medulla (HELLWEG, BAUMSTARK-KHAN, 2007; MAKALE, KING, 1993).

Subsequent stages of the syndrome primarily affect tissues with rapid turnover. Therefore bone marrow is one of the most radiosensitive organs. Acute whole body exposure to 0.7 – 4 Gy damages hematopoietic stem cells, rendering them non-proliferative by cell cycle arrest or cell death. This stage of the ARS, the hematopoietic syndrome, leads to pancytopenia, especially progressive lymphopenia. The loss of lymphocytes results in immunosuppression that increases susceptibility to infection, while thrombocytopenia leads to stronger bleeding tendencies. Without mitigating treatment, death occurs within 60 days after radiation exposure mainly due to sepsis (HELLWEG, BAUMSTARK-KHAN, 2007; LOPEZ, MARTIN, 2011).

Higher total body doses of 4 – 12 Sv lead to the next stage of the ARS, the gastrointestinal syndrome. The folds of the gastrointestinal tract are separated into crypts and villi and contain differently differentiated cells. The stem cells at the bottom of the crypt serve as a reservoir for intestinal progenitor cells, which differentiate into the epithelial cell types during migration towards the tip of the villus (SHAKER, RUBIN, 2010). Radiation-induced death of the stem cell reservoir results in a failure to replenish the epithelial cells, leading to detachment of the epithelial layer of the intestinal mucosa. Breakdown of the mucosal barrier increases the infection risk and is accompanied by symptoms such as abdominal pain, diarrhea, nausea, vomiting, gastrointestinal bleeding and disturbed fluid and electrolyte balances. Due to sepsis, death occurs within 3 – 10 days after radiation exposure (HELLWEG, BAUMSTARK-KHAN, 2007; LOPEZ, MARTIN, 2011; TANG et al., 2017).

At acute total body doses above 10 Sv, the neurovascular syndrome is elicited. This severe brain damage includes impairment of the blood-brain barrier, formation of intracranial edemas and inflammation of the meninges. Symptoms of this stage are severe nausea, headaches, loss of cognitive function, disorientation and confusion. No survival can be expected (HELLWEG, BAUMSTARK-KHAN, 2007; LOPEZ, MARTIN, 2011).

3.2.2. Late radiation effects

While the ARS describe the consequences of acute exposure to high IR doses, acute or chronic exposure to low doses do not show immediate effects, but may take years to develop. One of these late radiation effects is an increased risk of cancer (GRAMMATICOS et al., 2013; HELLWEG, BAUMSTARK-KHAN, 2007; KAMIYA et al., 2015; LOPEZ, MARTIN, 2011; TANG, LOGANOVSKY, 2018). The persistence of IR-related DNA damage may increase the statistical probability for malignant degeneration of a cell, rendering the increased cancer risk of low dose irradiation a stochastic effect (HELLWEG, BAUMSTARK-KHAN, 2007; KAMIYA et al., 2015). Since any damage to the genome may progress towards cancer, there is no dose threshold for stochastic radiation effects (KAMIYA et al., 2015). Epidemiological studies found an increased risk for bone marrow leukemia at doses as low as 1.5 mSv from fallout of nuclear tests and increased cancer risk for atomic bomb survivors exposed to doses of less than 100 mSv (TANG, LOGANOVSKY, 2018). The latent period of emergence of leukemia has been approximated to 7 – 10 years, while formation of solid tumors takes 20 – 30 years (GRAMMATICOS et al., 2013).

Other manifestations of late radiation effects include the formation of eye cataracts (KHAN et al., 2017), cardiovascular diseases (RAGHUNATHAN et al., 2017), radiation enteritis (WEBB et al., 2013), radiation pneumonitis (BLEDSOE et al., 2017) and the radiation fibrosis syndrome (STUBBLEFIELD, 2017).

3.3. Cellular radiation response

The cellular radiation response is predominantly a DNA damage response (DDR) since the DNA is the most sensitive structure for radiation-induced biological consequences. The DDR involves intracellular processes that lead to genome maintenance and DNA repair, as well as cell fate programs. Damage recognition and recruitment of repair proteins are the primary responses to DNA damage, augmented by contemporary regulation of the cell cycle and initiation of signaling pathways such as p53 and NF- κ B. Failure to repair DNA damage results in the stop of the cell cycle and initiation of cell programs instigating different fate scenarios as part of the DDR.

3.3.1. DNA damage

The perpetuation of cellular life depends on its genomic integrity. The genome, consisting of two complementary strands of DNA, encompasses the entirety of the functions and differentiation choices of a cell. As long as the integrity of the DNA can be ensured, the cell can fulfill its purpose in the organism. Mutations that lead to the transformation of the cell originate from damage to the DNA. The various types of DNA damage are induced by a plethora of endogenous and exogenous factors that can react with DNA and produce erroneous base modifications or breaks in the DNA backbone (CHATTERJEE, WALKER, 2017).

Base modifications are among the damage that occurs naturally due to cellular metabolism or during replication. ROS are molecules with potent oxidative capabilities such as hydroxyl radicals. ROS are by-products of electron-transfer processes during metabolism that perform signaling functions under physiological conditions. In excess, ROS can become pathological and oxidize a plethora of molecules such as the DNA backbone, inducing DNA single strand breaks (SSB) and DSB, or the bases of the DNA creating oxidized bases. The oxidized bases formamidopyrimidine, 7,8 dihydro-8-oxoguanine or thymine glycol lack binding capacity to the complementary base and result in unsuccessful transcription, blocked replication or SSB formation (CHATTERJEE, WALKER, 2017; DI MEO et al., 2016; ZOROV et al., 2014). Error-prone polymerases lack proof-reading capacity that would ensure a faithful insertion of nucleotides via thermodynamic stability and geometric selection of nucleotides as well as exonuclease function to remove incorrectly inserted nucleases. Therefore improper selection of nucleotides results in base substitution, single base insertion or deletion errors (CHATTERJEE, WALKER, 2017). Base deamination is a process in which the bases adenine, guanine or cytosine lose the exocyclic amine group and become hypoxanthine, xanthine and uracil respectively. Deamination can occur spontaneously and leads to mismatched DNA bases (CHATTERJEE, WALKER, 2017). Abasic sites (also apurinic/apyrimidic sites; AP sites) are locations at which the N-glycosyl bond between the nitrogenous base and the sugar phosphate backbone of the DNA is broken and the base

is lost. The bond between base and backbone can hydrolyze spontaneously or as part of the base excision repair (BER) pathway. The loss of the base renders the AP site inherently unstable and prone to become a SSB (CHATTERJEE, WALKER, 2017). Defective topoisomerases, proteins that remove superhelical tension on the DNA during replication or transcription, can result in SSB formation (CHATTERJEE, WALKER, 2017). Breakage of single stranded DNA may lead to the formation of DSB during replication and therefore need to be repaired in a timely manner (CALDECOTT, 2008; KHORONENKOVA, DIANOV, 2015; NASSOUR et al., 2016).

3.3.1.1. Radiation-induced DNA damage

IR is an exogenous DNA damaging agent that induces various types of DNA lesions, including SSB and DSB. The formation of clustered DNA damage characterized as multiple SSB, AP sites and DSB, can be caused by densely IR and adds to the difficulty of repair (CHATTERJEE, WALKER, 2017; SAGE, SHIKAZONO, 2017).

Multiple SSB that occur at locations in close proximity can destabilize the DNA further and create a DSB, which is able to trigger apoptosis (JACKSON, BARTEK, 2009; MEHTA, HABER, 2014; SANTIVASI, XIA, 2014). Due to the error-proneness of DSB repair, this kind of lesion increases the chance of chromosomal aberrations and are considered to be the most detrimental type of radiation-induced DNA damage (MLADENOV et al., 2013).

One of the earliest responses to DNA DSB is the phosphorylation of histone H2AX in the vicinity of the lesion site creating the histone variant γ H2AX that can be used as a marker for the detection of DNA DSB (ROGAKOU et al., 1998). The histone is phosphorylated at S139 by kinases associated with DSB such as DNA-PK or ATM (KINNER et al., 2008). The phosphorylation can spread out over a range of 2 Mbp and functions as an anchor for several protein complexes such as the MRN complex. This makes γ H2AX a key player for recruitment of DNA repair proteins such as 53BP1 (BHARGAVA et al., 2017; KINNER et al., 2008; LEE et al., 2018).

3.3.2. DNA repair

DNA damage repair relies on the recognition of different damage types by damage sensors and subsequent selection of the appropriate repair pathway.

3.3.2.1. Single strand break repair

Oxidation-induced SSB can be detected by the poly(ADP-ribose) polymerase-1 (PARP1), which is recruited to the lesion. PARP1 binding to the SSB promotes addition of branched chains of poly(ADP-ribose) units (PAR) to PARP1 itself initiating recruitment of repair factors to the damage site. The poly(ADP-ribose) glycohydrolase (PARG) rapidly degrades PAR, rendering PARP1 available for

detection of further damage. Among the recruited repair factors is the X-ray repair cross-complementing protein 1 (XRCC1) that functions as a scaffold stabilizing the repair complex. The repair complex consists of proteins for DNA end processing, gap filling and final ligation of the strands. Key players in DNA end processing are polynucleotide kinase 3'-phosphatase (PNKP), AP endonuclease 1 (APE1) and aprataxin (APTX), which reinstate the damaged ends to conventional 3'-hydroxyl and 5'-phosphate groups. Gaps in the base sequence are filled by different sets of proteins depending of the gap size. Short patches are filled by DNA polymerase β (pol β) and ligated via DNA ligase 3, (Lig3) while long patches require a complex containing stabilizing factors such as the replicating factor C (RFC) and the proliferating cell nuclear antigen (PCNA) as well as gap-processing factors such as the flap endonuclease 1 (FEN1) and pol β . FEN1 removes patches of 2-12 nucleotides, which are refilled by pol β . The long gap is sealed by the Lig 1 (CALDECOTT, 2008).

3.3.2.2. Double strand break repair

There are two distinct repair pathways for DNA DSB: Homologous recombination (HR) and non-homologous end-joining (NHEJ). The alternative end-joining (Alt-EJ) is a backup pathway that uses the facilities of both HR and NHEJ.

HR is a high fidelity repair pathway with slow kinetics. Due to the necessity of template chromatids, HR is only active in the S- and G2-phase of the cell cycle (MLADENOV et al., 2013). As depicted in Figure 1, in the beginning of HR repair, the MRN complex is recruited to the damage site, consisting of the proteins meiotic recombination 11 (MRE11), Rad50 and Nijmegen breakage syndrome protein 1 (NBS1). The MRN complex facilitates downstream processes of HR repair like DNA end resection and recruitment of subsequently needed repair proteins (LEE et al., 2018). Rad50 stimulates DNA binding of the complex and activation of MRE11, the core protein of the MRN complex. MRE11 exhibits double strand DNA (dsDNA) exo- and single strand DNA (ssDNA) endonuclease activity. NBS1 associates the endonuclease C-terminal binding protein 1 interacting protein (CtIP) to the MRN complex. For DNA end resection, MRE11 and CtIP create ssDNA endonuclease activity-induced breaks followed by digest towards the DSB via exonuclease activity of MRE11 and the exonuclease 1 (EXO1) in order to produce 3' ssDNA overhangs (LEE et al., 2018; LIU, HUANG, 2016; MLADENOV et al., 2013, 2016). The breast cancer type-1 susceptibility protein (BRCA1) is able to form complexes with different proteins and assist in HR at several points. In association with CtIP, BRCA1 positively affects end resection by removing the NHEJ initiating complex of the replication timing regulatory factor 1 (RIF1) and p53 binding protein 1 (53BP1) from the DSB. The endonuclease activity of MRE11 and CtIP are important for repair pathway choice, as they have been found able to release the Ku70/80 heterodimer from DNA ends, steering the DSB repair towards HR (CHAPMAN et al., 2013; GUO et al., 2018; JASIN, ROTHSTEIN, 2013; LEE et al., 2018; LIU, HUANG, 2016).

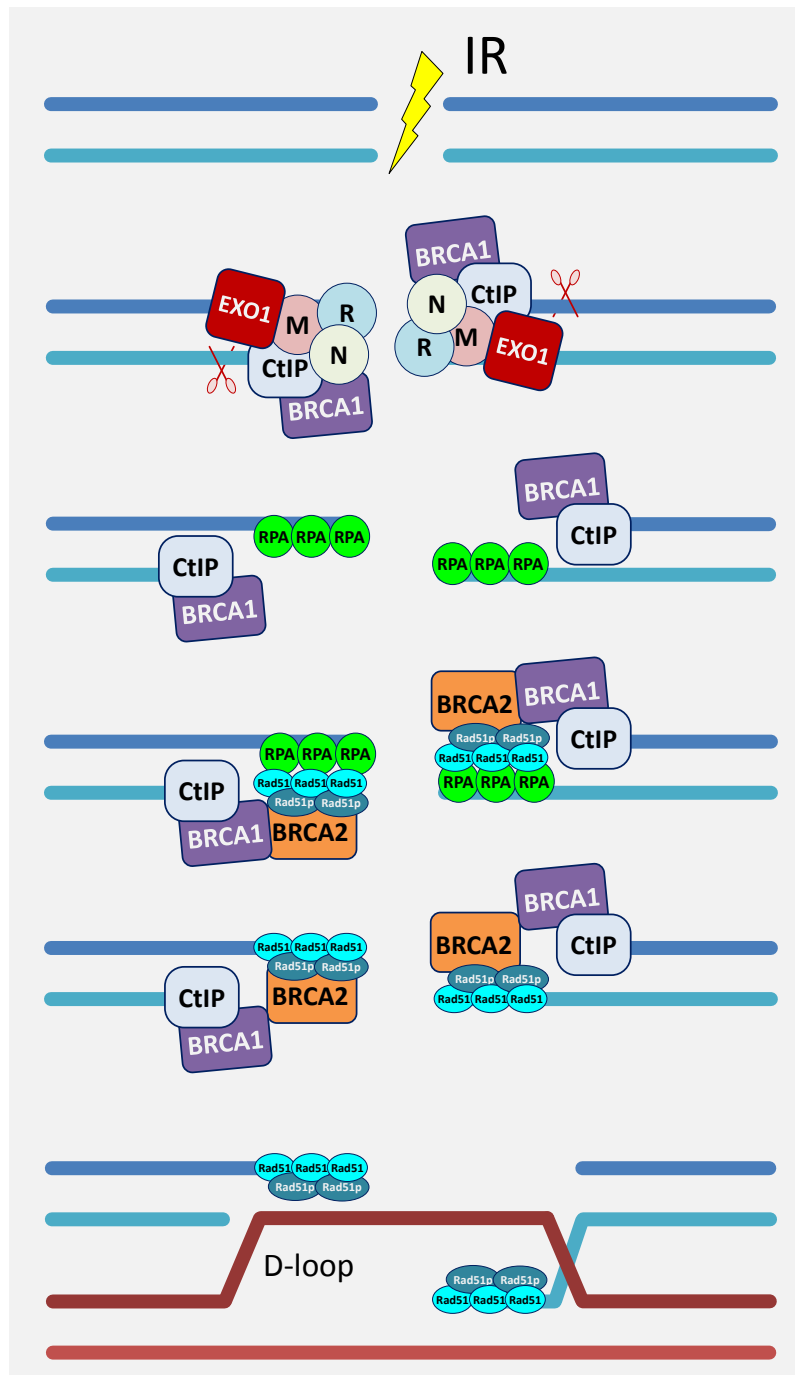


Figure 1 Initiation of the HR repair pathway

Assembly of HR relevant repair proteins and processes including D-loop formation and strand invasion is explained in the paragraph *DNA repair*. The DNA double strand break, induced by ionizing radiation (IR, yellow lightning) is indicated as a discontinuation of the two complementary strands (blue, cyan). Red scissors indicate endo- and exonuclease activity. The repair of DNA DSB via HR is continued in Figure 2 after D-loop formation in the template strands (red). Schematics were modified from existing literature (MLADENOV et al., 2013).

The 3' ssDNA overhang produced by DNA end resection rapidly recruits the replication protein A (RPA) to coat the overhang, which activates checkpoint kinase 1 (CHK1) via phosphorylation by ataxia and rad3 related (ATR) kinase (GOTO et al., 2015; MLADENOV et al., 2013). BRCA1 proceeds to recruit breast cancer type-2 susceptibility protein (BRCA2), Rad51 and Rad51 paralogs to the RPA coated ssDNA. BRCA2 initiates replacement of RPA with Rad51 to form a nucleoprotein filament structure stabilized by the Rad51 paralogs (LEE et al., 2018; MLADENOV et al., 2013, 2016). The Rad51 nucleoprotein filament invades the template dsDNA in search for the sequence homologous to the damaged DNA section, thereby creating a displacement loop (D-loop) structure (MLADENOV et al., 2013, 2016). After finding homology in the D-loop (synapsis), the farthest Rad51 protein is removed in a Rad54-dependent manner to reveal a 3' -OH end that facilitates strand elongation (CRICKARD, GREENE, 2018; MLADENOV et al., 2013, 2016).

Upon the initiation of this repair-associated DNA synthesis HR can branch into two sub-pathways, depending on whether one or both DNA ends are engaged, as shown in Figure 2. The D-loop invading strand can be elongated for a limited distance before it dissociates from the homologous sequence and re-ligates to the original strand, serving as a template for the second strand break to be repaired. This process is called synthesis-dependent strand annealing (SDSA) and is the most frequent outcome of homologous recombination repair (MLADENOV et al., 2013). In another sub-pathway, called the DSB repair (DSBR), both DSB ends are engaged and the D-loop additionally associates with the non-invading strand and a Holliday junction of four DNA strands is formed (LILLEY, 2017; MLADENOV et al., 2013, 2016). The formation of Holliday junctions in this process is important as it can result in cross-over of the involved strand-sections depending on the resolution of the Holliday junction. After simultaneous synthesis of both strands the Holliday junctions are resolved by a group of proteins called Holliday junction resolvases. Resolvases include the Bloom's syndrome helicase (BLM), topoisomerase 3a (Top3a), the nuclease GEN1 and the SLX4 endonuclease complex containing SLX1, SLX4, MUS81 and EME1. BLM brings two adjacent junctions together to be unlinked by Top3a. GEN1 and the SLX4 complex proceed to cleave diametrically opposite strands and resolve the junction. Depending on the spatial configuration of the strands in the Holliday junction, the information of the template chromatid may cross over to the site of the original DSB (LILLEY, 2017; MLADENOV et al., 2013, 2016).

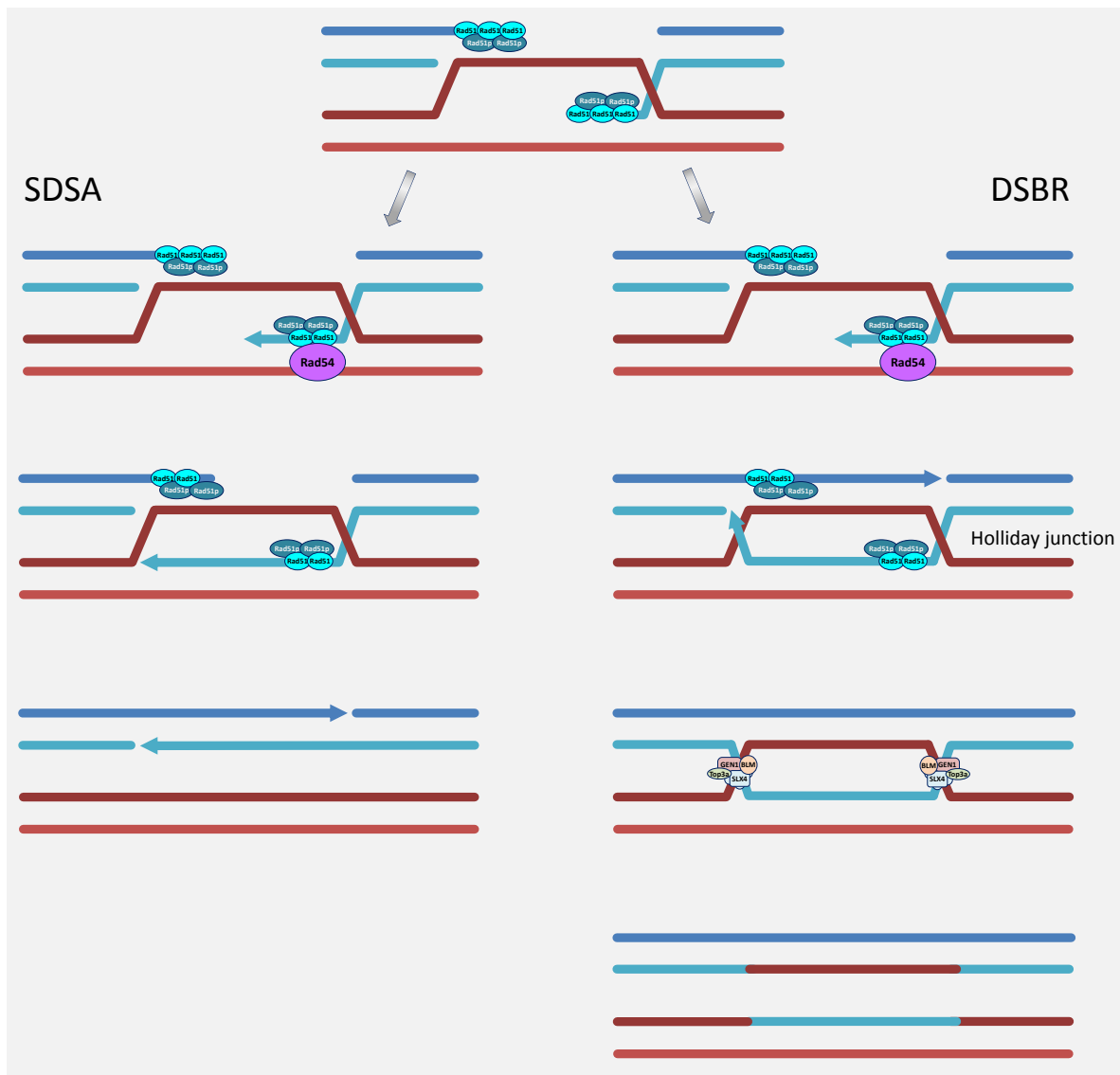


Figure 2 Resolution of the HR repair pathway

Elongation of DNA strands at homologous sites and resolution of the repair is explained in paragraph *DNA repair*. The previous steps of HR repair are shown in Figure 1. The silver arrows indicate the possible branches of the repair pathway into synthesis-dependent strand annealing (SDSA) and DSB repair (DSBR). Arrows in the DNA strand indicate the direction of synthesis. Schematics were modified from existing literature (MLADENOV et al., 2013)

NHEJ is a fast-acting yet error-prone repair pathway that is able to act throughout the cell cycle independent on sister chromatids as templates. In the classical NHEJ repair, as seen in Figure 3, the DNA DSB is detected by the proteins Ku70 and Ku80 that heterodimerize to form an asymmetric toroid structure. The Ku70/80-dimer protects the DNA ends from nucleolytic degradation and thereby guide repair pathway choice towards NHEJ. A complex of RIF1 and 53BP1, activated by Ku, additionally blocks DNA resection and promotes NHEJ pathway choice. DNA-bound Ku70/80 then recruits DNA-dependent protein kinase (DNA-PK) to the damage site. DNA-PK recruitment results in dimerization of the protein followed by auto-phosphorylation of the catalytic subunit DNA-PKcs.

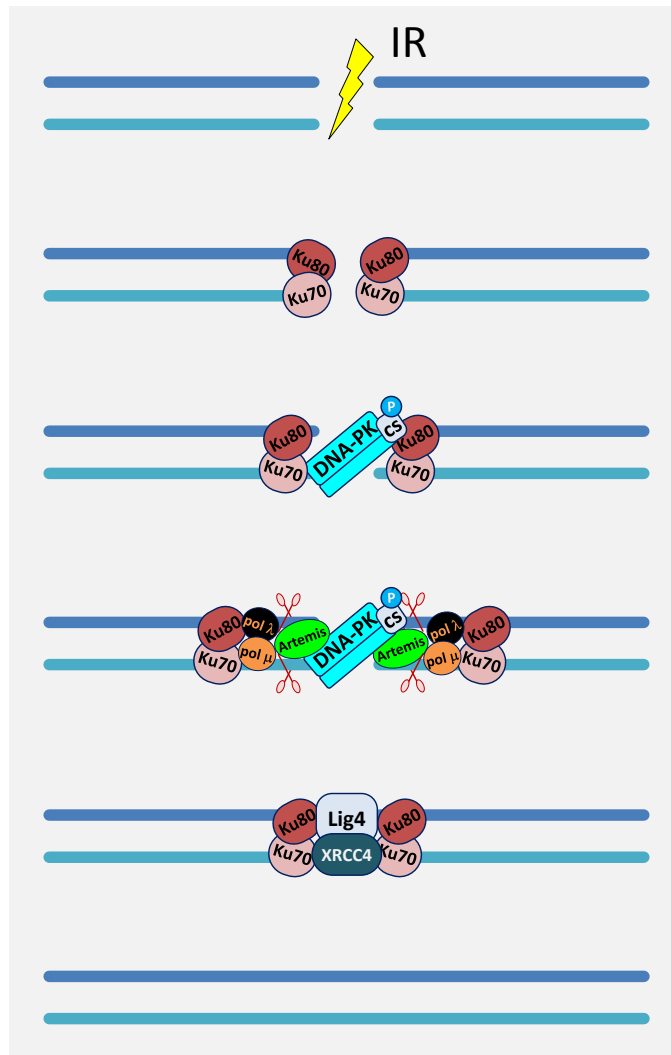


Figure 3 Non-homologous end-joining pathway of DNA DSB repair

The repair of DNA double strand breaks via NHEJ is explained in paragraph *DNA repair*. The DNA double strand break, induced by ionizing radiation (IR, yellow lightning) is indicated as a discontinuation of the two complementary strands (blue, cyan). Red scissors indicate endo- and exonuclease activity. Schematics were modified from existing literature (MLADENOV et al., 2013).

The activated kinase recruits and phosphorylates DNA processing enzymes Artemis, DNA polymerase μ and λ (pol μ and λ respectively). Artemis is a nuclease that together with pol μ and pol λ generates ligatable DNA ends. The processed DNA ends are re-ligated by the Lig4/XRCC4 complex and this restores DNA integrity. The DNA end processing and ligation act indiscriminately of the genetic information and aims to seal the breaks in a timely manner resulting in a possible alteration of the DNA sequence at the junction (CHAPMAN et al., 2013; ESCRIBANO-DIAZ et al., 2013; GOODWIN, KNUDSEN, 2014; ILIAKIS et al., 2015; LEE et al., 2018; LOBRICH, JEGGO, 2017; MAIER et al., 2016; MLADENOV et al., 2013, 2016).

Alt-EJ can act as a backup pathway to both HR and NHEJ throughout all phases of the cell cycle. DNA DSB recognition by PARP-1 as a low-affinity competitor to Ku70/80 initiates this repair pathway. PARP-1 proceeds to recruit the MRN complex and CtIP to the damage site initiating DNA end resection. Further recruitment of DNA polymerase θ (pol θ), a translesion polymerase, suppresses the ATPase activity of Rad51 and thereby inhibits formation of the Rad51 nucleofilament. Pol θ elongates each strand using the opposite single stranded DNA overhang as template preparing the strands for subsequent ligation. The Werner syndrome helicase (WRN) together with Lig1 and Lig3 proceed to re-ligate the strands (MLADENOV et al., 2013, 2016).

3.3.2.3. ATM-dependent signaling

Parallel to DNA repair, signaling cascades are initiated in response to DNA damage. The various signaling pathways that play a role in the DDR may also modulate DNA repair. A cornerstone of DNA damage signaling is Ataxia telangiectasia mutated (ATM). The kinase acts as key regulator in the DDR to DSB. ATM is a PI3K-like protein kinase (PIKK) with a catalytic domain similar to phosphatidylinositol 3 lipid kinases (PI3K) that forms inactive homodimers. The MRN complex recruits ATM to the damage site and enhances its kinase activity. The dimer separates into active monomers that auto-phosphorylate ATM at serine 1981 (S1981). In HR active ATM phosphorylates CtIP and EXO1, facilitating DNA end resection, as well as p53 and RPA, initiating Rad51 replacement of RPA (LEE et al., 2018; MENON, POVIRK, 2014; MLADENOV et al., 2013, 2016). ATM also phosphorylates p53 and CHK2 in order to modulate cell cycle arrest (DONG et al., 2018; MENON, POVIRK, 2014) as well as the KRAB-associated protein 1 (KAP-1) thereby promoting local chromatin relaxation and access for repair proteins to the DNA damage site (FERNANDEZ-CAPETILLO, NUSSENZWEIG, 2008; LOBRICH, JEGGO, 2017). In NHEJ repair, pol λ has been shown to be activated by ATM in addition to DNA-PKcs (SASTRE-MORENO et al., 2017).

DNA-PKcs, activated by auto-phosphorylation, can also be activated by ATM via phosphorylation at threonine (T) 2609 and T2647. ATM on the other hand can be negatively regulated by DNA-PKcs via phosphorylation at multiple sites. This interaction provides evidence for crosstalk between ATM and DNA-PKcs that may regulate DNA pathway choice (ZHOU et al., 2017).

Exposure to IR induces NF- κ B activation that has been shown to be dependent on ATM and NBS1 (FANG et al., 2014; HABRAKEN et al., 2003; HELLWEG et al., 2018). NF- κ B can also be activated by DNA-PK (SABATEL et al., 2011). Activation of NF- κ B thereby provides further regulation of DNA damage repair (GODWIN et al., 2013). ATR was shown to competitively bind the NK- κ b essential modulator (NEMO) and thereby repress ATM-mediated NF- κ B activation (SABATEL et al., 2011).

3.3.3. Cell cycle arrest

3.3.3.1. Cell cycle phases

The cell cycle is the continuous life cycle of a cell and is divided into several phases (G1, Synthesis, G2 and Mitosis) corresponding to the cellular activity in preparation of the subsequent phases. Most notable among the cell cycle phases are the DNA synthesis phase (S-phase), in which the DNA is replicated and the Mitosis (M-phase), in which the cells split the replicated DNA to opposing cells sides and then divide, in a process called cytokinesis, to create two equal daughter cells containing each a set of replicated DNA (SCHAFER, 1998). Progression through the different cell cycle phases is tightly regulated via activation of cyclin-dependent kinases (CDKs) and expression of cyclin proteins (VERMEULEN et al., 2003). CDKs are stably expressed during the cell cycle and are only activated when bound to cyclins. Protein levels of cyclins vary in a periodic manner corresponding to the respective cell cycle phase enabling a concerted CDK activation to progress the cell cycle in an orderly manner (VERMEULEN et al., 2003). The cell cycle phases, the DNA integrity checkpoints and the corresponding cyclin levels are depicted in Figure 4.

3.3.3.2. Cell cycle regulation

One exception to the periodical expression of cyclin proteins is cyclin D, which is expressed upon growth factor/mitogen stimulation of the cell, enabling cyclin D to initiate cell cycle progression (GIACINTI, GIORDANO, 2006; VERMEULEN et al., 2003).

Cyclin D can bind to CDK4 and CDK6, which are held inactive via complexation with proteins of the INK4 family, leading to activation of the kinases and phosphorylation of the retinoblastoma protein (pRb) (DARZYNKIEWICZ et al., 2015; NAKAYAMA et al., 2001). The hypo-phosphorylated protein pRb acts as a suppressor of cycle progression by binding to proteins of the E2F family of transcription factors. Phosphorylation of pRb releases the transcription factor, which positively regulates transcription of proteins necessary for later phases, including cyclin A, E and the cell-division-cycle 25 (cdc25) protein (DARZYNKIEWICZ et al., 2015; GIACINTI, GIORDANO, 2006; SUR, AGRAWAL, 2016; VERMEULEN et al., 2003).

Cyclin E complexes with CDK2, thus activating the kinase leading to hyper-phosphorylation of pRb and establishing a positive feedback loop of mitogen-independent activation of E2F. The inactivation of pRb marks a restriction point in the G1-phase, upon which the cell is committed to progression into the S-phase (BERTOLI et al., 2013; GIACINTI, GIORDANO, 2006; VERMEULEN et al., 2003). The cyclin E/CDK2 complex further phosphorylates the CDK inhibitor p27, marking it for proteasomal degradation resulting in the release of the cyclin A/CDK2 complex (BERTOLI et al., 2013; DARZYNKIEWICZ et al., 2015; NAKAYAMA et al., 2001; VERMEULEN et al., 2003).

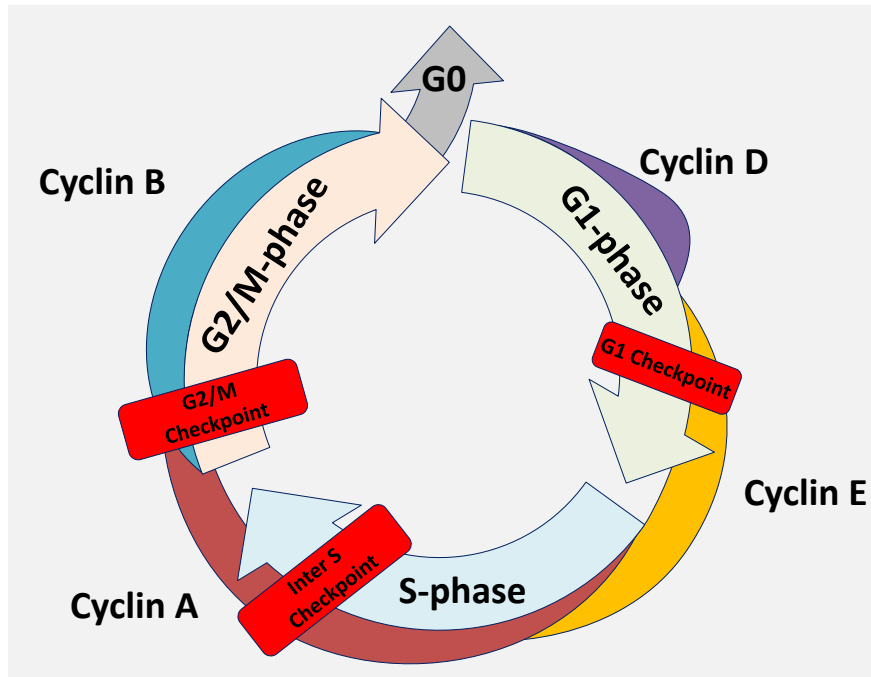


Figure 4 The cell cycle and DNA damage checkpoints

The cell cycle progresses through G1-phase (green) with an increasing cyclin D concentration (violet). Cyclin E concentrations (yellow) begin to rise in late G1-phase and start to fall during S-phase (blue). Cyclin A concentrations (brown) increase at the beginning of S-phase and into G2-phase and mitosis (G2/M-phase, orange). Cyclin B is present during G2/M-phase. DNA integrity is verified at the end of G1-phase, during S-phase and before mitosis in G2 phase at the DNA damage checkpoints. Cells can exit the cell cycle into G0 (grey). Schematics were modified from existing literature (SCHAFFER, 1998). The processes involved in cell cycle progression are explained in the paragraph *Cell cycle*

The cyclin A/CDK2 complex regulates factors responsible for initiating and maintaining DNA replication (TAKEDA, DUTTA, 2005; VERMEULEN et al., 2003). Cyclin A is expressed throughout S- and G2-phase of the cell cycle and is only degraded during mitosis (DARZYNKIEWICZ et al., 2015; VERMEULEN et al., 2003). During DNA replication cyclin A is sequestered in the nucleus, bound to CDK2, while during late G2-phase and early mitosis, it associates with CDK1 and regulates orderly the chromosome segregation before being degraded in proteolytic manner (DARZYNKIEWICZ et al., 2015; VERMEULEN et al., 2003).

Cyclin B levels rise during G2-phase of the cell cycle and forms a complex with CDK1 in preparation of cell division. At the beginning of mitosis, the complex translocates into the nucleus initiating mitosis. Its functions include phosphorylation of nuclear lamins in order to help disassembly of the nucleus and other proteins that initiate centrosome separation and spindle assembly. At the end of mitosis, cyclin B/CDK1 activates the anaphase promoting complex that catalyzes ubiquitination and

subsequent degradation of cyclin A and B, enabling the cell to go into anaphase of mitosis and divide (BROWN et al., 2007; LINDQVIST, 2010; VERMEULEN et al., 2003).

3.3.3.3. NF- κ B-associated regulation of cell cycle progression

NF- κ B is able to regulate the cell cycle in all phases either via transcriptional promotion of cyclins and CDKs or via activation of modulating factors such as p21 and p27. Progression through G1 is supported by NF- κ B via promotion of cyclin D and CDK6 expression. The RelA transcription targets cyclin A, cyclin B and CDK2 are able to control progression through S-phase, G2 phase and mitosis in a NF- κ B promoted manner. NF- κ B-dependent expression of S-phase kinase-associated protein 2 (SKP2) further promotes cell cycle progression via subsequent degradation of CDK inhibitor p27. Induction of p21 expression in a NF- κ B-associated manner regulates cell cycle progression on the other hand in a negative manner (LEDOUX, PERKINS, 2014).

3.3.3.4. DNA integrity checkpoints

For maintenance of genetic stability, DNA damage checkpoints assess DNA integrity and halt cell cycle progression in order to facilitate repair. The checkpoints are positioned before entering S-phase (G1/S checkpoint), during S-phase and in G2-phase (G2/M checkpoint) before entry into mitosis (BERTOLI et al., 2013; IYER, RHIND, 2017; VERMEULEN et al., 2003).

DNA damage by IR is recognized by damage recognition kinases such as ATM and ATR. ATM and ATR regulate cell cycle arrest via phosphorylation of p53 and CHK2 in response to DNA damage (PAWLIK, KEYOMARSI, 2004; VERMEULEN et al., 2003).

The cell cycle arrest at the G1/S checkpoint is dependent on p53. Activation of p53 leads to transcription of p21, which binds to the cyclin E/CDK2 complex thereby blocking phosphorylation of pRb inhibiting its release from the transcription factor E2F. Bound to pRb, E2F stays dormant and the cell cycle cannot progress (EL-DEIRY, 2016; PAWLIK, KEYOMARSI, 2004).

The S-phase checkpoint is activated via ATR-detected lesions in the DNA, by intrinsic factors such as misconducted DNA replication or extrinsic factors such as IR (IYER, RHIND, 2017). During replication, polymerases stall at lesions while the helicase continues to unwind the DNA. Separation of these enzymes leads to the generation of single stranded DNA which is coated with RPA. ATR is recruited to the RPA-ssDNA complex of the stalled replication fork and phosphorylates CHK1 which proceeds to phosphorylate cdc25, a phosphatase regulating the activation of cyclin/CDK complexes (GOTO et al., 2012; GOTO et al., 2015; IYER, RHIND, 2017). Phosphorylated cdc25 is degraded resulting in inhibition of CDK activation and cell cycle arrest (BOUTROS et al., 2007; GOTO et al., 2012).

The most prominent arrest after IR exposure occurs at the G2/M checkpoint. Several cell types are reported to arrest at G2/M to varying degrees (CHEN et al., 2017; DONG et al., 2017; FURUSAWA et al., 2012; KIM et al., 2015a; QIAO et al., 2013; SMITH et al., 2016; YOU et al., 2014). CHK2 activation via ATM leads to inhibition of cdc25 in a p53-independent manner (PAWLIK, KEYOMARSI, 2004). Activation of p53 via ATM can induce arrest via various ways. Expression of 14-3-3 proteins that bind cdc25 blocks cyclin B/CDK1 activation, while p21 mediates nuclear sequestration or degradation of the cyclin B/CDK1 complex. Damage recognition via ATR at the G2/M checkpoint leads to CHK1-induced cdc25 degradation using the same mechanism as in S-phase, blocking cyclin B/CDK1 activation (CHEN, 2016; GOTO et al., 2012; GOTO et al., 2015; LI et al., 2018; PAWLIK, KEYOMARSI, 2004; VERMEULEN et al., 2003). Without cyclin B/CDK1 initiating mitosis, the cells arrest in G2 phase.

3.4. Cell fates

Damage induced by IR has a chance to be too complex or too abundant for sufficient repair. In response to a prolonged cell cycle arrest, programs can be initiated that decide the ultimate outcome of the cell. Controlled programs include cell death via apoptosis or via autophagy. Another option for a controlled cell fate is the induction of a permanent cell cycle arrest leading to cellular senescence. The induced damage may also disrupt the initiation of those controlled programs. Such disruption usually leads to an uncontrolled cellular demise, such as necrosis or mitotic catastrophe.

3.4.1. Cell death

Cell death by IR occurs via several possible mechanisms including apoptosis, necrosis, autophagy and mitotic catastrophe (ERIKSSON, STIGBRAND, 2010; NIKOLETOPOULOU et al., 2013; PAWLIK, KEYOMARSI, 2004; SMITH et al., 2017; YUAN et al., 2017). Apoptosis is a programmed process that results in distinct biochemical and morphological changes like breakdown of nuclear DNA and cell shrinking. During this process the cell membranes stay intact and the cytoplasm is retained in apoptotic bodies, which renders apoptosis a non-inflammatory mechanism (ELMORE, 2007). Cellular stress, like IR, or extrinsic factors, like the FAS-ligand binding to the apoptosis-inducing receptor FAS (CD95) lead to the activation of caspase proteins facilitating the apoptotic degradation of the cell (ELMORE, 2007; HENGARTNER, 2000; PAWLIK, KEYOMARSI, 2004).

Mitotic catastrophe describes cell death as a result of a faulty mitosis and is frequently observed in solid tumors after radiotherapy. If the cell fails to recognize damaged DNA at the DNA damage checkpoints and thereby progresses unimpeded through the cell cycle, the cell enters mitosis with erroneous DNA. Damage like hyper-amplified centrosomes or inter-chromosome conjunctions might lead to aberrant segregation of chromosomes that incites the caspase-machinery and results in apoptotic cell death (CASTEDO et al., 2004; ERIKSSON, STIGBRAND, 2010).

3.4.2. Cellular senescence

One of the various cell fates that can occur due to exposure to IR is a persistent proliferative arrest also known as cellular senescence. It is a protective mechanism to prevent irreparably damaged cells from proliferation (SHAO et al., 2016). Damaged cells that go into cell cycle arrest in order to repair damage may also permanently stay in arrest.

The markers for the senescence-associated phenotype include increased p21 (CDKN1A), p16^{Ink4} (CDKN2A), p38 (mitogen-activated protein kinase 14, MAPK14), senescence-associated β -

galactosidase activity, cytokine secretion as well as growth inhibition (KANG et al., 2015; WANG et al., 2011; WERNER et al., 2014). Intracellular signaling for stress-induced premature senescence (SIPS) starts at the impact of radiation exposure (DNA DSB) and continues via several axes. One is the ATM-driven DDR leading to the expression of p16 as well as stabilization of p53 with downstream transcription of p21. The CDKs p21 and p16 both inhibit cell cycle progression and thereby facilitate growth arrest (BARASCU et al., 2012; DEBACQ-CHAINIAUX et al., 2010; KANG et al., 2015). An ATM-independent senescence pathway is mediated via p38 (DEBACQ-CHAINIAUX et al., 2010; WANG et al., 2011; WERNER et al., 2014). Exposure to cellular stresses leads to 1) the induction of the p38 signaling pathway that mediates stabilization of p53 – inducing senescence via p21 as mentioned above – and 2) the activation of NF- κ B, engaging transcription of inflammatory cytokines hallmarking the senescence-associated secretory phenotype (SASP) (CUADRADO, NEBREDA, 2010; KANG et al., 2015; WERNER et al., 2014).

3.5. Nuclear factor κ B

The nuclear factor kappa-light-chain-enhancer of activated B-cells (NF- κ B) is a key regulator in the response to infection, cell injury and various kinds of cellular stress. As such, NF- κ B governs the transcription of proteins necessary for a plethora of physiological processes including immune functions, inflammation, autophagy, cellular senescence, cell survival, proliferation and differentiation (BEGALLI et al., 2017; DIDONATO et al., 2012; HELLWEG, 2015; HELLWEG et al., 2011; HOESEL, SCHMID, 2013; LI, VERMA, 2002; VALLABHAPURAPU, KARIN, 2009; WU et al., 2015).

3.5.1. The NF- κ B family

In mammalian cells, the NF- κ B family is composed of five proteins that can form homo- and heterodimeric complexes: RelA (p65), RelB, c-Rel, NF- κ B1 (p50/p105) and NF- κ B2 (p52/p100). The dimers bind to DNA promoters of a wide range of target genes including inflammation, proliferation and cell cycle control. The NF- κ B subunits share a highly conserved N-terminal region of 300 amino acids (Rel-homology domain) that is responsible for protein-protein interactions (dimerization, I κ B regulation), DNA binding and nuclear translocation (BEGALLI et al., 2017; SOUBANNIER, STIFANI, 2017). RelA, RelB and c-Rel possess a transcriptional activating domain (TAD) unlike the subunits p50 and p52, which are formed by proteolytic partial degradation of the precursor proteins p100 and p105 respectively (HELLWEG et al., 2016; O'DEA, HOFFMANN, 2009; VALLABHAPURAPU, KARIN, 2009). Activation of different dimer combinations can be triggered via the canonical, the non-canonical and the genotoxic signaling pathways (HELLWEG et al., 2016; O'DEA, HOFFMANN, 2009; TEGOWSKI, BALDWIN, 2018).

For a rapid activation, the transcription factor is inactively located in the cytoplasm bound to the inhibitor of NF- κ B (I κ B), a family of proteins including I κ B α , I κ B β and I κ B ϵ . I κ B proteins all possess an ankyrin-repeat domain that is used to bind to the NF- κ B subunits and mask their nuclear localization sequence, thereby holding the transcription factor in the cytoplasm (BEGALLI et al., 2017; COURTOIS, FAUVARQUE, 2018; IMBERT, PEYRON, 2017). The precursor proteins p100 and p105 contain ankyrin-repeat domains and can act self-inhibitory in the non-canonical pathway on p52 and p50 (HELLWEG et al., 2016; O'DEA, HOFFMANN, 2009).

3.5.2. Canonical NF- κ B signaling pathway

The canonical NF- κ B signaling pathway, depicted in Figure 5, is activated by inflammation inducing ligands binding to cytokine receptors such as the tumor necrosis factor receptor-1 (TNFR1), pathogen-recognizing Toll-like receptors (TLR) or antigen-binding T-/B-cell receptors (HELLWEG et al., 2016; O'DEA, HOFFMANN, 2009). In case of TNFR1, the conformational change upon binding of its ligand tumor necrosis factor (TNF) leads to receptor trimerization and subsequent recruitment of the adapter protein TNFR1-associated DEATH domain (TRADD), E3 ubiquitin ligases of TNFR-associated factor family (TRAF) and the kinase receptor-interacting serine/threonine-protein-1 (RIP1).

TRADD and RIP1 both contain DEATH domain (DD) sequences that can bind to the cytosolic DD of TNFR1 (MICHEAU, TSCHOPP, 2003; ROY et al., 2018; VALLABHAPURAPU, KARIN, 2009). TRAF2/5 bound to the TNFR1:TRADD:RIP1 complex initialize recruitment of the E3 ubiquitin ligases cellular inhibitor of apoptosis protein (cIAP1/2) that catalyze poly-ubiquitination of RIP1 on lysine 63 (K63) (SHI, SUN, 2018). RIP1 poly-ubiquitination leads to the recruitment of the TGF β -activated kinase 1 (TAK1) and the I κ B kinase (IKK) complexes (CHEN, 2012; ROY et al., 2018). The TAK1 complex consists of the subunits TAK1, TAB1 and TAB2. The RIP1 poly-ubiquitin chain binds to the TAB2 subunit of the TAK1-complex, which leads to the auto-phosphorylation and thereby activation of the complex via TAK1. The IKK complex consists of the catalytic subunits IKK α , IKK β and the scaffolding subunit IKK γ (NEMO).

The IKK complex is recruited via binding of the RIP1 poly-ubiquitin chain to NEMO enabling TAK1-mediated phosphorylation of S177 and S181 of IKK β (CHEN, 2012; MCCOOL, MIYAMOTO, 2012; ROY et al., 2018). The activated IKK complex proceeds to phosphorylate I κ B α at S32 and S36, thereby targeting the inhibitor for recognition by the β -transducing repeat-containing protein (β -TrCP). Subsequent K48 poly-ubiquitination via the associated E3 ubiquitin ligase complex leads to degradation via the 26S proteasome (COURTOIS, FAUVARQUE, 2018; HELLWEG et al., 2016). Dissociation of I κ B α from the I κ B:NF- κ B complex uncovers the nuclear localization sequence of

NF- κ B. The activated NF- κ B dimer then translocates into the nucleus and binds to the κ B consensus sequences, facilitating the transcription of target genes (HELLWEG et al., 2016; ROY et al., 2018; VALLABHAPURAPU, KARIN, 2009).

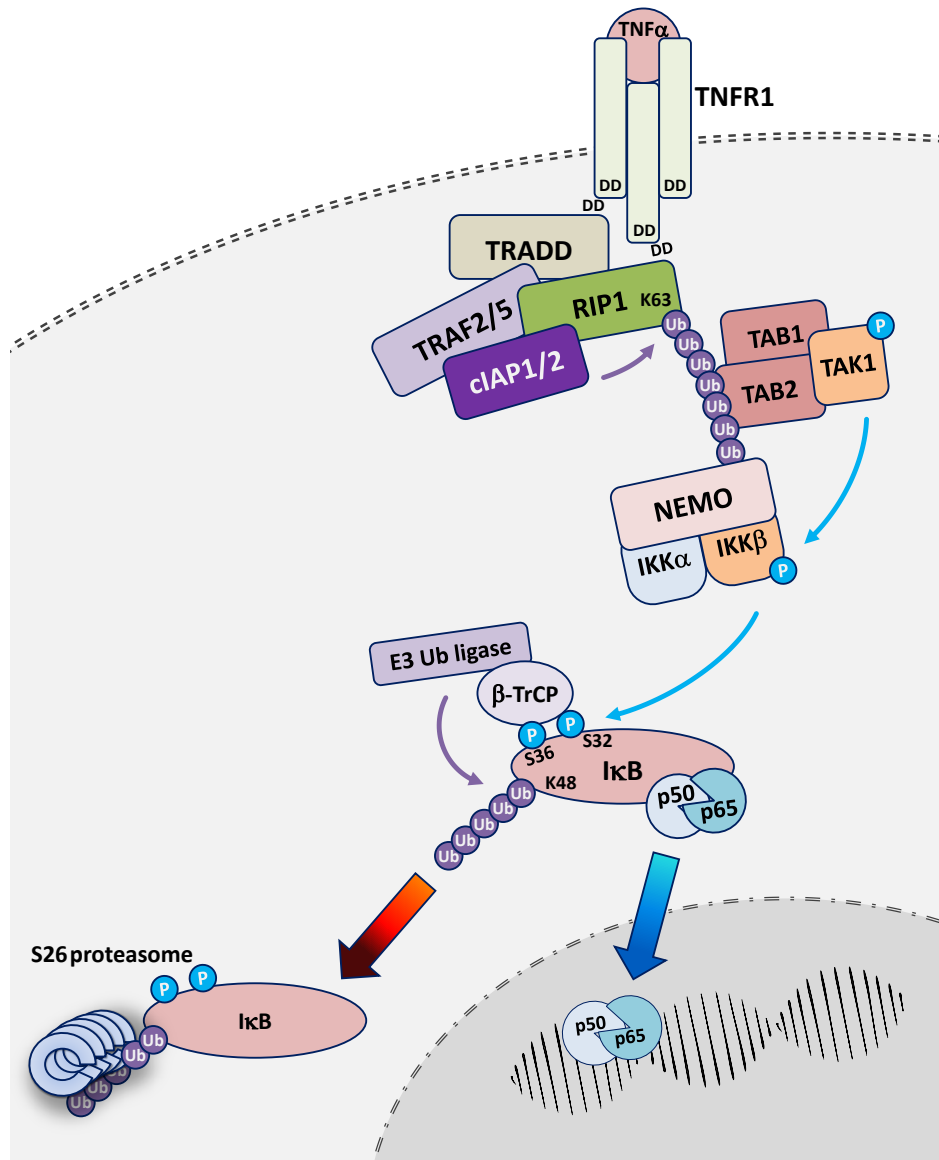


Figure 5 TNF- α initiated activation of NF- κ B via the canonical pathway.

The canonical activation of NF- κ B via TNF- α is detailed in the paragraph Canonical NF- κ B signaling pathway. Small violet arrows indicate ubiquitination, while small blue arrows indicate phosphorylation. The big yellow-red arrow indicates a junction of the pathway towards proteasomal degradation of I κ B, while the big green-blue arrow indicates a junction towards nuclear NF- κ B translocation.

The TLR/IL-1R pathway for NF- κ B activation, Figure 6, relies on signal transduction via the cytosolic Toll/IL-1 receptor (TIR) domain of the respective receptor, which contains DD sequences (KAWAI, AKIRA, 2007; VALLABHAPURAPU, KARIN, 2009). Cytokines such as interleukin-1 (IL-1) and pathogen-associated molecular patterns (PAMP) such as lipopolysaccharide (LPS) bind to the respective

receptors triggering recruitment of adapter proteins which correspond to the bound dimerized receptor (KAPLAN-TURKOZ et al., 2013). The key adapters mediating the signaling cascade are myeloid differentiation primary response gene 88 (MyD88) and TIR-domain-containing adapter inducing IFN- β (TRIF).

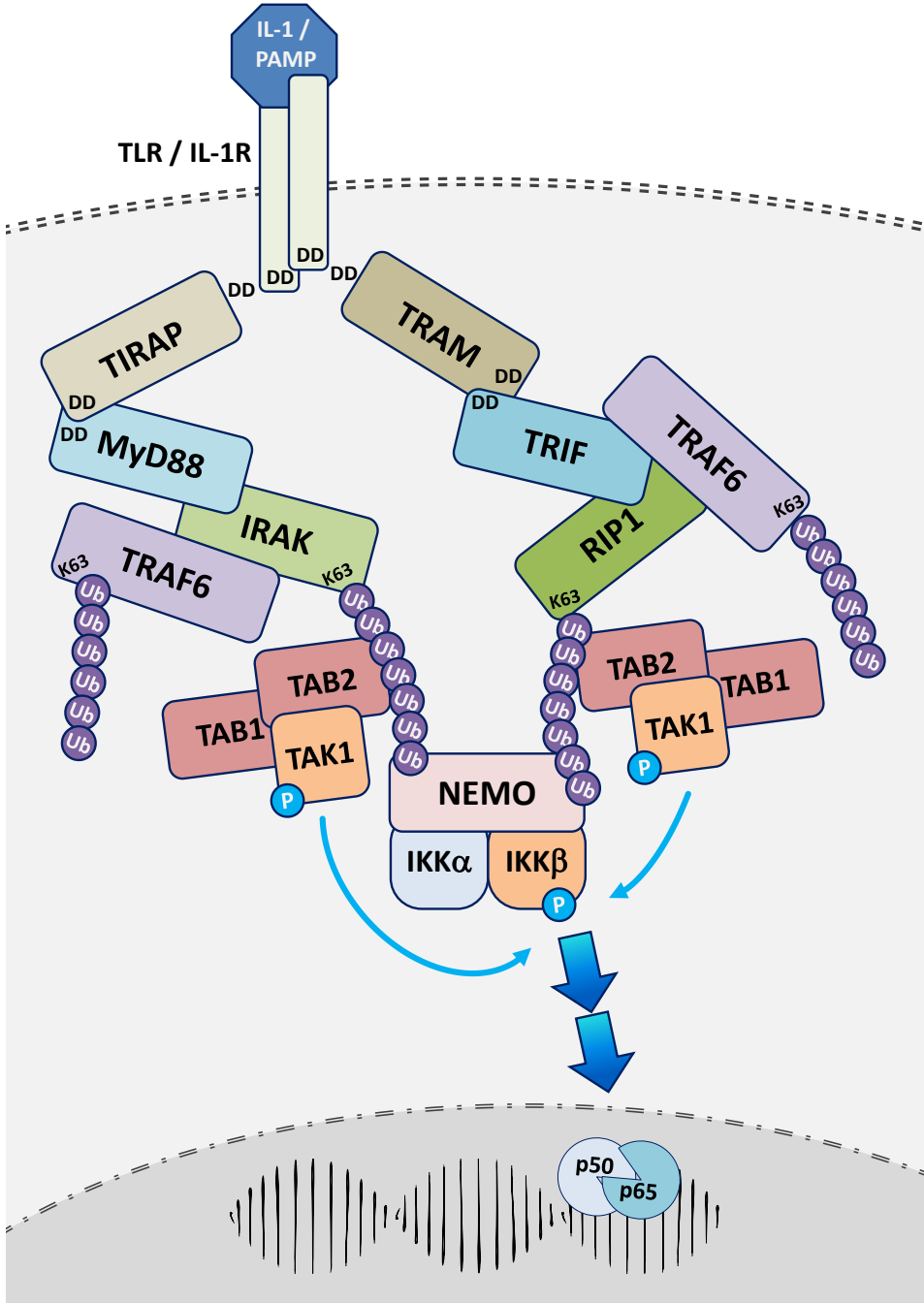


Figure 6 PAMP / IL-1 initiated activation of NF- κ B via the canonical pathway.

The canonical activation of NF- κ B via TLR is detailed in the paragraph Canonical NF- κ B signaling pathway. Small blue arrows indicate phosphorylation. The double green-cyan arrows indicate NF- κ B activation via the mechanisms described before, including proteasomal degradation of I κ B and nuclear translocation of the NF- κ B subunits (Figure 5).

While TLR9 and TLR3 can directly bind to the DD sequences of MyD88 and TRIF, respectively, TLR2 and TLR4 need to form bridges via additional adapter proteins, TIR-containing adapter protein (TIRAP) and TIR-domain-containing adapter molecule (TRAM), mediating interaction with MyD88 and TRIF (KAWAI, AKIRA, 2007; VALLABHAPURAPU, KARIN, 2009). Since DD sequences can interact with each other, the lack of direct interplay of TLR2 and TLR4 with MyD88 and TRIF has been attributed to the electrostatic surfaces of the TIR domains. The TIR of TLR4 and MyD88 are both highly electro-positive, inhibiting reciprocal action. TIRAP on the other hand is electro-negative, promoting interaction with both TLR4 and MyD88 (VALLABHAPURAPU, KARIN, 2009). Upon activation of TRIF mediated signaling, RIP1 and TRAF6 are recruited to the receptor complex and both targeted for poly-ubiquitination by TRAF6. The poly-ubiquitin chains then promote the TAK1-mediated activation of IKK β . In MyD88-mediated signaling, IL-1R-associated kinase (IRAK) proteins and TRAF6 are recruited to the receptor/adapter complex and initialize K63 poly-ubiquitination of TRAF6 and IRAK (ADHIKARI et al., 2007). Similar to RIP1, poly-ubiquitination mediates NF- κ B activation (ADHIKARI et al., 2007; KAWAI, AKIRA, 2007; VALLABHAPURAPU, KARIN, 2009).

3.5.3. Non-canonical NF- κ B signaling pathway

In the non-canonical (alternative) NF- κ B pathway, depicted in Figure 7, stabilization of the NF- κ B inducing kinase (NIK) is the key mechanism for transcriptional NF- κ B activity. In resting cells, alternative activation of NF- κ B is inhibited due to rapid degradation of NIK in a proteasome-dependent manner. NIK is associated with TRAF3, which acts as an adaptor for the E3 ubiquitin ligases cIAP1/2 and TRAF2 (COURTOIS, FAUVARQUE, 2018; VALLABHAPURAPU, KARIN, 2009). Interaction of NIK with the cIAP1/2:TRAF2:TRAF3 complex promotes K48 poly-ubiquitination of NIK and thereby targets it for degradation by the 26S proteasome. Humoral stimulation of certain TNFR-superfamily receptors, like the B-cell activation factor receptor (BAFFR), CD40, Fn14 or receptor activator of NF- κ B (RANK), leads to recruitment of the NIK associated ubiquitin ligase complex. Upon binding to the receptor:ligand complex, TRAF2 ubiquitinates cIAP1/2 and itself on K63. The ubiquitination of cIAP1/2 promotes K48 poly-ubiquitination of TRAF3 and subsequent degradation. Removal of TRAF3 consequently stabilizes NIK resulting in its activation via auto-phosphorylation. Activated NIK phosphorylates IKK α , which in turn phosphorylates the p100 subunit of the NF- κ B dimer (VALLABHAPURAPU, KARIN, 2009). Phosphorylated p100 is recognized by the E3 ubiquitin ligase β -TrCP and processed into p52 via partial proteasomal degradation of the self-inhibiting ankyrin-repeat domains. The p52:RelB dimer can translocate into the nucleus where it is transcriptionally active. NIK stabilization has been shown to additionally induce NF- κ B activation via the canonical pathway (TEGOWSKI, BALDWIN, 2018; VALLABHAPURAPU, KARIN, 2009).

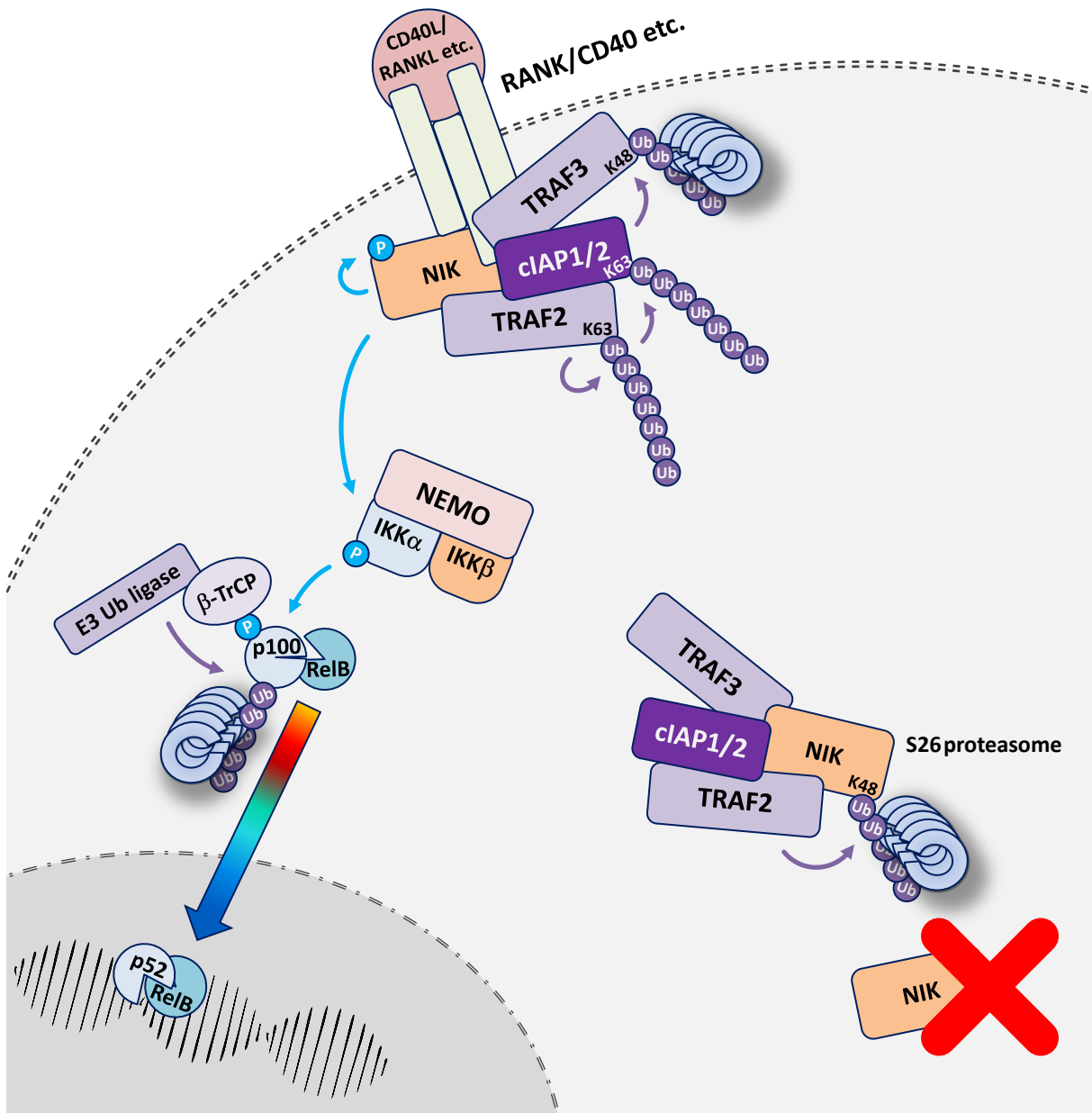


Figure 7 Non-canonical activation of NF-κB.

The non-canonical activation of NF-κB is detailed in the paragraph *Non-canonical NF-κB signaling pathway*. Small violet arrows indicate ubiquitination, while small blue arrows indicate phosphorylation. The big arrow colored yellow-to-blue indicates NF-κB activation via the mechanisms described before, including proteasomal degradation of IκB and nuclear translocation of the NF-κB subunits (Figure 5). The red cross indicates removal of the NIK protein.

3.5.4. Genotoxic stress-induced NF- κ B activation

While the canonical and alternative NF- κ B pathways are initiated by intra- and extracellular ligands binding to their appropriate receptors, the genotoxic stress-induced pathway is triggered entirely intracellularly. After recognition of DNA DSB via the cellular DDR mechanisms, NEMO undergoes a series of posttranslational modifications. The scaffolding protein for the IKK complex can dissociate from the kinases upon genotoxic stress and interact with importin 3 (IPO3) instigating nuclear import (HWANG et al., 2015; WANG et al., 2017b). This nuclear, IKK-free NEMO associates with p53-induced DEATH domain protein (PIDD) and RIP1 to form a heterotrimer that accumulates in the nucleus (COURTOIS, FAUVARQUE, 2018; MCCOOL, MIYAMOTO, 2012; WANG et al., 2017b; YANG et al., 2011). The NEMO:PIDD:RIP1 complex is joined by PARP-1. PARP-1 is a chromatin-associated enzyme acting as a DNA damage sensor and can be recruited to damage sites such as SSB and DSB (WANG et al., 2017b). The main function of PARP-1 is addition of PAR to itself and other proteins in a process called poly(ADP-ribosyl)ation (PARylation). Damage-associated PARP-1 auto-PARylates and dissociates from the lesion site (PASCAL, 2018; STILMANN et al., 2009). PARP-1 uses the PAR chain to anchor itself and protein inhibitor of activated STATy (PIASy) to the NEMO:PIDD:RIP1 complex. PIASy post-translationally modifies NEMO by addition of small ubiquitin like modifier 1 (SUMO) at K277 and K309, the binding sites for IKK, in a SUMO E3 ligating manner (COURTOIS, FAUVARQUE, 2018; HELLWEG, 2015; MCCOOL, MIYAMOTO, 2012). PARP-1 additionally PARylates activated ATM monomers thereby attaching it to the NEMO-associated complex (STILMANN et al., 2009). ATM, which has kinase activity for serine:glutamine structures, proceeds to specifically phosphorylate nuclear NEMO at S85 (WU et al., 2006). Phosphorylation at S85 is surmised to control mono-ubiquitination of NEMO at K277 and K309 in a cIAP-dependent manner. This post-translational modification presumably replaces the SUMOylation signal, a notion supported by the fact that cIAP binds to the same motif on NEMO as PIASy. The mono-ubiquitin signal at K277 and K309 has been shown to promote nuclear export of the ATM:NEMO complex (COURTOIS, FAUVARQUE, 2018; JIN et al., 2009; MCCOOL, MIYAMOTO, 2012; WANG et al., 2017b).

Cytoplasmic involvement of NEMO and IKK activation has been subject to discussion favoring different models of interaction. One model, Figure 8, focusses on the actions of the E3 ubiquitin ligase X-linked inhibitor of apoptosis (XIAP) and of ELKS, a protein rich in the amino acids glutamic acid (E), leucine (L), lysine (K) and serine (S). After the modified ATM:NEMO complex has left the nucleus, ELKS associates with the complex and is K63 poly-ubiquitinated by XIAP, which itself is associated with the TAK1:TAB2 complex. TAB2 of the TAK1 complex can bind the poly-ubiquitin chain, as well as the IKK:NEMO complex (COURTOIS, FAUVARQUE, 2018; MCCOOL, MIYAMOTO, 2012; WANG et al., 2017b; WU et al., 2010). As of now it is unknown by what mechanism XIAP and ELKS are brought in proximity for poly-ubiquitination.

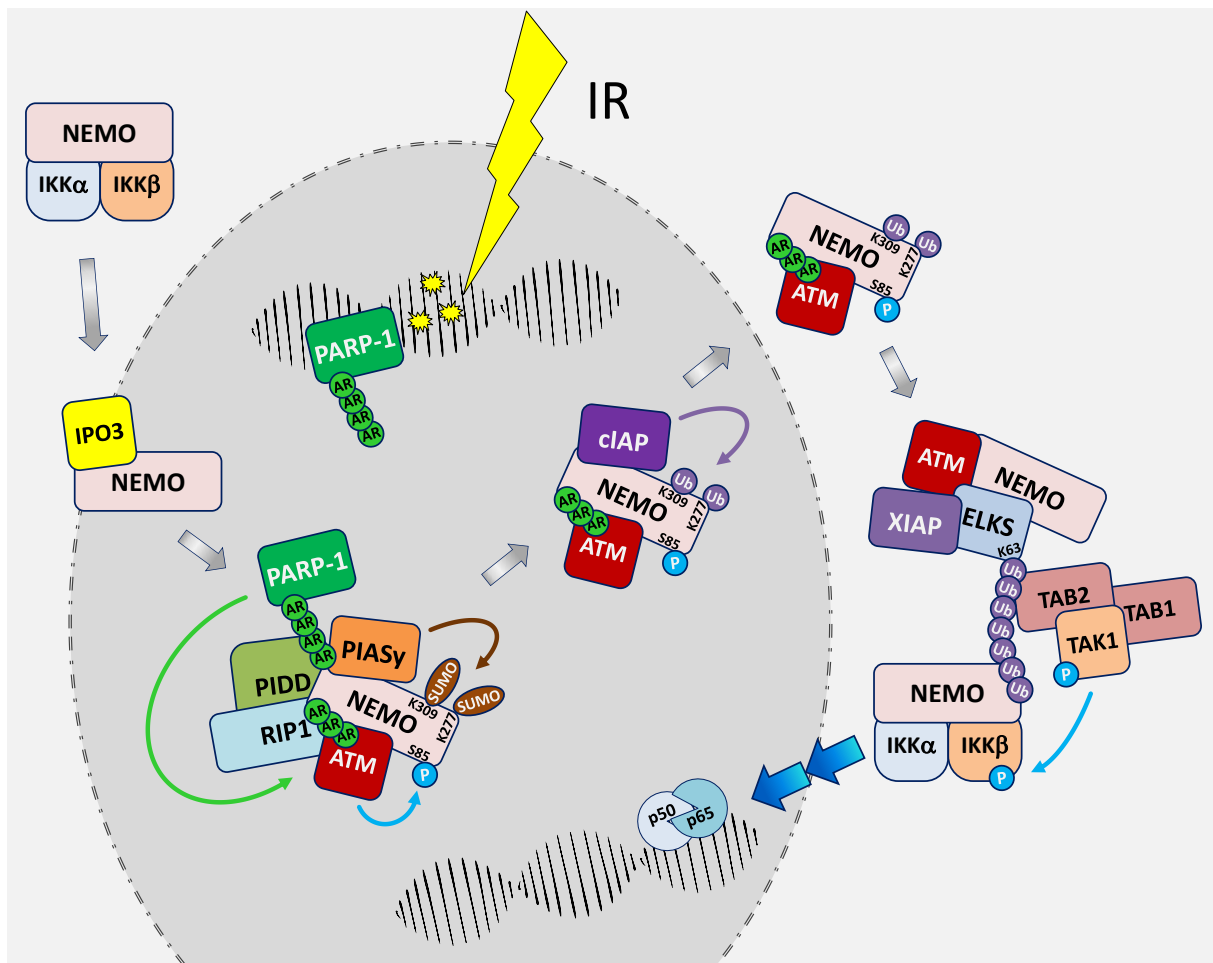


Figure 8 Genotoxic pathway of NF-κB activation – Model 1.

The activation of NF-κB in response to genotoxic stress is explained in detail in paragraph *Genotoxic stress-induced NF-κB activation*. The first model describes the intra-nuclear activity of NEMO independent of IKKα and IKKβ. The yellow polyangular shapes indicate DNA damage induced by ionizing radiation (IR, yellow lightning). Small green arrows indicate poly(ADP-ribosylation), small brown arrows indicate SUMOylation, small blue arrows indicate phosphorylation and small violet arrows indicate ubiquitination. The big silver arrow indicates the sequence of the steps undertaken by NEMO. The double blue-cyan arrows indicate NF-κB activation via the mechanisms described before, including proteasomal degradation of IκB and nuclear translocation of the NF-κB subunits (Figure 5). The mechanism visualized here is based on existing literature (COURTOIS, FAUVARQUE, 2018; HELLWEG, 2015; JIN et al., 2009; MCCOOL, MIYAMOTO, 2012; WANG et al., 2017b).

Another model, Figure 9, proposes involvement of cIAP and TRAF6 in the activation process of TAK1 (HINZ et al., 2010). Apart from forming the ATM:NEMO complex after DNA damage recognition, activated ATM can also exit the nucleus in a Ca²⁺-dependent manner without association to any other protein. This unbound, cytoplasmic ATM then proceeds to complex with TRAF6 triggering it to poly-ubiquitinate itself at K63. The poly-ubiquitin chain of the ATM:TRAF6 complex is used as an anchor for cIAP, the TAK1 complex via TAB2 and the IKK complex via NEMO. After association of this multi-complex, the E3 ubiquitin ligase cIAP adds a mono-ubiquitin signal to NEMO at K285 (HINZ et al.,

2010). Similar to canonical activation of IKK β the TAK1 complex phosphorylates IKK β leading to subsequent NF- κ B activation (BEGALLI et al., 2017; COURTOIS, FAUVARQUE, 2018; MCCOOL, MIYAMOTO, 2012; WANG et al., 2017b). In this model the role of the ATM:NEMO complex as a central mediator for the genotoxic NF- κ B pathway is disregarded, instead this model focuses on the calcium-mediated export of unbound ATM.

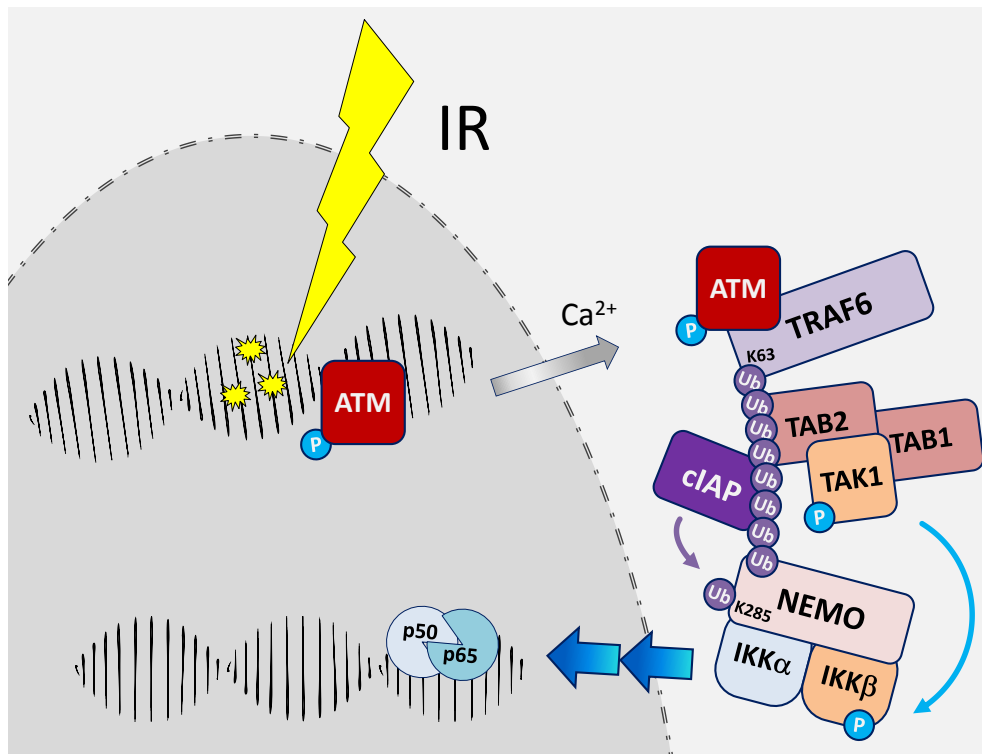


Figure 9 Genotoxic pathway of NF- κ B activation – Model 2.

The second model describes extranuclear activity of ATM. The yellow polyangular shapes indicate DNA damage induced by ionizing radiation (IR, yellow lightning). Small blue arrows indicate phosphorylation, while small violet arrows indicate ubiquitination. The big silver arrow indicates the nuclear export of ATM. The double blue-cyan arrows indicate NF- κ B activation via the mechanisms described before, including proteasomal degradation of I κ B and nuclear translocation of the NF- κ B subunits (Figure 5). For details, see text. The mechanism visualized here is based on existing literature (HINZ et al., 2010).

Other authors describe a model that tries to couple the previously described mechanisms of NEMO-associated IKK activation to cytoplasmic activity of RIP1, in addition to its nuclear role in facilitating SUMOylation of NEMO in assistance of PIDD, as depicted in Figure 10 (YANG et al., 2011). Nuclear RIP1 is SUMOylated by PIASy and is translocated out of the nucleus via an unknown mechanism in parallel to the ATM:NEMO complex. In the cytoplasm, RIP1 associates with the ATM:NEMO complex and is K63 poly-ubiquitinated either via ELKS:XIAP or TRAF6:cIAP (HINZ et al., 2010; WU et al., 2010).

The poly-ubiquitin chain enables TAB2-dependent binding of the TAK1:TAB2 complex and the subsequent phosphorylation of IKK β , engaging NF- κ B activation via the same follow-up mechanism as in the canonical pathway (COURTOIS, FAUVARQUE, 2018; MCCOOL, MIYAMOTO, 2012; YANG et al., 2011).

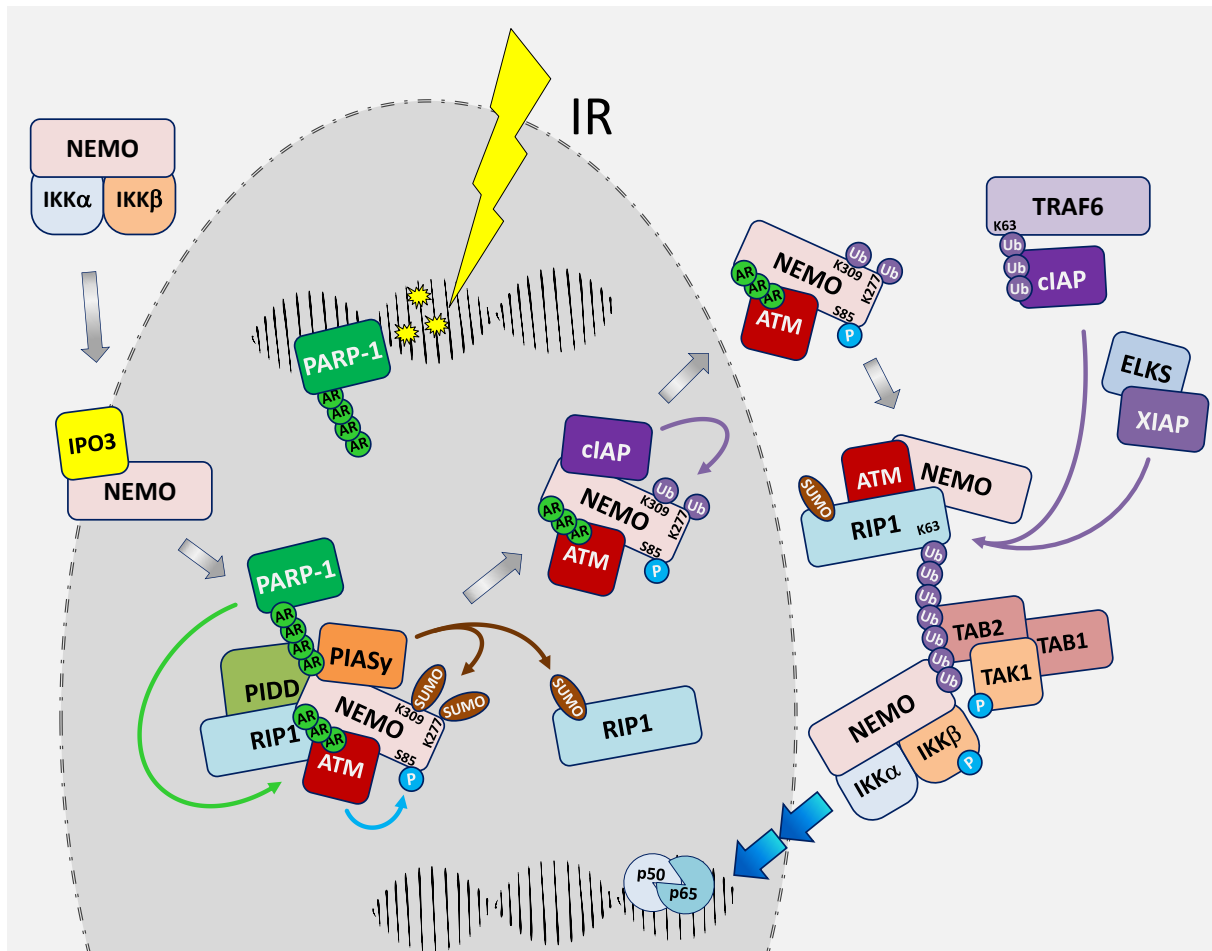


Figure 10 Genotoxic pathway of NF- κ B activation – Model 3.

The third model describes an alternative interaction of NEMO with SUMOylated RIP1. The yellow polyangular shapes indicate DNA damage induced by ionizing radiation (IR, yellow lightning). Small green arrows indicate poly(ADP-ribosylation), small brown arrows indicate SUMOylation, small blue arrows indicate phosphorylation and small violet arrows indicate ubiquitination. The big silver arrow indicates the sequence of the steps undertaken by NEMO. The double blue-cyan arrows indicate NF- κ B activation via the mechanisms described before, including proteasomal degradation of I κ B and nuclear translocation of the NF- κ B subunits (Figure 5). For details, see text. The mechanism visualized here is based on existing literature (COURTOIS, FAUVARQUE, 2018; HINZ et al., 2010; MCCOOL, MIYAMOTO, 2012; WU et al., 2010; YANG et al., 2011).

The described models may operate independently and in a cell type dependent manner. Although the mechanisms vary in their exact implementation, they all contribute to the hypothesis that the proteins ATM and NEMO play key roles in the activation of NF- κ B after detection of DNA damage.

Mainly, NEMO is described as a shuttle for damage-activated ATM to exit the nucleus. In the cytoplasm, ATM activates processes that bring poly-ubiquitin chains to the complex that can anchor the TAK1:TAB2 complex via TAB2 as well as the IKK complex via its associated NEMO. TAK1 then proceeds to activate IKK β leading to canonical I κ B phosphorylation and degradation, permitting NF- κ B nuclear translocation. Although not yet discussed in the literature, the varying processes initiated by ATM might occur in parallel, creating an ATM:ELKS:RIP1:TRAF6 complex with multiple anchors for TAB2, thereby enabling increased recruitment of the TAK1 complex. The resulting signal amplification could lead to prolonged NF- κ B activation. In favor of this idea is a comment by Yang et al. regarding a more sustained NF- κ B response via the genotoxic pathway compared to canonical activation (YANG et al., 2011).

3.6. The radiation-induced bystander effect

The radiation-induced bystander effects (RIBE) are characterized as the induction of cellular consequences in response to IR exposure concerning non-irradiated cells by means of intercellular communication. Besides intracellular regulation of cell cycle and cell fate, radiation-induced DDR includes the activation of signaling cascades that result in intercellular transfer of signal transmitters and damaging factors. In non-irradiated cells, the effects of radiation-stimulated communication range from the activation of intracellular signaling pathways and gene expression to the induction of DNA damage, chromosomal aberrations, cell death and oncogenic transformation. RIBE are considered to amplify and propagate the bystander signal in order to recruit immune cells for the initiation of damaged cell removal. In other instances, signaling initiated by RIBE produces responses in bystander cells that alleviate the symptoms of radiation injury in directly irradiated cells, a phenomenon called the rescue effect. The rescue effect manifests as a higher survival, better repair of DNA damage and radioresistance. RIBE can be similar to the consequences of direct radiation exposure and uses the same response mechanisms of cellular stress (ABRAMOWICZ et al., 2019; BRYANT et al., 2019; CHEN et al., 2011; DESAI et al., 2014; DIEGELER, HELLWEG, 2017; JELLA et al., 2018; KARTHIK et al., 2019; NAJAFI et al., 2014; TU et al., 2019; YU, 2019).

Factors facilitating RIBE traverse to other cells in a direct manner via gap junctions or are secreted in to the cellular microenvironment, where they are subsequently taken up by bystander cells in a paracrine manner (AUTSAVAPROMPORN et al., 2017; DIEGELER, HELLWEG, 2017; FARHOOD et al., 2019).

3.6.1. Gap-junctional transfer of RIBE-inducing factors

Cytoplasmic molecules that traverse to neighboring cells may use gap junctions that physically connect cells. Gap junctions are pores in the cell membrane that are generated by assembly of two hemichannels of connexin complexes. The connexin family of proteins consists of several isoforms that can complex into hexameric structures to form a connexin hemichannel. The resulting connexin channel permits transmission of signaling molecules like nitric oxide (NO), ROS and microRNAs (miRNA) thereby allowing communication between cells (AUTSAVAPROMPORN et al., 2017; AUTSAVAPROMPORN et al., 2013; AZZAM et al., 2003; DE TOLEDO et al., 2017; HEI et al., 2008; TOMITA et al., 2015).

3.6.2. Induction of RIBE via secreted soluble factors

Radiation-induced signaling promotes the production and secretion of soluble factors that initiate a humoral response in an auto-, para- and endocrine manner. The endocrine and immune associated induction of RIBE, termed abscopal effect, is observed *in vivo* in tissues far from the irradiated site and offers alternatives for treatment plans in radiation therapy involving a stimulated immune

response (DIEGELER, HELLWEG, 2017; FERNANDEZ-PALOMO et al., 2016; HABETS et al., 2016). Among the soluble factors are cytokines, chemokines and damage-associated molecular patterns (DAMP). They can bind to surface receptors of both irradiated and non-irradiated cells and incite signaling cascades like the canonical activation of the NF- κ B pathway and the MAPK signaling pathway (DIEGELER, HELLWEG, 2017; HEI et al., 2008). In addition to humoral signaling, secreted extracellular vesicles including exosomes represent another class of communicative mediator for RIBE. Extracellular vesicles are small membrane-enclosed vesicles that can contain lipids, proteins, RNA and DNA including DAMPS, miRNA, messenger RNA and non-coding RNA. The composition is highly dependent on the secreting cell type and the manner of stimulation. IR has been shown to increase extracellular vesicle secretion and to modulate their composition (ABRAMOWICZ et al., 2019; DIEGELER, HELLWEG, 2017; FARHOOD et al., 2019; MAIA et al., 2018; MO et al., 2018; SZATMARI et al., 2019). Furthermore, miRNA such as miR-34c and miR-1246 contribute to DNA damage in bystander cells via ROS induction and repression of Ligase 4 activity (MO et al., 2018; RASTOGI et al., 2018).

3.6.3. Amplification and propagation of bystander signals

Essential for propagation of bystander-related signaling is the establishment of positive feedback loops that lead to the production of signaling factors promoting the activation of further signaling pathways in a time-dependent manner. The radiation-induced expression of cytokines such as IL-1, IL-6, IL-8 and TNF- α can lead to the canonical activation of the NF- κ B signaling pathway. Target genes of NF- κ B include IL-1, IL-8 and TNF- α , the same cytokines that initiate NF- κ B activation. The continued activation of NF- κ B creates a paracrine feedback loop in bystander cells that propagates the radiation signal. The intercellular signaling incited by the secreted cytokines additionally acts as autocrine amplification for the irradiated cell and also at any downstream activated cell. The amplification leads to a prolonged expression of the signaling factors, thereby strengthening the initial signal impulse of the irradiated cell and retention of subsequent bystander signaling. The radiation-induced production of DAMPs such as the high mobility group box 1 (HMGB1) protein, and oxidized and free DNA can promote TLR-dependent activation of the MAPK and signal transducer and activator of transcription (STAT) pathways in addition to NF- κ B (DIEGELER, HELLWEG, 2017; FARHOOD et al., 2019; HEI et al., 2011; HEI et al., 2008; JELLA et al., 2018).

3.6.4. Cellular consequences of the radiation-induced bystander response

The effects of radiation-induced signaling in bystander cells have been shown to be of detrimental nature. In the first discovery of RIBE, sister chromatid exchanges were observed in 30 % of all cells although less than 1 % of the cell nuclei were irradiated (NAGASAWA, LITTLE, 1992). Since then, the formation of micronuclei, senescence induction, DNA damage, mutations, reduced cellular survival, genetic instability and oncogenic transformation in bystander cells have been attributed to RIBE (AUTSAVAPROMPORN et al., 2013; BRYANT et al., 2019; BUONANNO et al., 2011a; BURDAK-ROTHKAMM et al., 2008; FARHOOD et al., 2019; HAGELSTROM et al., 2008; HAMADA et al., 2007; HEI et al., 2004; KOBAYASHI et al., 2017; LEWIS et al., 2001; MLADENOV et al., 2018; MO et al., 2018; POLESZCZUK et al., 2015; PRISE et al., 2003; RASTOGI et al., 2018; SHAREEF et al., 2007; SOKOLOV et al., 2005; SPRUNG et al., 2015; SUZUKI, TSURUOKA, 2004; WIDEL et al., 2015; YANG et al., 2015; ZHAO et al., 2015). A variety of factors have been found to directly mediate these adverse RIBE including oxidative stress and miRNA-induced DNA damage (BUONANNO et al., 2011b; JELLA et al., 2018; KOBAYASHI, KONISHI, 2018; MO et al., 2018; RASTOGI et al., 2018; SAWAL et al., 2017; SHAO et al., 2003). Mechanistic studies imply involvement of ROS regulators such as cyclooxygenase 2 (COX-2) and inducible nitric oxide synthase (iNOS), DNA repair and DDR factors such as DNA-PKcs and ATM and modulation of NF- κ B and MAPK signaling pathways in the regulation of the bystander response (ARAVINDAN et al., 2014; CHAI et al., 2013; FARDID et al., 2017; FARHOOD et al., 2019; HEI, 2006; SAWAL et al., 2017; TU et al., 2019; TU et al., 2016; YU et al., 2017).

3.7. Aim of this thesis

Intercellular communication between irradiated tumor cells and the healthy tissue surrounding the target is an important aspect of radiation therapy. Investigation of these cell-to-cell interactions is not only a chance to understand tumor progression but also to support current therapeutic approaches. Deeper knowledge of non-targeted responses to IR can help in finding new strategies for tumor eradication by identifying new targets for medication and control the radiation-induced immune response.

The complete mechanism of RIBE induction is not yet fully understood but the vast potential for intracellular regulation, immune response modulation and intercellular signaling make the transcription factor NF- κ B and its downstream targets key mediators for the radiation-induced bystander response.

The aim of this work was to analyze and compare the cellular response to IR and RIBE of wildtype murine embryonic fibroblast (MEF wt) and MEF NEMO knock-out (NEMO ko) cells.

The hypothesis is that NEMO-deficiency in MEF cells, which results in a dysfunctional NF- κ B pathway, provides an ideal model system to study involvement of NF- κ B in RIBE. Cellular radiation and bystander responses were induced by exposure of MEF wt and NEMO ko cells to X-rays and treatment of the cells with medium conditioned by X-irradiated cells (bystander treatment).

To this end, the following endpoints were assessed after X-rays exposure and bystander treatment:

- The ability to form clonogenic colonies to elucidate role of NF- κ B in cellular survivability.
- The activity of β -galactosidase to demonstrate the induction of premature stress-induced senescence as an alternative to cellular demise.
- The distribution of cells in the cell cycle phases to observe the induction of cell cycle arrest as part of DNA damage repair.
- The kinetics of γ H2AX occurrence as a marker for DNA DSB and their repair as a function of time.

4. Material and Methods

4.1. Cell culture

4.1.1. Cell lines

MEF wt and MEF with a knock-out of the NEMO gene were used in this work to analyze the role of NF- κ B in radiation-induced bystander response. MEF NEMO ko cells were isolated from NEMO knock-out C57BL/6 female mice generated by crossing heterozygous NEMO^{+/-} mice (SCHMIDT-SUPPRIAN et al., 2000). Upon stimulation with TNF, IL-1 β and LPS, these NEMO deficient cells showed no NF- κ B DNA binding activity, no I κ B α degradation and no secretion of IL-6 and TNF- α (SCHMIDT-SUPPRIAN et al., 2000). Therefore, the NF- κ B pathway in MEF NEMO ko cells cannot be activated via the classical way and they can be used to elucidate the role of NF- κ B in cellular responses to radiation and other stressors.

4.1.2. Cell culture

Cells were cultured in 80 cm² culture flasks (Labsolute®, Th. Geyer, Renningen, Germany) in Alpha MEM Eagle medium (PAN Biotech, Aidenbach, Germany) supplemented with 10 % (v/v) fetal bovine serum (FBS; Biochrom AG, Berlin, Germany) and other supplements (see Table 1), under standard conditions (37 °C, 5 % CO₂, humid atmosphere).

Table 1 Cell culture medium supplements

Supplement	Concentration	Distribution
Penicillin	100 Units/ml	PAN Biotech, Aidenbach, Germany
Streptomycin	100 μ g/ml	PAN Biotech
Amphotericin B	2.5 μ g/ml	PAN Biotech
Neomycin	100 μ g/ml	PAN Biotech
Bacitracin	25 Units/ml	Sigma Aldrich, Steinheim, Germany
L-glutamine	2 mmol/l	PAN Biotech
Glucose	5.5 mmol/l	Merck, Darmstadt, Germany

For sub-cultivation, cells were washed with phosphate-buffered saline (PBS, Table 2), detached from the culture vessel using 0.05 % trypsin and 0.02 % ethylenediaminetetraacetic acid (EDTA, PAN Biotech), counted using a Luna™ Automated cell counter (logos Biosystems, Anyang-si, Korea) and seeded at a density of 3×10^3 cells/cm².

4.1.3. Cryoconservation and thawing of cells

For long term storage, the cells were detached from the culture flasks and resuspended in culture medium at a concentration of 2×10^6 cells / ml. In order to protect the cells from freezing-associated ruptures, the culture medium was supplemented with 10 % dimethyl sulfoxide (DMSO). Due to the organic solvent, the culture medium freezes as an amorphous ice crystal, thereby preserving the cells without additional stress. The cells were then placed at -80 °C in a freezing container (Nalgene Mr. Frosty, Thermo Fisher Scientific, Waltham, USA), which permits a slow cooling rate of 1 °C per minute. After 24 h, the frozen samples were placed in liquid nitrogen for long term storage.

After retrieval of the frozen samples, the cell suspension was slowly thawed and resuspended with 4 °C-cold culture medium in a 80 cm² culture flask. The cells are placed under standard culture conditions to attach and recuperate. Not all cells survived the thawing procedure, so the culture medium containing dead cells and residual DMSO was refreshed after 24 h.

Table 2 Composition of phosphate-buffered saline (PBS)

Phosphate buffered saline (PBS)	Concentration in ddH ₂ O
NaCl	137 mmol/l
KCl	2.3 mmol/l
Na ₂ HPO ₄ × 7 H ₂ O	4.3 mmol/l
KH ₂ PO ₄	1.4 mmol/l
pH	7.4

4.2. Treatment conditions

4.2.1. Addition of NF-κB activators and senescence inducers

For positive controls of NF-κB activation, cells were treated with recombinant mouse TNF-α or LPS in culture medium. In order to induce senescence, cells were treated with etoposide (Table 3). The topoisomerase II inhibitor etoposide can induce DNA DSB that lead to a permanent cell cycle arrest (NAGANO et al., 2016; SUN et al., 2017; YANG et al., 2017a).

Table 3 NF-κB activators and senescence inducers

Substance	Working concentration	Stock concentration	Solvent	Distribution
murine TNF-α	20 ng/ml	100 ng/μl	H ₂ O	Sigma Aldrich
LPS (<i>E. coli</i> O111:B4)	2 μg/ml	1 mg/ml	H ₂ O	Sigma Aldrich
Etoposide	12.5 μmol/l	50 mmol/l	DMSO	Cell Signaling, Danvers, USA

4.2.2. Irradiation and medium conditioning

For irradiation, cells were seeded in petri dishes ($\varnothing = 3$ cm, Labsolute[®], Th. Geyer) and were grown to 50 % confluency. Cells were exposed to different doses of X-rays (200 kV, 15 mA) generated by a Gulmay RS225 X-ray cabinet (X-Strahl, Surrey, GB) at a constant dose rate of 1 Gy/min at room temperature. Soft X-rays were removed using a 0.5 mm copper (Cu) filter, to reduce energy loss in the medium. Doses were determined using the UNIDOS^{webline} with an ionization chamber type TM30013 (PTW, Freiburg, Germany). Immediately after X-rays exposure, medium was refreshed to reduce effects of ROS produced in the cell culture medium by radiolysis of water.

For the induction of bystander effects, fresh medium was incubated with irradiated cells for 24 h in order to accumulate soluble factors secreted by the irradiated cells in response to X-rays exposure. The conditioned medium was filtered (Sartorius Minisart syringe filter with 5 μ m pore size, Sigma Aldrich) to avoid transfer of irradiated cells that may have detached from the irradiated culture and transferred onto untreated cells for the duration of the experiment.

4.3. Fluorescence-based assays

Fluorescence can be used in molecular biology to visualize or otherwise detect other molecules such as proteins, lipids or nucleic acids. Fluorophores are exposed to light of a certain wavelength. The electrons of the fluorophore are excited by the energy of the source light, raising the energy state for a short amount of time. Returning to the ground energy state, the electrons emit the excess energy as light of a wavelength that is longer than the wavelength of the excitation light (Stokes shift). This emitted light can be detected.

4.3.1. Immunofluorescence staining

Immunofluorescence staining is an established method to visualize intracellular structures, and the presence and abundance of proteins. Mostly, antibodies are used to bind to the proteins in question. A secondary antibody, coupled to a fluorophore, is subsequently used to bind to the primary antibody and enables detection of fluorescence localized to the protein in question.

Cells were seeded on glass coverslips (\varnothing 10 mm, Menzel-Gläser, Thermo Fisher Scientific, Waltham, USA) and grown to 50 % density. The seeded cells were then treated according to the experimental setup with either X-rays, conditioned medium, TNF- α or LPS. At certain time points of the experiment, cells on glass cover slips were fixed with 3.5 % formaldehyde in a Tris-buffered saline solution containing Tween-20 (TBST, Table 4) for 10 min at 4 °C.

Table 4 Composition of Tris-buffered saline with Tween-20 (TBST)

Tris-buffered saline with Tween-20 (TBST)	Concentration in ddH ₂ O
NaCl	150 mmol/l
Tris	50 mmol/l
Tween-20	0.05 % (v/v)
pH	7.5

Fixed cells were washed by rinsing the sample three times with TBST and swaying for 5 min on a tumbling mixer before the last aspiration. The cells were then permeabilized with TBST containing 1 % bovine serum albumin (BSA, Sigma Aldrich) and 0.05 % Triton X-100 (Sigma Aldrich) for 20 min at 4 °C. Permeabilized cells were incubated with the primary antibody diluted in Antibody Diluent (Zytomed Systems, Berlin, Germany) for 45 min at room temperature in a wet chamber to avoid evaporation of antibody solution and drying of the sample. Antibody Diluent was used to efficiently block unspecific binding sites during staining. After staining with the primary antibody, cells were washed and then incubated with the secondary antibody diluted in Antibody Diluent for 45 min at room temperature in the dark. Afterwards, cells were washed 3 times with TBST and incubated with 0.05 µg/ml DAPI (4',6-Diamidin-2-phenylindol, Table 5) diluted in Antibody Diluent for 10 min at room temperature. Cells were washed and the coverslips were placed onto a glass slide (VWR International, Darmstadt, Germany) with mounting medium (DAKO, Carpinteria, USA). Samples were analyzed via fluorescence microscopy using a Zeiss Axio Imager.M2 fluorescence microscope (Carl Zeiss AG, Ulm, Germany). Fluorescence was excited using a HPX-R120 mercury short arc reflector lamp (JENA GmbH, Jena, Germany) as light source and captured after application of Zeiss fluorescence filter sets 38 (BP 525/50 nm), 43 (BP 605/70 nm) and 49 (BP 445/50 nm). Images were produced using the Zeiss AxioCam MRm camera and processed using the Zeiss AxioVision40 V4.8.2 software.

Table 5 Specifications of DAPI

DAPI	
$\lambda_{\text{Excitation}}$	358 nm
$\lambda_{\text{Emission}}$	461 nm
Distribution	Sigma Aldrich
Working concentration	0.05 $\mu\text{g/ml}$

4.3.1.1. *NF- κ B activation*

For assessment of NF- κ B activation, nuclear translocation of NF- κ B subunit p65 was determined using a primary antibody against p65 and a secondary antibody coupled to the Alexa Fluor 488 (AF488) fluorophore (Table 6). The cell nucleus was visualized by DAPI staining. Kinetics of p65 translocation were determined using cells treated with 8 Gy X-rays. The incubation time identified for maximal translocation was used in the following experiments. For control of signal intensity, cells were treated with 2 $\mu\text{g/ml}$ LPS (*E. coli* O111:B4) and 20 ng/ml murine TNF- α (Table 3). Exposure time for microphotography was kept constant during the experiment.

Table 6 Antibodies for p65 immunofluorescence staining

Antibodies	Primary	Secondary
Epitope / Fluorophore	NF- κ B subunit p65	IgG / Alexa Fluor 488
Target species	Mouse / Human	Rabbit
Host species	Rabbit monoclonal, clone: E379	Goat polyclonal
$\lambda_{\text{Excitation}}$		495 nm
$\lambda_{\text{Emission}}$		519 nm
Distribution	Abcam, Cambridge, GB	Thermo Fisher Scientific, Waltham, USA
Dilution	1 : 150	1 : 1000

4.3.1.2. *DNA damage*

For the detection of γ H2AX as a marker of the cellular response to DNA DSB, a primary antibody against human H2AX phosphorylated at serine 139 was used (Table 7). The antibody has been shown to detect γ H2AX foci also in MEF cells (BOGLIOLO et al., 2007). A secondary antibody coupled to the northern lights 557 (NL557) fluorophore was applied for detection of the primary antibody (Table 7). DAPI staining was used for visualization of cell nuclei. The microphotography exposure time for γ H2AX and nucleus detection was determined using a positive control of cells exposed to 2 Gy X-rays and kept constant for every other experimental condition.

Table 7 Antibodies for γ H2AX immunofluorescence staining

Antibodies	Primary	Secondary
Epitope / Fluorophore	H2AX phosphorylated at Serine 139	IgG / Northern Lights 557
Target species	Human	Rabbit
Host species	Rabbit	Donkey
$\lambda_{\text{Excitation}}$		557 nm
$\lambda_{\text{Emission}}$		574 nm
Distribution	R&D systems, Minneapolis, USA	R&D systems
Dilution	1 : 150	1 : 300

4.3.2. Fluorescence image analysis

For the evaluation of fluorescence microscopic images, the Zeiss image analysis software ZEN 2.5 blue edition was used. The images were taken in two channels, the DAPI channel that shows the cell nuclei and a channel for the fluorochrome of the secondary antibody. The primary tool of the analysis software “image analysis” uses sequential application of sub-tools. The sub-tool “automated segmentation” creates gates that can be separately analyzed. The sub-tool “count” can numerically assess the number of gates, while the sub-tool “intensity mean of channel” measures signal intensities of a selected channel within the gates.

For the analysis of p65 nuclear translocation, the location of p65 within the cell was visualized in the AF488 channel. The “automated segmentation” allows determination of the nucleus area using an intensity threshold in the DAPI channel. The mean fluorescence intensity in the AF488 channel was then measured within the nucleus gate in order to determine the amount of p65 translocated into the nucleus. For relative assessment of p65 translocation, the signal intensities within the nucleus were compared between treated and untreated cells.

For γ H2AX foci detection, the nucleus area was delineated as before and the number of γ H2AX foci within the nucleus was quantified automatically. An “automated segmentation” using an intensity threshold in the NL557 channel enabled numerical assessment of γ H2AX foci within the nucleus. The threshold was set for each experiment separately using images of cells exposed to 2 Gy X-rays as a reference. The absolute numbers of γ H2AX foci in cell nuclei exposed to different doses of X-rays or conditioned medium were compared to their respective untreated controls. For statistical accuracy, conditions with less than 800 analyzed cell nuclei were not taken into consideration.

4.3.3. Flow cytometry

With flow cytometry large quantities of cells stained with fluorescent dyes or immunofluorescent probes can be rapidly analyzed and sorted. The flow cytometer retrieves cells from a sample and applies a fluid at distinct pressure to create a sheath around the cells aligning them in single file. This single file of cells is drawn into the flow cytometer and passed through a series of lasers of certain wavelength to excite the fluorophores. With the help of an argon-laser at $\lambda = 488$ nm, the cellular size (forward scatter, FSC) and internal complexity (side scatter, SSC) are assessed to yield information on the cells independent of any staining. The detector for FSC is placed at 180° to the laser origin and detects the light scattered from the cell surface, indicating the relative size of the measured particle. The detector for the SSC is placed at 90° to the laser at the level of the cell stream and detects light reflected from internal structures of the measured particle. Since not only cells but also any kind of debris and salt crystals are measured, the FSC and SSC measurements are used to distinguish between cells and non-cellular particles as well as different populations of cells based on size and complexity. Fluorescent signals emitted by dyes or conjugated antibodies are measured with a detector placed at 90° to the laser, same as the SSC. Using dichroic mirrors, light of a distinct wavelength is filtered to the fluorescence detectors whilst the rest is reflected toward the SSC detector. The filtered light detected in the respective channel gives a measure of the relative amount of fluorochrome-coupled antibodies or dyes bound to the target structure, thereby enabling a quantitative assumption about e.g. the total DNA content and the expression status of proteins.

4.3.3.1. Cell cycle analysis

The distribution of cells in different phases of the cell cycle is determined by assessing the total DNA content of single cells. The DNA content correlates to the cell cycle phase, featuring cells in G1-phase with chromosomes consisting of single chromatids, cells in G2/M-phase with a double set of chromatids, cells in S-phase with an intermittent amount of DNA and cells in sub-G1 phase with less DNA than G1 cells. The cells are stained with DNA intercalating fluorescent dyes like propidium iodide (PI, Table 8) or DAPI and are assessed via flow cytometry. Different approaches have specific advantages and disadvantages. The spectral excitation range of PI allows for the use of machines with only an argon laser. The PI staining itself requires RNA digestion prior to application of the dye, as the dye can bind single-stranded nucleic acids. Therefore the sample needs to be fixed in -20°C ethanol to allow for modification of intracellular structures post-fixation. DAPI can be used on formaldehyde-fixed cells as it only binds to double-stranded DNA but the spectral excitation range of DAPI requires a flow cytometer with a violet laser diode at $\lambda = 405$ nm (TELFORD, 2011). For technical reasons, the detection of stained DNA necessitated the use of single-laser measurements; therefore PI staining of ethanol-fixed samples was performed.

Table 8 Specifications of propidium iodide

Propidium iodide	
$\lambda_{\text{Excitation}}$	535 nm
$\lambda_{\text{Emission}}$	617 nm
Distribution	Sigma Aldrich
Working concentration	2.5 $\mu\text{g/ml}$

Cells were seeded in petri dishes ($\varnothing = 3$ cm, Th. Geyer) and grown to 50 % density. The seeded cells were then treated according to the experimental setup with either X-rays or conditioned medium (see *Treatment conditions*). After addition of fresh (X-rays) or conditioned medium, the cells were incubated for different periods of time. Subsequent to the incubation, the cells were detached with trypsin/EDTA and fixed in -20 °C ethanol (final concentration 70 %) for 24 h. The ethanol was then diluted with PBS and cells were centrifuged at 500 g. Cells were treated with 20 Units/ml RNase as well as 1 % (v/v) Triton X-100 and stained with 2.5 $\mu\text{g/ml}$ PI in PBS for 60 min. Without removing excess PI from the cell suspension, the cells were measured in the flow cytometer FACScan (BD Biosciences, Franklin Lakes, USA). The fluorescence of PI was detected after passing through a 585/42 nm bandpass filter. The Flowing Software 2.5.1 (created by Perttu Terho, Turku Centre for Biotechnology, Finland) (SAHRANESHIN SAMANI et al., 2014) was used to analyze the data. After selecting the cell population in a dot plot of FSC and SSC (Figure 11 A), the population was screened for cell aggregates that would disrupt the single cell based assessment of the DNA content. An accumulation of two cells in G1-phase that is measured as one single event has the same light intensity as one cell in G2/M-phase and would therefore give a wrong result. Cell aggregates were detected by measuring the width of the PI fluorescence signal for each event and displaying it in relation to the area of the fluorescence peak (Figure 11 B). After removing cell aggregates such as doublets from the measurement, the PI intensity of single cells was assessed. The resulting histogram shows the cell cycle distribution of the measured cell population. In untreated, slowly proliferating cells such as MEF, most of the cells are in G1-phase depicted by a large peak of a set intensity. A second smaller peak at twice the intensity of the G1 peak contains cells in G2/M-phase. Cells between those two peaks can be in S-phase. The absolute intensity is irrelevant for mention, as the cells of the population are normalized to the total cell number in each experiment.

The distribution of the fluorescence intensity of the cells followed a Gaussian distribution in all phases, and was calculated using the peak height and width. Thereby the fractions of cells within G1- and G2/M-phase were accurately determined. The fraction of cells in S-phase was extrapolated by subtraction of the number of cells in G1- and G2/M-phase from the total cell number (Figure 12). Cells in sub-G1 phase are noticeable as a peak with a lower intensity than G1 cells.

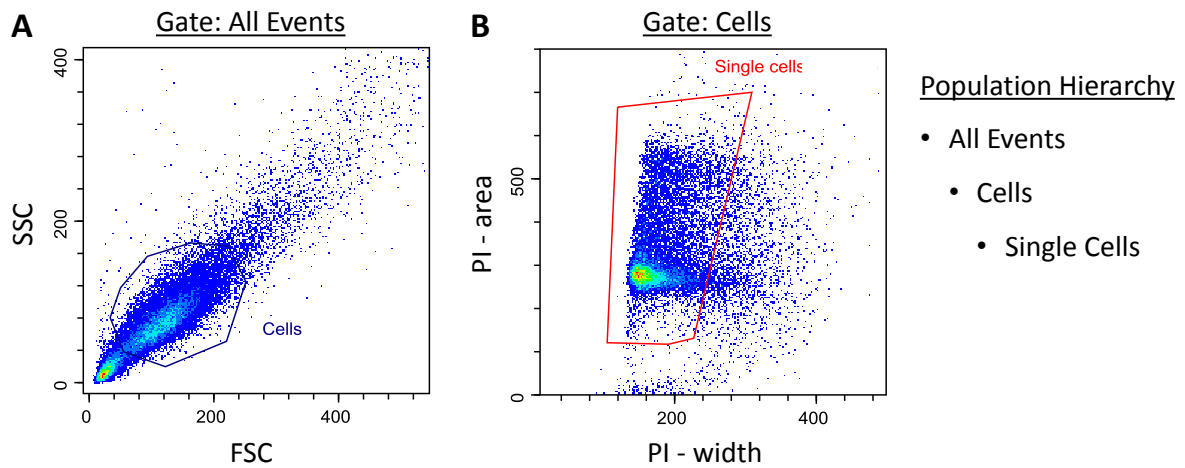


Figure 11 Gating scheme for cell cycle analysis

In flow cytometry, cells can be determined by physical parameters such as their relative size and internal complexity or by labeling cell specific constituents with fluorescent labels. For assessing the cell cycle progression, cells were stained with propidium iodide (PI). At first all measured events of the sample in question are depicted collectively in a dot-plot that gives information of the relative size (FSC) or the internal complexity (SSC). The dot plot (A) shows a population of events with similar size and complexity that can be assumed to be the cellular component of the sample (Gate: Cells). A population of smaller size and complexity is commonly expected to consist of cellular debris and medium impurities such as salts or unbound fluorescent particles. The flow cytometric cell cycle analysis quantifies the amount of stained DNA in each measured cell. Therefore, a dot plot showing the previously gated cellular portion of the sample (B) is used to consider the fluorescent signal of PI. The axes of the dot plot show the relative area of the fluorescent signal as well as the relative width of the signal. Two or more agglomerated cells will present the sum of their signal intensities but also a size-dependently increased signal width as the cell cluster takes longer to pass through the laser of the flow cytometer compared to single cells. The dot plot shows a population that is spread out on both axes. The spread along the area-axis shows the cell cycle progression of the measured cells, while the spread on the width-axis shows aggregation of cells. For the final evaluation of the cell cycle phases only single cells were considered (Gate: Single cells).

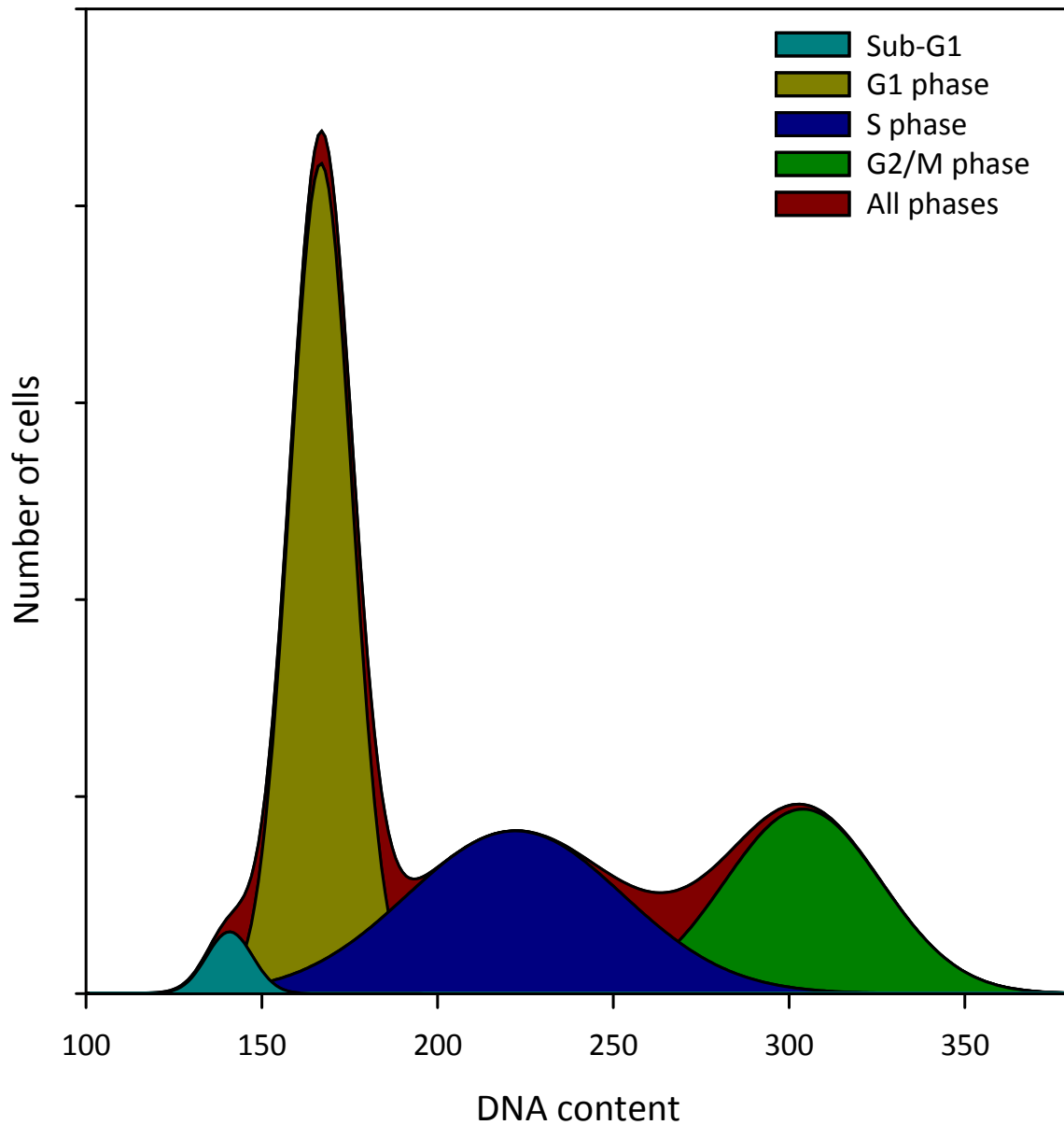


Figure 12 Histogram of DNA content

The cell cycle phases of single cells displayed in a histogram show the amount of cells at a signal intensity that directly corresponds to the relative DNA content of the cell. The distribution pattern of the separate phases is Gaussian and can be mathematically derived from the fluorescence histogram of all single cells (red). The sub-G1 phase (cyan) is noticeable in the total curve as an irregularity of the first peak of the total curve. This first peak corresponds to the G1-phase (golden) and makes up most of the cell population in untreated cells. The S-phase (blue) is the second discernable peak of the total curve and has a broad base as it consists of all intermediate DNA contents between G1- and G2/M-phase. The last peak, the G2/M-phase (green), shows cells with twice the amount of DNA than G1-cells.

4.4. Cellular senescence

4.4.1. β -galactosidase assay

Cells outside of the cell cycle, living yet not proliferating, can show signs of cellular senescence. The most widely used senescence biomarker is senescence-associated- β -galactosidase activity (DEBACQ-CHAINIAUX et al., 2009). Under non-senescent conditions lysosomal β -galactosidase activity is measured at acidic pH of 4.5. A cell undergoing replicative or induced senescence shows increased lysosome number and function, represented by increased β -galactosidase activity, that is detectable at a pH of 6.0 (LEE et al., 2006). The cytochemical conversion of the chromogenic β -galactosidase substrate 5-bromo-4-chloro-3-indoyl- β -D-galactopyranoside (X-gal) to an insoluble blue compound in a citric acid/sodium phosphate buffer at pH 6.0 allows bright-field microscopic detection of senescent cells (DEBACQ-CHAINIAUX et al., 2009).

Cells were seeded in petri dishes ($\emptyset = 3$ cm, Th. Geyer) at a density of 1×10^2 cells/cm² and allowed to settle down for 24 h. Due to long recovery times necessary to ascertain senescence induction, a low seeding density was chosen in order to prevent overgrowth of the cells.

According to the experimental setup, the cells were then either treated with 12.5 μ mol/l DNA damaging anti-cancer drug etoposide (LEONTIEVA et al., 2012; NAGANO et al., 2016), with conditioned medium, or cells were directly X-irradiated according to the *Treatment conditions*. Cells received fresh medium 24 h after the etoposide/conditioned medium treatment or directly after X-irradiation. After a recovery period of 6 days, senescent cells were detected using a senescence-associated β -galactosidase staining kit (Cell Signaling). After aspiration of culture medium and washing with PBS, cells were treated with the fixative solution included in the staining kit for 15 min at room temperature. The fixed cells were washed with PBS and then stained at 37 °C for 24 h with an X-gal staining solution provided in the kit. Pictures of stained cells were obtained using a 20 \times magnification in bright-field on a Zeiss Axiovert inverse microscope with the AxioCam Mrc5 camera using the Zeiss AxioVision40 V4.5.0.0 software.

Since senescent cells can be detected via a blue coloration of the cellular corpus, each image was assessed for the parameters cell confluency and blue coloration. The confluency was determined using the PHANTAST ImageJ macro (JACCARD et al., 2014). For blue coloration, a color threshold was used to isolate pixels with a hue of 99° to 240° (Figure 13), corresponding to a green to blue color (LOGVINENKO, 2015).

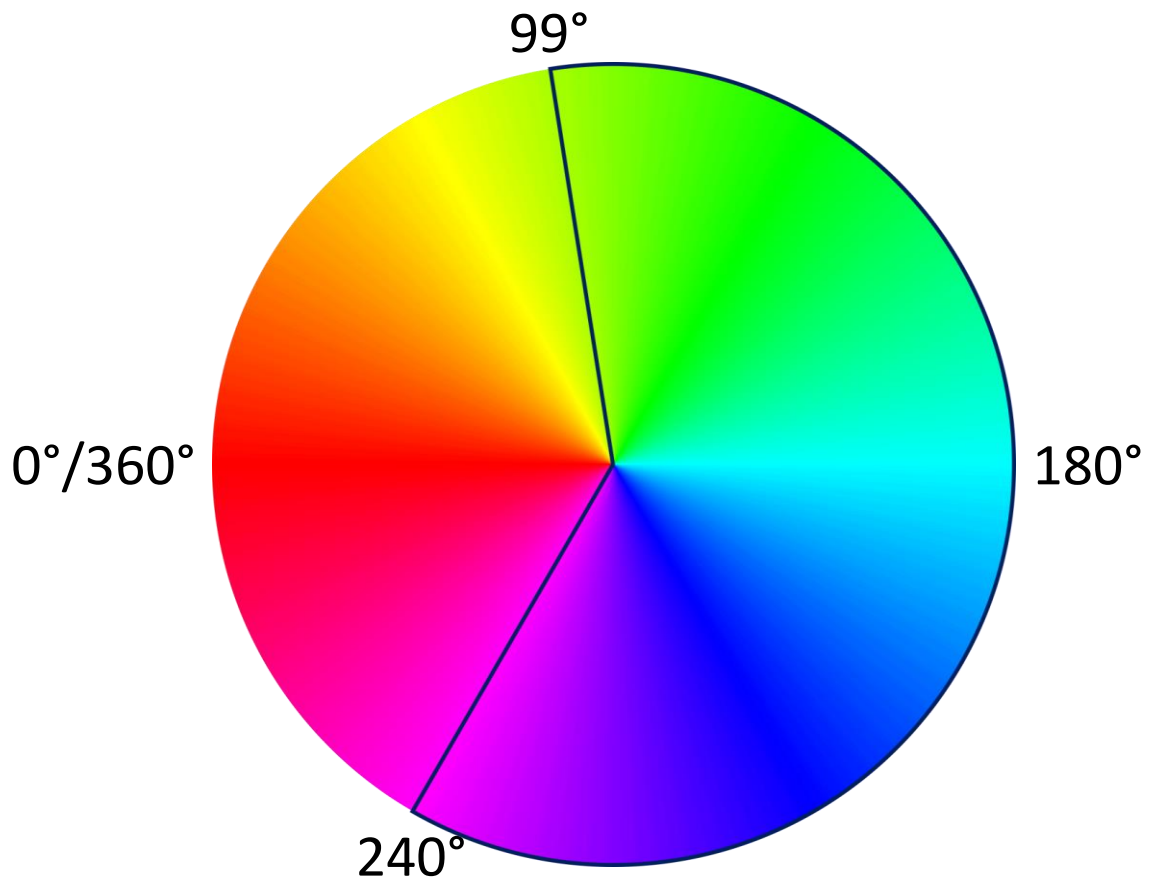


Figure 13 Angular display of color hue in the hue / saturation / brightness (HSB) color space

In the HSB model of color space, the color is composed of three parameters: Hue, Saturation and Brightness. While saturation and brightness can be expressed as a percentage, hue is represented as an angle of a circle displaying the full visible color spectrum. 0°/360° indicate the color red and 180° a light blue. A color threshold in a range of 99° - 240° isolated colors on the spectrum between green and blue.

For blue coloration the lower end of the range was defined using untreated cells in order to exclude artifacts due to cell edges. The upper end of the range was defined using 12 $\mu\text{mol/l}$ etoposide-treated cells for a distinct blue coloration. Colored pixels were correlated to the cell confluency to discern the amount of blue coloration in cells (LOZANO-GERONA, GARCIA-OTIN, 2018; SHLUSH et al., 2011). Cellular coloration values were normalized to values of untreated cells.

4.5. Clonogenic survival

4.5.1. Colony forming ability assay

The determination of cellular survival of different cell types after exposure to IR is an essential tool in radiation biology. The colony formation assay determines the ability of a cell to form a colony from one single cell after exposure to increasing doses of IR. Macroscopically discernable colonies of at least 50 clonogenically identical cells ensure genuine representation of the mitotically active fraction of cells. Cells lethally damaged by IR may undergo a few divisions before settling in mitotic arrest (PUCK, MARCUS, 1956; PUCK et al., 1957).

MEF cells of 50 % density were irradiated with X-rays of 1 to 8 Gy or treated with conditioned medium for 24 h (conditioning doses 1 to 8 Gy). Irradiated cells were seeded for colony formation in petri dishes ($\varnothing = 6$ cm, Th. Geyer) directly after radiation exposure or after a repair period of 24 h. Bystander cells were seeded for colony formation after treatment with conditioned medium for 24 h. For colony formation, cell seeding density accounts for producing 50 clonogenic colonies. After a time period of 10 days, the colonies were fixed and stained with a 3.5 % formaldehyde solution containing 1 g/l crystal violet. The colonies were counted and the plating efficiency (PE) was calculated by dividing the number of colonies by the number of seeded cells (Equation 1).

$$PE = \frac{\# \text{ colonies}}{\# \text{ seeded cells}} \quad \text{Equation 1}$$

The survival fraction (S) after treatment was then calculated according to Equation 2 by dividing the PE of the sample by the mean PE of all untreated samples.

$$S = \frac{PE_{\text{irradiated sample}}}{PE_{\text{untreated sample}}} \quad \text{Equation 2}$$

The relative survival of cells directly exposed to X-rays can be approximated using regression models. The two prevalent mathematical models are the linear-quadratic model (LEA, CATCHESIDE, 1942; MCMAHON, 2018) and the single-hit multi-target model (PUCK, MARCUS, 1956). While these models are primarily means to visualize the survival curve of irradiated cells, they are useful tools to determine parameters that help in comparing the survival of different conditions.

4.5.2. Linear-quadratic model

The linear-quadratic model (Equation 3, Figure 14) describes best the response to exposure with low doses of radiation.

$$S = e^{-(\alpha D + \beta D^2)} \quad \text{Equation 3}$$

IR-induced damage can be categorized in different types of lesions, such as lethal lesions, sub-lethal and potentially lethal lesions. Lethal lesions are seen as damage to intracellular sites that are non-repairable and ultimately lead to the demise of the cell. Sub-lethal lesions represent repairable lesions that can become lethal only by interaction with similar damage to produce a damage site that cannot be repaired. Potentially lethal lesions are sub-lethal lesions that only become lethal under certain circumstances, like mitotic failure. Mechanistic explanations for the linear-quadratic model base upon these damage categories, their interaction and repair capacity (MCMAHON, 2018).

In the linear-quadratic model, cell death by lethal lesions occurs proportionally to an increased dose, but sub-lethal lesions can further reduce the survival fraction if they are too accumulated to be repaired. Accumulation of sub-lethal lesions can generate complex damage sites or additional lethal lesions, thereby adding an exponential curvature to the otherwise linear survival curve. Mathematically, the linear α term dominates lower dose ranges, while the β term gains prominence at higher doses. The combination of both terms in a α/β ratio corresponds to the degree of curvature at a dose at which the linear α and the quadratic β term contribute equally. Cells with a low α/β ratio show a distinctive curvature known as 'shoulder' indicative for damage resistance and repair capacity. The 'shoulder' section becomes gradually reduced with an increasing α/β ratio (MCMAHON, 2018; WANG et al., 2010).

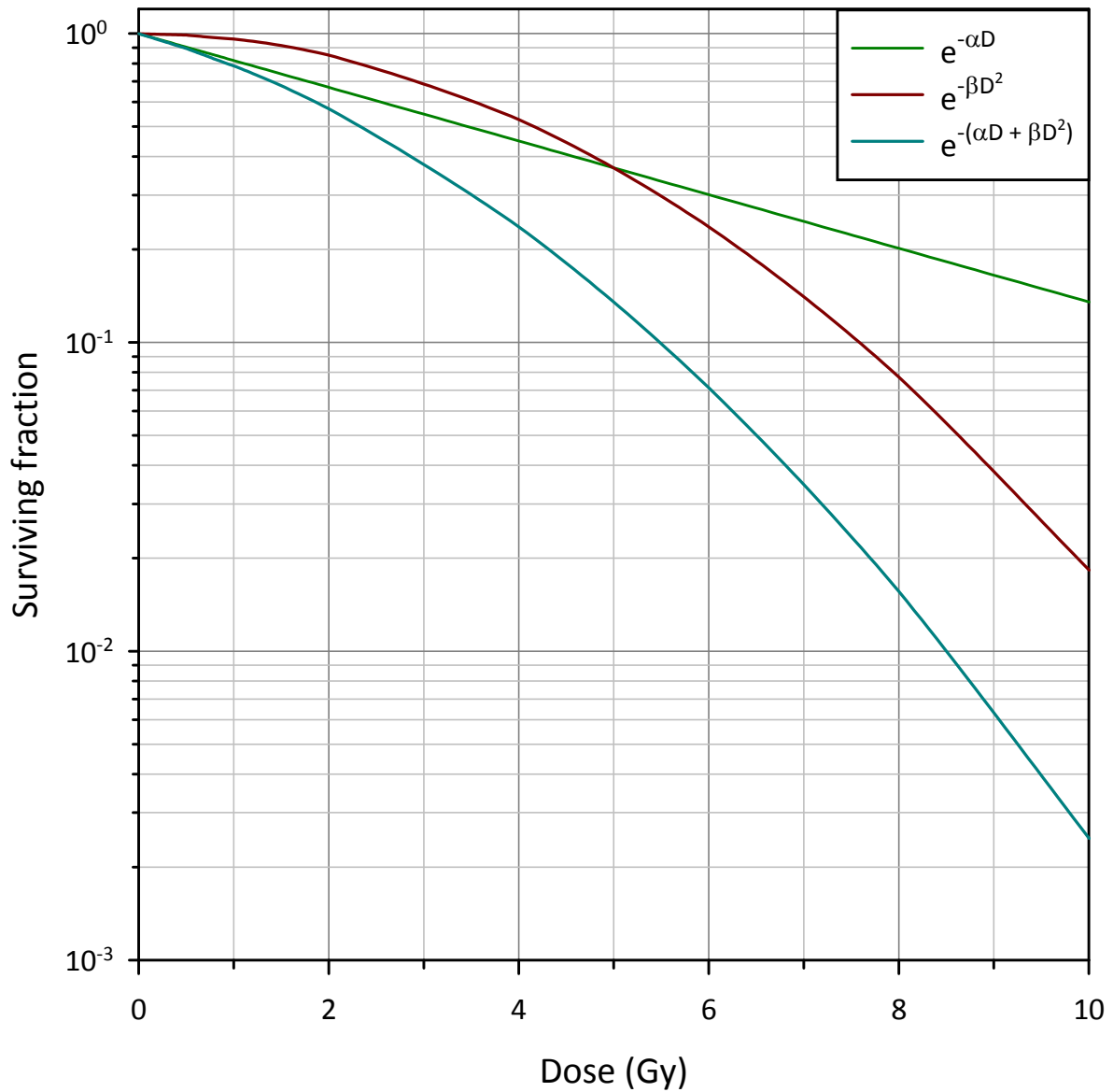


Figure 14 The linear-quadratic model

The linear-quadratic model for estimating dose-response relationships after exposure to IR produces a regression line for survival data points. In order to fully assess the surviving fraction, the curve of the linear-quadratic model implements two assumptions of radiation impact into one formula. The first assumption is that cellular survival behaves in a linear manner to lower radiation doses (green) that can be modeled using the formula $e^{-(\alpha D)}$. The second assumption is that the surviving fraction at higher doses corresponds exponentially to increasing doses (red), resulting in a steep decline of the curve described by the formula $e^{-(\beta D^2)}$. The combination of both formulae results in a realistic presentation of the survival after exposure to IR (blue, $e^{-(\alpha D + \beta D^2)}$).

4.5.3. Single-hit multi-target model

The single-hit multi-target model (Equation 4, Figure 15) describes very well the survival after high dose radiation exposure.

$$S = 1 - (1 - e^{-D/D_0})^n \quad \text{Equation 4}$$

For this model the incorporation of sub-lethal damage is different than for the linear-quadratic model. A cell is assumed to have n targets that need to be inactivated before the cell is killed (MCMAHON, 2018; YU et al., 2005). Any inactivation of a target is considered to be a sub-lethal damage. Therefore, only accumulations of sub-lethal damage lead to cell death. At high doses, the slope of the survival curve (D_0) correlates to the dose (D) needed to reduce survival to 37 % ($1/e$). The number of targets n is the intercept of the y -axis at 0 Gy and the extrapolation of the exponential part of the survival curve.

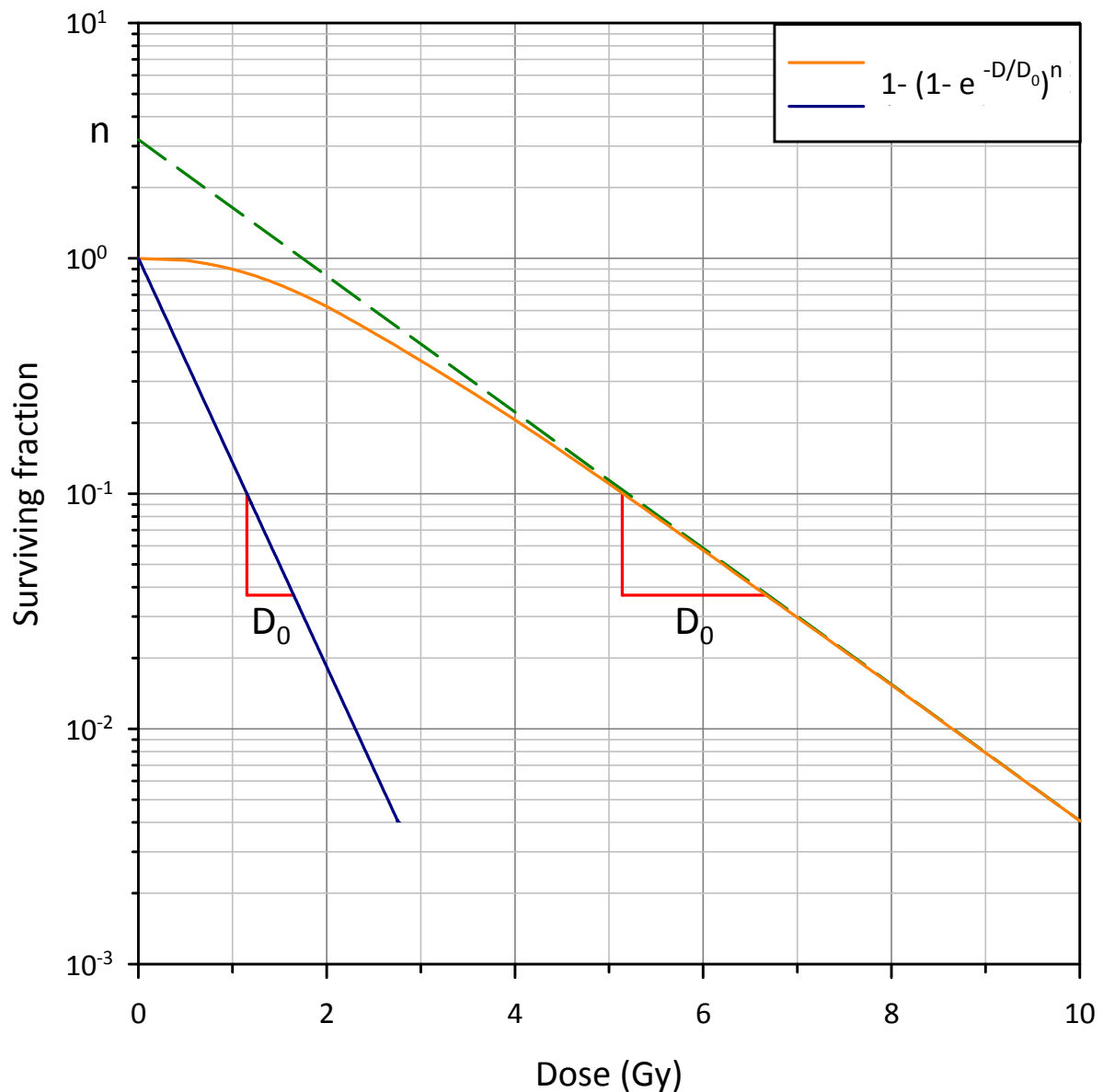


Figure 15 The single-hit multi-target model

The single-hit multi-target model for assessment of cellular survival after IR exposure is based on the assumption that a number of targets (n) within the cell must be inactivated by radiation to reduce the surviving fraction. This variable together with the dose that corresponds to the slope of the curve (D_0), allows the estimation of the sensitivity to the radiation quality the cells were exposed to. The combination of the variables into the formula $(1 - 1(1 - e^{-D/D_0})^n)$ results in a survival curve with a shoulder (cyan) for $n > 1$ that indicates an efficient repair of radiation damage. Extrapolating the slope of the survival curve onto the y-axis of the graph (green dotted line) results in the number of targets (n) that needs to be hit to kill the cell. For doses in the non-linear range of the curve, the damage to the cell is considered sub-lethal. With increasing radiosensitivity of the cell or radiation qualities of high biological effectiveness, the slope will be steeper and the shoulder will cease to exist (blue).

4.6. Statistics

Each experiment was repeated up to six times with up to six replicates each. For statistical evaluation of the measured results, the arithmetic mean as well as standard error (SE) was determined, factoring in the different numbers of repeats and replicates. In order to verify statistical significance of differences between conditions, samples were first subjected to the Shapiro-Wilk normality test and the Brown-Forsythe equal variance test. If both tests were passed, the samples were compared using Student's t-test. If normality or equal variance could not be ascertained, the samples were compared using the Mann-Whitney Rank Sum test. Means and SE were calculated using Microsoft® Office Excel 2010 (Microsoft Deutschland GmbH, Munich, Germany). Shapiro-Wilk, Brown-Forsythe, Student's t-test and Mann-Whitney Rank Sum test as well as regression analyses were performed using SigmaPlot 13.0 (Systat Software, Inc., San Jose, CA, USA).

5. Results

RIBE affect the radiation response especially in non-irradiated cells near the radiation-exposed tissue volume and might modulate the outcome of radiotherapy or increase the probability for secondary tumor formation. Therefore cellular responses of X-irradiated cells and cells treated with radiation-conditioned medium were compared. The radiobiological endpoints in question were clonogenic survival, stress-induced cellular senescence, cell cycle progression and DNA damage induction. Additionally, the activation of NF- κ B in bystander cells was assessed by immunofluorescence visualization of nuclear translocation of the NF- κ B subunit p65. The radiation response in MEF cell lines of differing NF- κ B status was compared. Using the NF- κ B (-) MEF NEMO ko cell line, the mechanistic relevance of the transcription factor was determined (1) for the radiobiological endpoints after direct X-irradiation and (2) in non-irradiated bystander cells that were treated with conditioned medium from X-irradiated cells.

5.1. Direct Exposure to X-rays

5.1.1. Cellular survival

Using the colony forming ability assay for assessment of clonogenic survival, the dose-effect relationship for survival after X-ray exposure was determined. In order to compare the survival curves, the linear-quadratic model was employed as it fitted the acquired data better than the single-hit multi-target model.

MEF wt and NEMO ko cells were exposed to X-rays up to 8 Gy and plated either immediately or 24 h after irradiation to allow for repair. With both, immediate plating and late plating, MEF wt cells showed a reduced relative survival with increasing X-ray dose (Figure 16). At 8 Gy the survival amounted to 0.01 (Table 9). The curves showed a slight shoulder up to 1 Gy, indicating repair of sub-lethal damage. While the decrease of the surviving fraction was significant for each curve, starting at 2 Gy based on the preceding dose, no significant difference was found for the two plating modalities when compared to each other with the linear-quadratic model (Table 10).

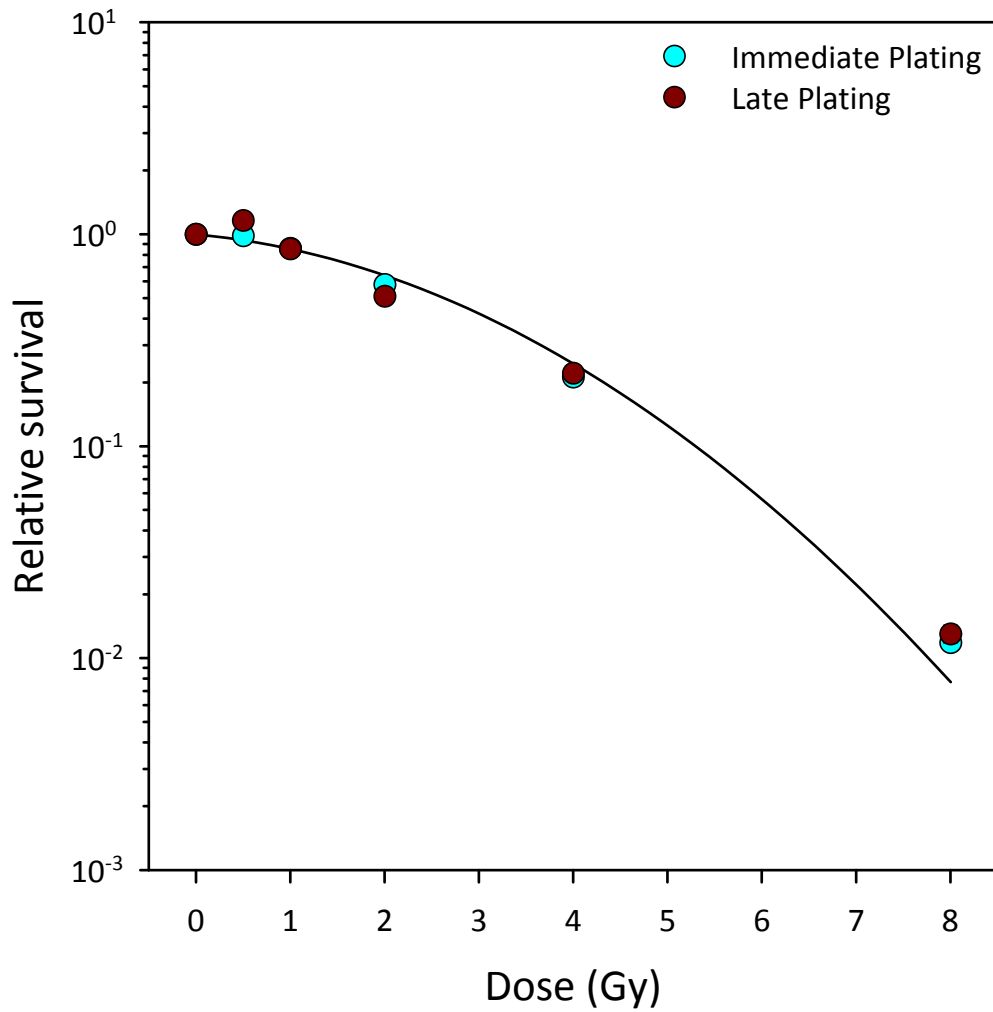


Figure 16 Cellular survival of MEF wt cells after direct exposure to X-rays – Immediate Plating vs. Late Plating

MEF wt cells were plated for clonogenic colony formation immediately (cyan) and 24 h (Late Plating, dark red) after X-irradiation of up to 8 Gy. Macroscopic colonies were counted after 10 days and the surviving fraction was determined. The regression for the survival curve was determined with the linear-quadratic model.

A minimum of 1200 colonies were analyzed. Mean \pm SE, n = 8 with six technical replicates in each experiment. If the SE is not visible, it is smaller than the symbol.

Table 9 Survival data for X-irradiated MEF wt (Immediate Plating and Late Plating)

Dose (Gy)	Immediate Plating		Late Plating	
	Mean surviving fraction \pm SE	p-value	Mean surviving fraction \pm SE	p-value
0	1.00 \pm 0.02		1.00 \pm 0.02	
0.5	0.99 \pm 0.03	0.737	1.16 \pm 0.06	0.021
1	0.86 \pm 0.02	0.003	0.85 \pm 0.05	< 0.001
2	0.58 \pm 0.02	< 0.001	0.51 \pm 0.02	< 0.001
4	0.21 \pm 0.01	< 0.001	0.22 \pm 0.01	< 0.001
8	0.01 \pm 0.00	< 0.001	0.01 \pm 0.00	< 0.001

Table 10 Parameters of the survival curves determined by the linear-quadratic model and statistics for X-irradiation of MEF wt (Immediate vs. Late Plating)

Parameters	Mean \pm SE (Immediate Plating)	Mean \pm SE (Late Plating)	p-value
α	0.11 \pm 0.02	0.08 \pm 0.04	0.804
β	0.06 \pm 0.00	0.07 \pm 0.01	0.563
α/β	1.81 \pm 1.98	1.16 \pm 1.92	

Figure 17 shows the survival of MEF NEMO ko plated immediately and 24 h after exposure to up to 8 Gy X-rays. The relative survival for both plating modalities decreased without a shoulder in the curves resulting in a surviving fraction of 0.02 at 8 Gy. The reduction of survival was significant starting at 2 Gy based on the preceding dose (

Table 11). Similar to the clonogenic survival of MEF wt cells, the dose-effect curves for immediate and late plating of MEF NEMO ko cells were not significantly different in the linear-quadratic model (Table 12).

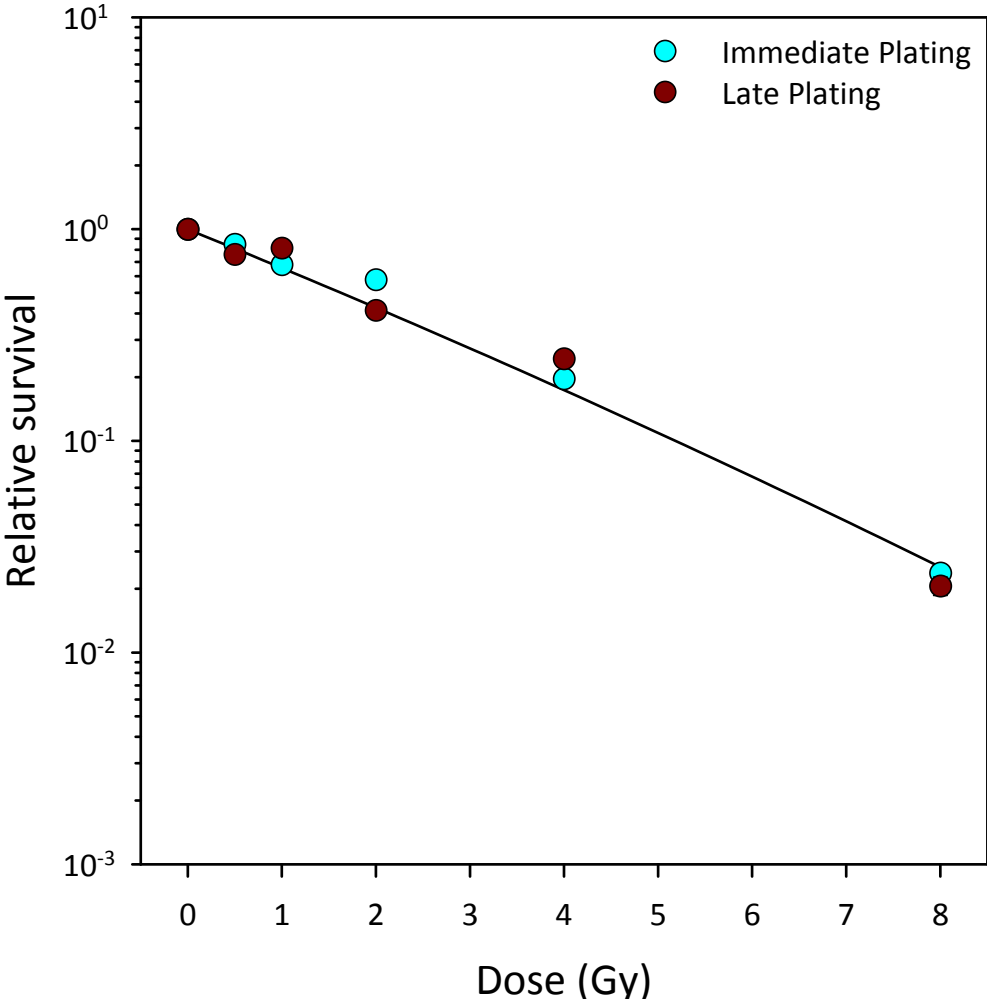


Figure 17 Cellular survival of MEF NEMO ko cells after direct exposure to X-rays – Immediate Plating vs. Late Plating

MEF NEMO ko cells were plated for clonogenic colony formation immediately (cyan) and 24 h (Late Plating, dark red) after X-irradiation of up to 8 Gy. Macroscopic colonies were counted after 10 days and the surviving fraction was determined. The regression for the survival curve was determined with the linear-quadratic model.

A minimum of 1200 colonies were analyzed. Mean ± SE, n = 7 with six technical replicates in each experiment. If the SE is not visible, it is smaller than the symbol.

Table 11 Survival data for X-irradiated MEF NEMO ko (Immediate Plating and Late Plating)

Dose (Gy)	Immediate Plating		Late Plating	
	Mean surviving fraction \pm SE	p-value	Mean surviving fraction \pm SE	p-value
0	1.00 \pm 0.03		1.00 \pm 0.02	
0.5	0.85 \pm 0.05	0.017	0.76 \pm 0.04	< 0.001
1	0.68 \pm 0.04	0.013	0.82 \pm 0.03	0.329
2	0.58 \pm 0.03	0.041	0.41 \pm 0.02	< 0.001
4	0.20 \pm 0.01	< 0.001	0.24 \pm 0.02	< 0.001
8	0.02 \pm 0.00	< 0.001	0.02 \pm 0.00	< 0.001

Table 12 Parameters of the survival curves determined by the linear-quadratic model and statistics for X-irradiation of MEF NEMO ko (Immediate vs. Late Plating)

Parameters	Mean \pm SE (Immediate Plating)	Mean \pm SE (Late Plating)	p-value
α	0.41 \pm 0.04	0.42 \pm 0.04	0.967
β	0.01 \pm 0.01	0.00 \pm 0.01	0.872
α/β	62.81 \pm 1.96	101.08 \pm 1.85	

The survival fractions of immediately plated MEF wt and NEMO ko cells are depicted in Figure 18. The survival of MEF wt cells was slightly higher at doses of 0.5 and 1 Gy compared to MEF NEMO ko cells, and lower at 8 Gy, delineating the MEF wt curve with a low-dose shoulder and a steeper drop at the highest tested dose. This resulted in a significant difference of the curve shapes in the linear-quadratic model (Table 13).

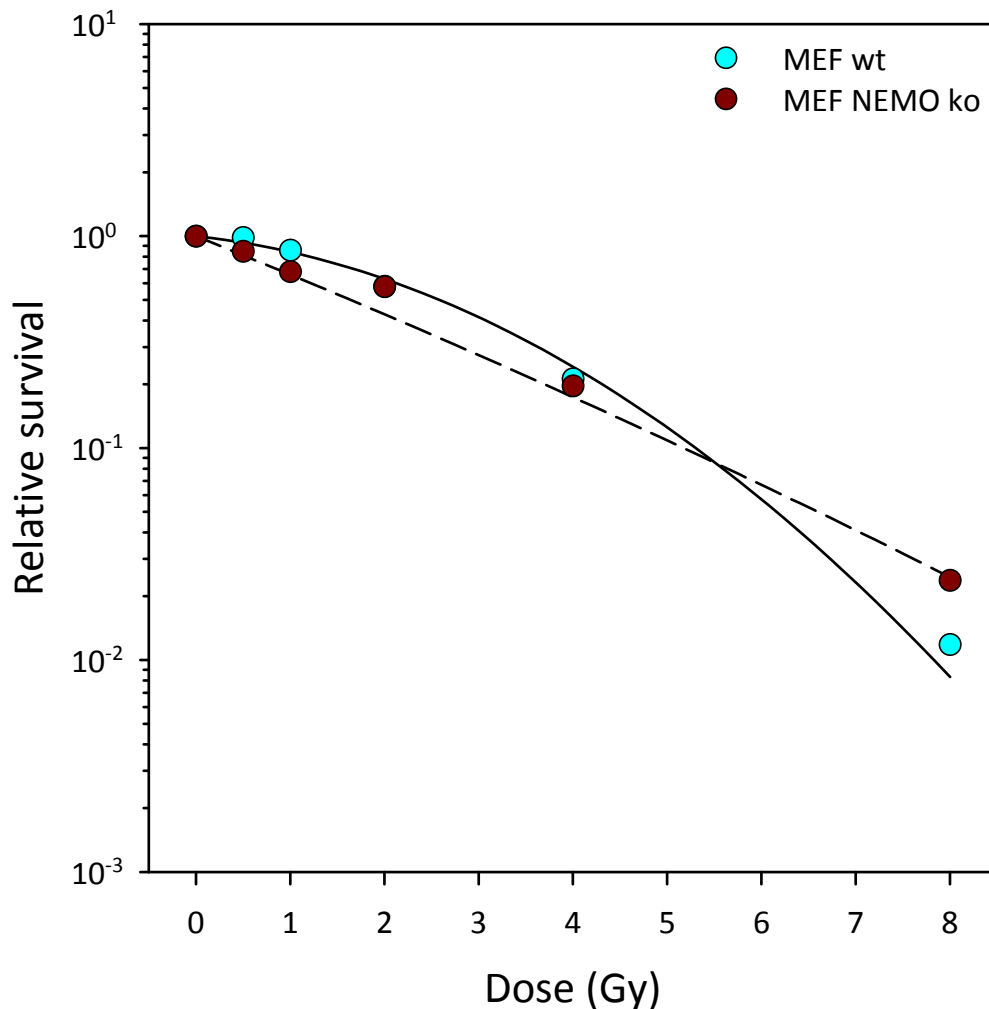


Figure 18 Cellular survival of immediately plated MEF wt and NEMO ko cells after direct exposure to X-rays

Comparison of relative survival of MEF wt (cyan, straight line) and NEMO ko (dark red, dashed line) cells, immediately plated for clonogenic colony formation, after X-irradiation of up to 8 Gy. The regression for the survival curve was determined with the linear-quadratic model.

A minimum of 1200 colonies were analyzed. Mean \pm SE, n = 7-8 with six technical replicates in each experiment. If the SE is not visible, it is smaller than the symbol.

In Figure 19, the survival fractions of late plated MEF wt and NEMO ko cells are compared. The 0.5 Gy data point of MEF wt cells was slightly higher than that of MEF NEMO ko and slightly lower at 8 Gy, the differences between the curves were significant in the linear-quadratic model (Table 14).

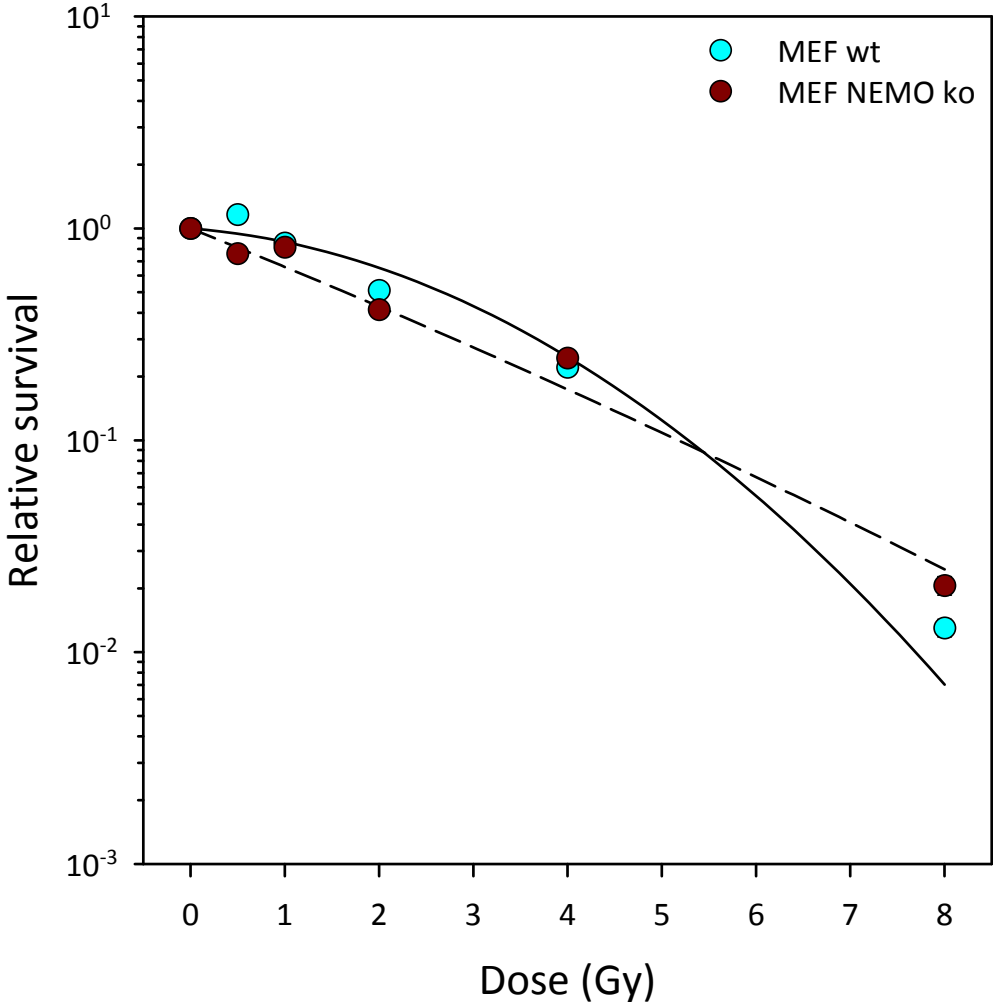


Figure 19 Cellular survival of late plated MEF wt and NEMO ko cells after direct exposure to X-rays

Comparison of relative survival of MEF wt (cyan, straight line) and NEMO ko (dark red, dashed line) cells, plated for clonogenic colony formation 24 h after X-irradiation of up to 8 Gy. The regression for the survival curve was determined with the linear-quadratic model.

A minimum of 1200 colonies were analyzed. Mean \pm SE, n = 7-8 with six technical replicates in each experiment. If the SE is not visible, it is smaller than the symbol.

Table 13 Parameters of the survival curves determined by the linear-quadratic model and statistics for X-irradiation and Immediate Plating (MEF wt vs. MEF NEMO ko)

Parameters	Mean ± SE (MEF wt)	Mean ± SE (MEF NEMO ko)	p-value
α	0.11 ± 0.02	0.41 ± 0.04	< 0.001
β	0.06 ± 0.00	0.01 ± 0.01	< 0.001
α/β	1.81 ± 1.98	62.81 ± 1.96	

Table 14 Parameters of the survival curves determined by the linear-quadratic model and statistics for X-irradiation and Late Plating (MEF wt vs. MEF NEMO ko)

Parameters	Mean ± SE (MEF wt)	Mean ± SE (MEF NEMO ko)	p-value
α	0.08 ± 0.04	0.42 ± 0.04	< 0.001
β	0.07 ± 0.01	0.00 ± 0.01	< 0.001
α/β	1.16 ± 1.92	101.08 ± 1.85	

5.1.2. Cellular senescence

The analysis of cellular survival after exposure to IR using the colony forming ability assay permitted the assessment of remaining dividing cells. Any mitotically inactive yet living cell is counted as dead, since no colony can arise. Therefore, the stress-induced senescence of MEF wt and NEMO ko cells was investigated by determining the β -galactosidase activity at a pH of 6.0.

Representative images of the stained cells are given in Figure 20. Brightfield microscopy at 20 \times magnification presented a blue coloration after enzymatic cleavage of X-gal via β -galactosidase at pH 6.0. Exposure to 8 Gy X-rays and 12.5 μ mol/l etoposide increased β -galactosidase activity in both MEF wt and NEMO ko cells.

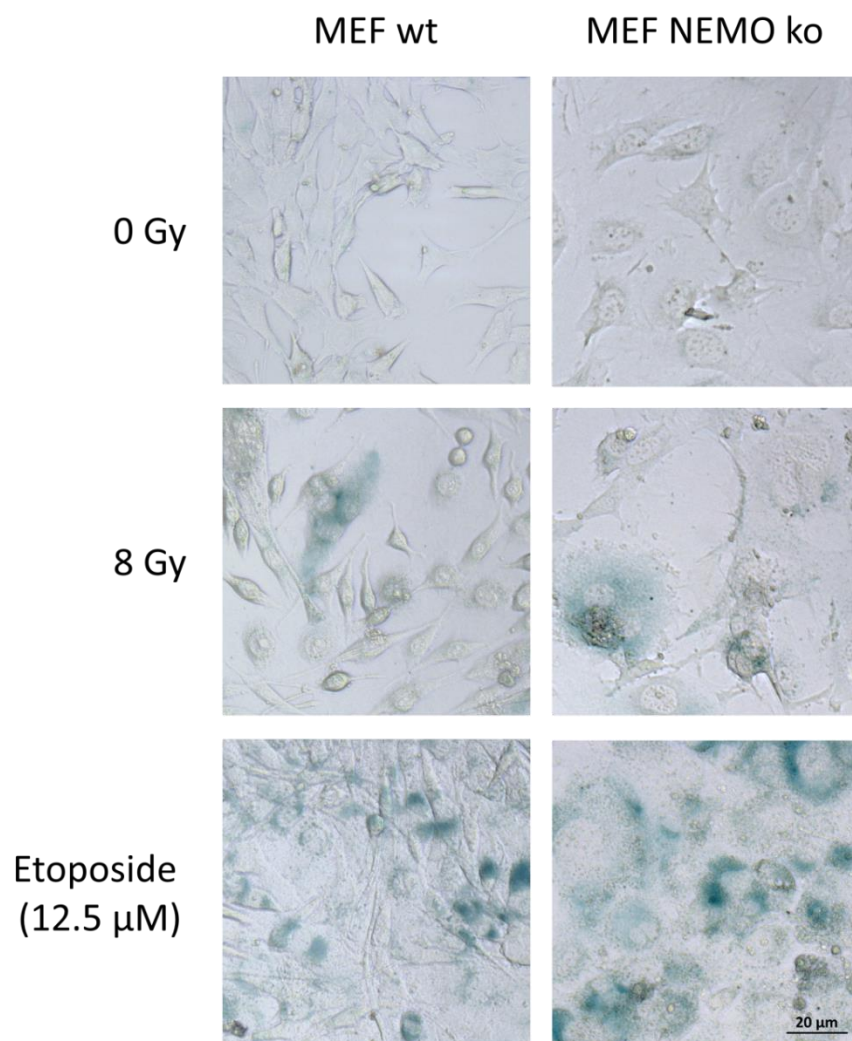


Figure 20 β -galactosidase activity after direct X-rays exposure

Activity of β -galactosidase in MEF wt (left) and MEF NEMO ko (right) cells after exposure to different doses of X-rays or 24 h treatment with 12.5 μ mol/l etoposide. Cells were stained at pH 6.0 after 6 days of recovery in α -medium. Brightfield microscopy at 20 \times magnification.

As shown in Table 15 and Figure 21, the β -galactosidase activity of MEF wt cells increased significantly after exposure to 8 Gy X-rays compared to the mock-irradiated control. Doses below 8 Gy failed to significantly increase senescence-associated β -galactosidase activity in MEF wt cells.

In MEF NEMO ko cells, a X-ray dose of 2 Gy was sufficient to increase the activity of β -galactosidase significantly compared to mock-irradiated cells. Exposure to 4 and 8 Gy of X-rays resulted in a dose-dependent increase of β -galactosidase activity.

Treatment with 12.5 μ mol/l etoposide resulted in a strong increase of β -galactosidase activity, which was significant for both cell lines.

β -galactosidase response towards senescence-inducing stresses of MEF NEMO ko cells was significantly more extensive compared to wildtype cells (4 Gy: $p < 0.001$, 8 Gy: $p < 0.001$).

The NF- κ B status of MEF cells appears to contribute to withstanding the senescence-inducing effects of X-rays and chemotherapeutics.

Table 15 Relative β -galactosidase activity of MEF wt and MEF NEMO ko after X-irradiation and etoposide treatment

Dose (Gy)	MEF wt		MEF NEMO ko	
	Mean \pm SE	p-value vs 0 Gy	Mean \pm SE	p-value vs 0 Gy
0	1.00 \pm 0.05		1.00 \pm 0.12	
2	1.05 \pm 0.06	0.815	1.50 \pm 0.22	0.021
4	1.16 \pm 0.06	0.166	3.64 \pm 0.42	< 0.001
8	2.36 \pm 0.20	< 0.001	6.13 \pm 1.00	< 0.001
Etoposide	6.31 \pm 0.50	< 0.001	18.89 \pm 1.49	< 0.001

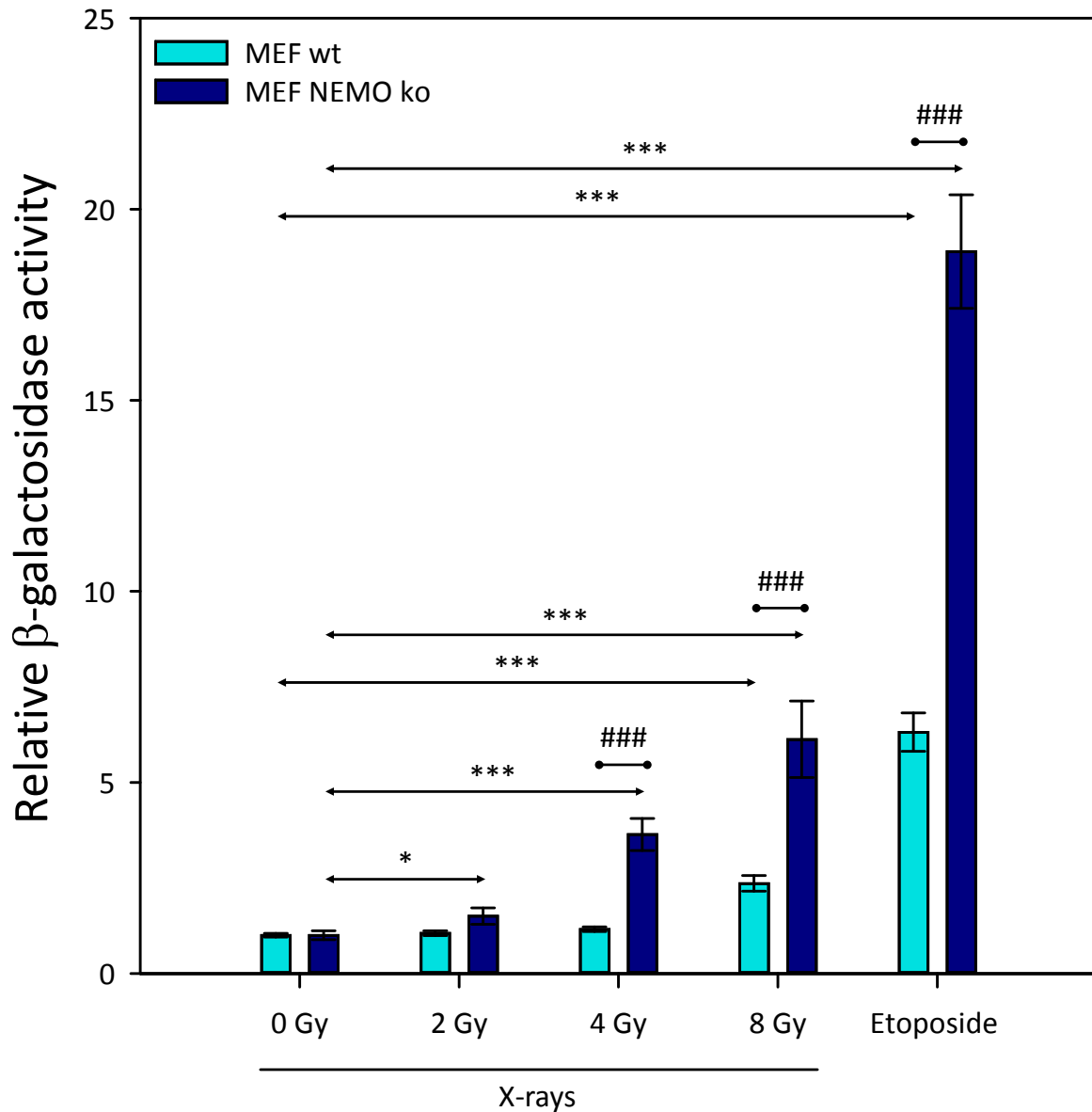


Figure 21 Relative cellular senescence after direct X-rays exposure

Relative amount of β -galactosidase positive MEF wt (cyan) and MEF NEMO ko (dark blue) cells after exposure to different doses of X-rays or 24 h treatment with 12.5 $\mu\text{mol/l}$ etoposide. Cells were stained at pH 6.0 after 6 days of recovery in α -medium. An asterisk (*) indicates a significant difference compared to 0 Gy. A diamond (#) indicates a significant difference between cell lines. A minimum of 700 cells were analyzed. Mean \pm SE, n = 6, * p < 0.05, *** / ### p < 0.001.

5.1.3. Apoptosis and cell cycle progression

Besides mitotic inactivation of a cell, the clonogenic survival assay does not discriminate dying and dead cells. Apoptosis as one cell death pathway is marked by compartmentalization of fragmented DNA. The cellular DNA content was assessed with a pan-DNA PI staining. Flow cytometrically-recorded events containing less DNA than cells in G1/G0 phase were assigned to the sub-G1 portion of the cell cycle and are indicative for formation of apoptotic bodies.

Over a time course of 48 h after X-irradiation, a very small relative amount of both MEF wt and MEF NEMO ko cells was in the sub-G1 population as seen in Figure 22 and Table 16. Irradiation with 8 Gy X-rays did not significantly change the proportion of sub-G1 cells. There were no significant differences between MEF wt and MEF NEMO ko cells.

Without an indication of an apoptotic cell fate in the cell cycle analysis, further tests for apoptosis were not pursued.

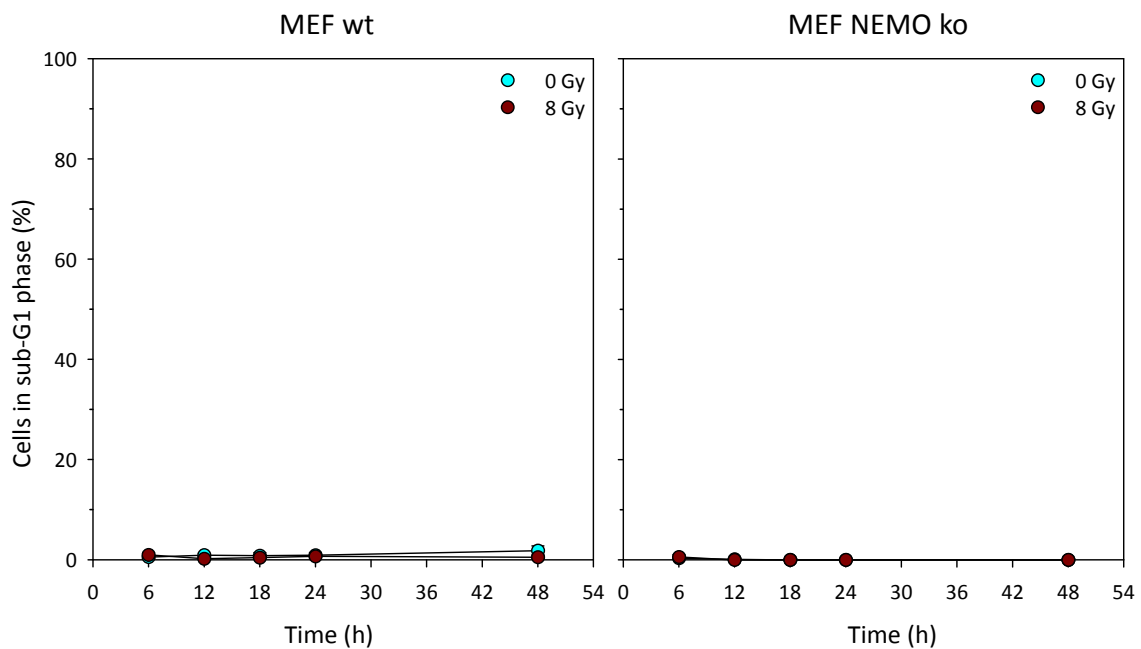


Figure 22 Percentage of cells with a sub-G1 DNA content after direct X-rays exposure

Amount of MEF wt (left) and MEF NEMO ko (right) cells with sub-G1 DNA content up to 48 h after exposure to 0 Gy (cyan) and 8 Gy (dark red) X-rays. A minimum of 200'000 cells were analyzed. Mean \pm SE, n = 6. If the SE is not visible, it is smaller than the symbol.

Table 16 Percentage of MEF wt and MEF NEMO ko cells with sub-G1 DNA content (mean \pm SE) up to 48 h after X-irradiation with 8 Gy.

Time (h)	MEF wt			MEF NEMO ko		
	0 Gy	8 Gy	p-value	0 Gy	8 Gy	p-value
6	0.59 \pm 0.36	1.01 \pm 0.43	0.505	0.36 \pm 0.28	0.59 \pm 0.49	0.937
12	0.96 \pm 0.37	0.24 \pm 0.22	0.307	0.11 \pm 0.05	0.00 \pm 0.00	0.152
18	0.85 \pm 0.55	0.47 \pm 0.29	0.721	0.00 \pm 0.00	0.00 \pm 0.00	0.122
24	0.94 \pm 0.46	0.71 \pm 0.46	0.930	0.00 \pm 0.00	0.00 \pm 0.00	0.228
48	1.87 \pm 0.89	0.54 \pm 0.34	0.532	0.00 \pm 0.00	0.00 \pm 0.00	0.138

In order to repair DNA damage induced by IR, cell cycle control checkpoints give the cell time for DNA repair by arresting the cell cycle progression. These arrests are denoted depending on the cell cycle phase in question and can be recognized as a higher fraction of cells in that phase.

The amount of MEF wt and NEMO ko cells in the different cell cycle phases after irradiation with 8 Gy X-rays is shown in Table 17 and Figure 23. Irradiation led to a significant decrease of MEF wt cells in G1-phase of the cell cycle 6 and 12 h after radiation exposure. The distribution in G1-phase returned to the same level as untreated cells after 18 h. At this time point, a significant decrease in S-phase cells was noticed, which returned to untreated levels at 24 h. The amount of G2/M cells started out unchanged at 6 h but increased strongly 12 h after X-irradiation. This increase is commonly known as a G2/M-arrest. The arrest slowly resolved, with a weak but significant increase of cells in G2/M-phase at 18 h and no change in G2/M-level from 24 h onwards.

MEF NEMO ko cells showed a slightly different G2/M-arrest progression. A significant reduction in G1-phase cells was observed at 12 h after X-rays exposure. Cells in S-phase were present to a significantly lower extent 12 to 18 h after exposure. A G2/M-arrest on the other hand was noticeable 6 to 18 h post-irradiation resolving completely after 24 h.

Noticeable was a steep shift of cell cycle phase distribution towards the G1-phase with longer incubation times as an effect of contact growth inhibition in petri dishes.

Between the cell lines there were significant differences for both 0 and 8 Gy (Table 18). MEF NEMO ko cells showed a higher proportion of cells in G2/M-phase at later time points (0 Gy: 18 to 48 h) compared to MEF wt. The amount of cells in G1- (0 Gy: 6 and 18 h, 8 Gy: 18 and 24 h) and S-phase (0 Gy: 6 h) were accordingly smaller. The cell number in G2/M-phase over time reflects the progression speed of the respective cell line through the cell cycle. A larger number at late time points indicates a slower progression through the cell cycle.

To summarize, the NF- κ B status of MEF cells appears to modify the sensitivity for G2/M cell cycle arrest induction.

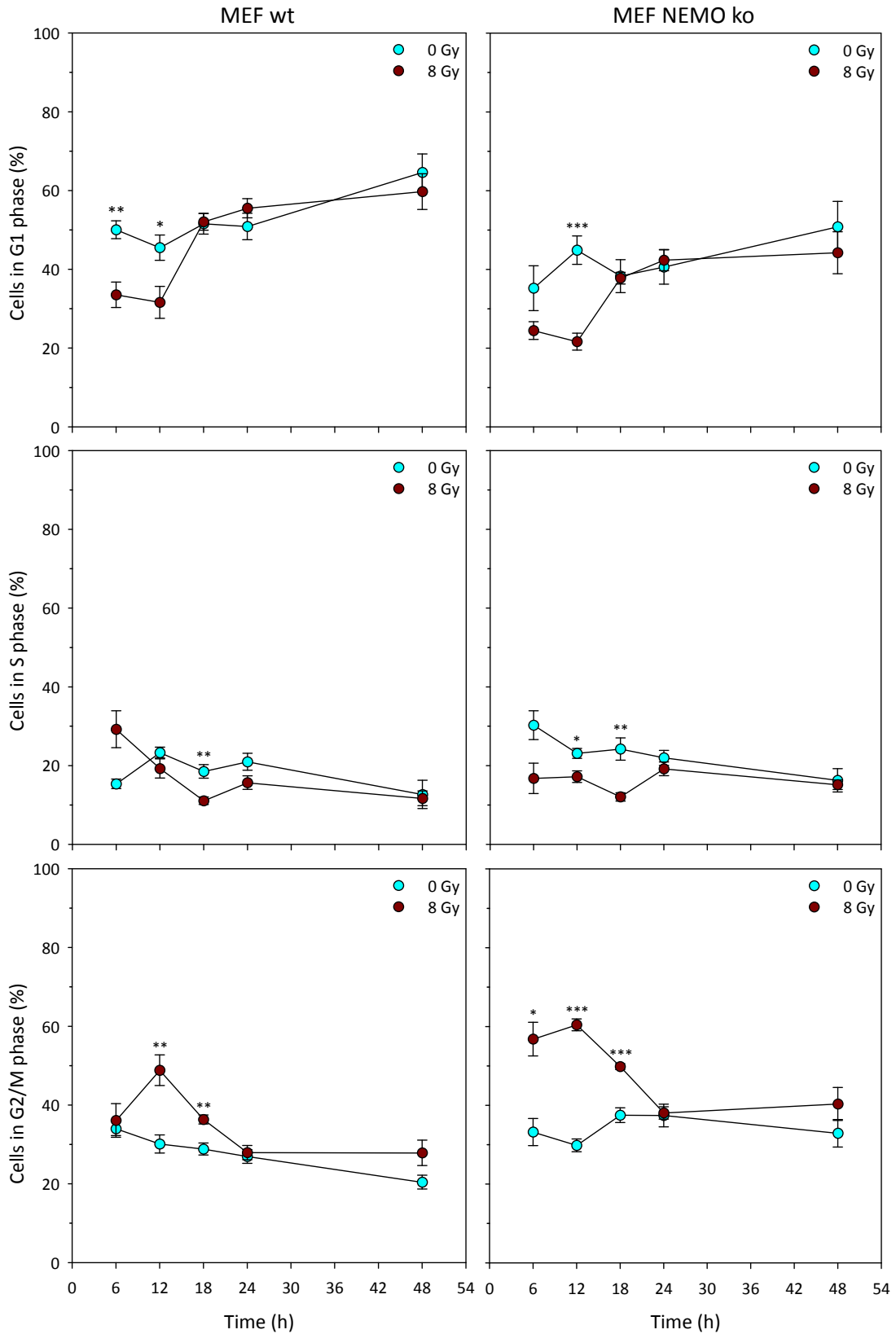


Figure 23 Cell cycle phase distribution after direct X-rays exposure

Amount of MEF wt (left) and MEF NEMO ko (right) cells in G1, S and G2/M cell cycle phases up to 48 h after exposure to 0 Gy (cyan) and 8 Gy (dark red) X-rays. An asterisk (*) indicates significant difference compared to 0 Gy.

A minimum of 200'000 cells were analyzed. Mean \pm SE, n = 6, * p < 0.05, ** p < 0.01, ***p < 0.001.

Table 17 Percentage of MEF wt and MEF NEMO ko cells in G1, S and G2/M cell cycle phases up to 48 h after X-irradiation with 8 Gy.

G1		MEF wt			MEF NEMO ko		
Time (h)	0 Gy	8 Gy	p-value	0 Gy	8 Gy	p-value	
6	50.05 ± 2.26	33.53 ± 3.21	0.002	35.22 ± 5.71	24.46 ± 2.24	0.065	
12	45.51 ± 3.23	31.62 ± 4.05	0.023	44.89 ± 3.62	21.64 ± 2.16	< 0.001	
18	51.59 ± 2.64	52.07 ± 2.13	0.897	38.30 ± 4.19	37.77 ± 1.49	0.409	
24	50.90 ± 3.37	55.53 ± 2.43	0.309	40.61 ± 4.36	42.36 ± 2.71	0.573	
48	64.62 ± 4.69	59.74 ± 4.54	0.494	50.84 ± 6.44	44.24 ± 5.33	0.480	

S		MEF wt			MEF NEMO ko		
Time (h)	0 Gy	8 Gy	p-value	0 Gy	8 Gy	p-value	
6	15.38 ± 1.21	29.23 ± 4.67	0.105	30.25 ± 3.66	16.74 ± 3.86	0.099	
12	23.31 ± 1.36	19.27 ± 2.42	0.199	23.09 ± 1.25	17.18 ± 1.47	0.013	
18	18.53 ± 1.73	11.08 ± 0.96	0.003	24.20 ± 2.85	12.05 ± 1.06	0.004	
24	20.98 ± 2.15	15.67 ± 1.72	0.112	21.96 ± 1.91	19.16 ± 1.74	0.282	
48	12.68 ± 3.59	11.69 ± 1.85	0.815	16.26 ± 2.98	15.13 ± 1.21	0.741	

G2/M		MEF wt			MEF NEMO ko		
Time (h)	0 Gy	8 Gy	p-value	0 Gy	8 Gy	p-value	
6	33.99 ± 1.75	36.09 ± 4.29	0.721	33.20 ± 3.43	56.81 ± 4.27	0.025	
12	30.12 ± 2.30	48.85 ± 3.88	0.001	29.83 ± 1.61	60.44 ± 1.51	0.001	
18	28.83 ± 1.53	36.32 ± 1.15	0.003	37.49 ± 1.87	49.84 ± 0.74	<0.001	
24	26.93 ± 1.74	27.93 ± 1.81	0.712	37.42 ± 2.90	38.07 ± 1.58	0.491	
48	20.42 ± 1.75	27.86 ± 3.22	0.085	32.90 ± 3.49	40.35 ± 4.20	0.244	

Table 18 Error probability (p-value) for comparison of MEF wt and MEF NEMO ko cells G1, S and G2/M cell cycle phases up to 48 h after X-irradiation with 8 Gy.

Time (h)	0 Gy			8 Gy		
	G1	S	G2/M	G1	S	G2/M
6	0.022	0.003	0.994	0.130	0.259	0.061
12	0.906	0.915	0.926	0.090	0.541	0.039
18	0.023	0.123	0.006	< 0.001	0.556	< 0.001
24	0.102	0.860	0.009	0.004	0.201	0.001
48	0.127	0.511	0.008	0.057	0.194	0.041

5.1.4. DNA damage

Of the damage that IR can induce to the DNA, DSB are the most detrimental. While the repair of one DNA strand makes use of the undamaged strand as a template, a DSB is repaired using a chromatid template in case of HR repair, or the broken ends are cut off and re-ligated in case of NHEJ. Thus, the fidelity of DSB repair is dependent on the repair pathway choice, with HR being precise and NHEJ being error-prone. The complexity of the damage can increase to an irreparable level or whole sections of DNA are lost from the genome if they are lacking a centromere and are packaged in micronuclei.

As one of the first steps of DSB repair, the H2AX histones around the break site are phosphorylated at S139. This modification, termed γ H2AX, serves as a marker for DNA DSB and was detected using immunofluorescence staining.

The absolute number of γ H2AX foci per nucleus of MEF wt and NEMO ko cells after irradiation with different doses of X-rays is shown in Table 19 and Figure 24, the significance of differences is displayed in Table 20 and Table 21. One hour after irradiation with 2 Gy X-rays, the number of γ H2AX foci was significantly increased compared to the mock-irradiated control. X-irradiation with 4 Gy resulted in an even higher number of γ H2AX foci. At 4 h after irradiation with 2 Gy X-rays, the number of γ H2AX foci was slightly yet significantly elevated, while at 4 Gy the number was about four times higher than in the mock-irradiated control. 24 h after irradiation with 2 Gy X-rays, the number of γ H2AX foci slightly but significantly increased, compared to the mock-irradiated control, similar to the 4 h time point. The elevation was more strongly pronounced after administration of 4 Gy X-rays.

The amount of γ H2AX foci for each dose decreased significantly with each time increment ($p < 0.001$), reflecting the capabilities of MEF wt cells to repair the damage with time. This repair resulted in a drop of γ H2AX foci at 2 Gy to almost the level of the mock-irradiated control 24 h after irradiation, while 4 Gy X-rays appeared to inflict more lasting damage.

In samples not exposed to X-irradiation, the number of γ H2AX foci decreased with time. As these samples stayed at room temperature during the irradiation procedure (mock-irradiation), the cells might have suffered stress-induced DNA DSB, which were repaired under culture conditions during the following 24 h. Cell division may have a dilutive effect on the mean amount of γ H2AX foci.

MEF NEMO ko cells exhibited a significant increase in γ H2AX foci at 1 h after exposure to 2 Gy X-rays. The number of foci 4 h after X-irradiation increased significantly by a factor of two at 2 Gy compared to mock-irradiated cells and by a factor of four at 4 Gy. At 24 h after X-irradiation, the number of foci in MEF NEMO ko cells increased significantly for 2 Gy and 4 Gy.

For irradiated samples, the number of foci dropped significantly with time, similar to MEF wt cells. Stress-induced DSB increased in mock-irradiated MEF NEMO ko after 4 h incubation under culture conditions, which decreased to almost zero after 24 h.

In comparison to MEF wt, NF- κ B (-) MEF cells featured significantly more γ H2AX foci in irradiated samples 1 and 4 h after X-irradiation ($p < 0.001$). At 24 h the damage in MEF NEMO ko cells was reduced to levels lower than the wildtype, suggesting a more efficient but delayed repair. While mock-irradiated MEF NEMO ko cells seemed to sustain stress-induced damage similar to MEF wt cells, the γ H2AX foci manifest with a delay.

The NF- κ B status of a MEF cells appears to change the sensitivity towards DNA DSB formation as well as the repair kinetics of DNA damage.

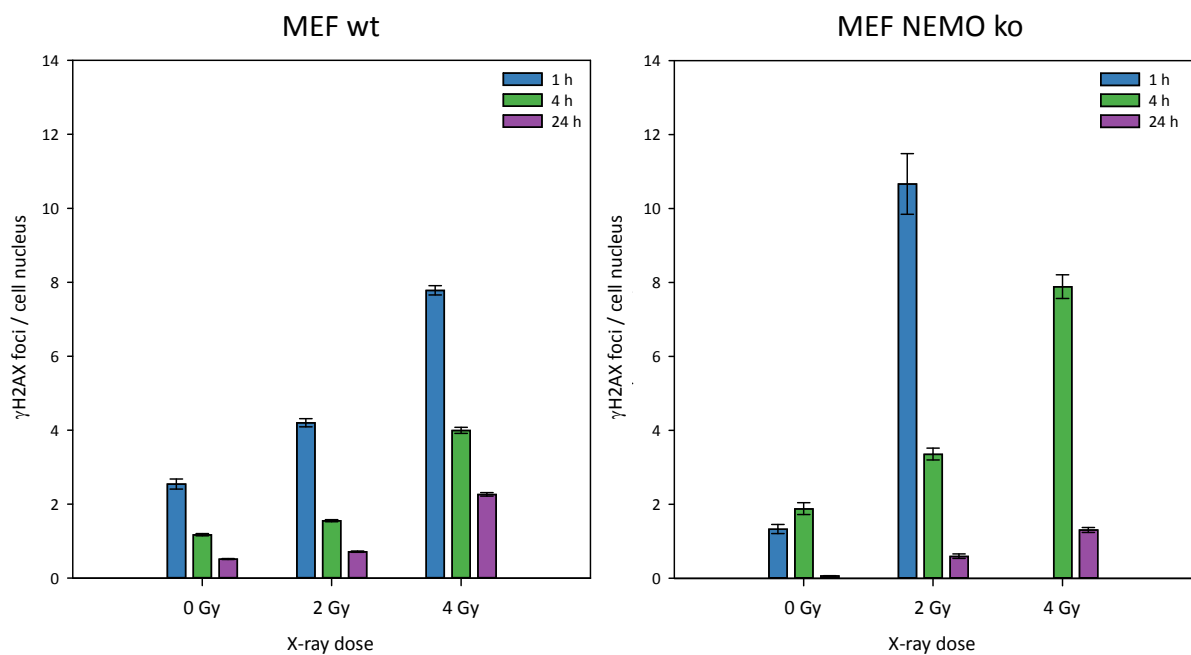


Figure 24 γ H2AX foci per cell nucleus after direct X-rays exposure

Absolute number of γ H2AX foci / cell in MEF wt (left) and MEF NEMO ko (right) cells at different time points after exposure to X-ray doses 2 and 4 Gy. Cells on coverslips were fixed after 1 (blue), 4 (green) and 24 hours (purple) then stained for fluorescent microscopy. A minimum of 800 cell nuclei were analyzed. Mean \pm SE, n = 1-3.

Table 19 Kinetics of γ H2AX foci (mean \pm SE) in MEF wt vs. MEF NEMO ko after X-irradiation

Time (h)	MEF wt			MEF NEMO ko		
	Dose (Gy)					
	0	2	4	0	2	4
1	2.54 \pm 0.14	4.20 \pm 0.11	7.78 \pm 0.13	1.33 \pm 0.12	10.67 \pm 0.02	
4	1.17 \pm 0.03	1.55 \pm 0.03	3.99 \pm 0.08	1.88 \pm 0.16	3.36 \pm 0.16	7.89 \pm 0.32
24	0.52 \pm 0.01	0.72 \pm 0.02	2.26 \pm 0.05	0.07 \pm 0.01	0.60 \pm 0.06	1.31 \pm 0.07

Table 20 Error probability (p-value) between doses at different time points for γ H2AX foci in MEF wt vs. MEF NEMO ko after X-irradiation

1 h	MEF wt			MEF NEMO ko		
Dose (Gy)	Dose (Gy)					
	0	2	4	0	2	4
0						
2	< 0.001			< 0.001		
4	< 0.001	< 0.001				
4 h	Dose (Gy)					
Dose (Gy)	0	2	4	0	2	4
0						
2	< 0.001			< 0.001		
4	< 0.001	< 0.001		< 0.001	< 0.001	
24 h	Dose (Gy)					
Dose (Gy)	0	2	4	0	2	4
0						
2	< 0.001			< 0.001		
4	< 0.001	< 0.001		< 0.001	< 0.001	

Table 21 Error probability (p-value) between time points for different doses regarding γ H2AX foci in MEF wt vs. MEF NEMO ko after X-irradiation

0 Gy		MEF wt			MEF NEMO ko		
		Time (h)					
Time (h)		1	4	24	1	4	24
1							
4		< 0.001			< 0.001		
24		< 0.001	< 0.001		< 0.001	< 0.001	
2 Gy		MEF wt			MEF NEMO ko		
		Time (h)					
Time (h)		1	4	24	1	4	24
1							
4		< 0.001			< 0.001		
24		< 0.001	< 0.001		< 0.001	< 0.001	
4 Gy		MEF wt			MEF NEMO ko		
		Time (h)					
Time (h)		1	4	24	1	4	24
1							
4		< 0.001			< 0.001		
24		< 0.001	< 0.001		< 0.001	< 0.001	

5.2. Bystander treatment with conditioned medium

5.2.1. NF- κ B nuclear translocation

The first step in analyzing the role of NF- κ B in the bystander response was to determine whether the transcription factor can be activated by bystander treatment. To this end, MEF wt cells were exposed to 4 and 8 Gy X-rays or treated with conditioned medium of 4 and 8 Gy conditioning doses. Furthermore, MEF wt cell were treated with TNF- α (20 ng/ml) or LPS (2 μ g/ml) inducing NF- κ b activation via the TNFR1 or the TLR/IL-1R mediated canonical pathway. The samples, fixed 1 h after the respective treatment, were subjected to immunofluorescence staining with an antibody against the NF- κ B subunit p65. The fluorescence intensity of the antibody was assessed within the nucleus of each cell as a measure for translocation of the transcription factor into the nucleus of the cell. The signal intensity was normalized to the 0 Gy control of each treatment. For TNF- α and LPS the signal intensity was normalized to 0 Gy X-irradiated samples.

As displayed in Table 22 and Figure 25, directly irradiated cells showed a significant increase in NF- κ B activation of about 40 % after exposure to 4 and 8 Gy X-rays compared to the mock-irradiated control. Bystander cells exhibited a significant NF- κ B activation of 10 and 20 % after incubation with medium of conditioning X-ray doses of 4 and 8 Gy respectively compared to untreated. Treatment with TNF- α or LPS lead to a 25 and 30 % increase in NF- κ B activation respectively.

These results strongly indicate involvement of the transcription factor in the bystander response, justifying further investigation.

Table 22 Nuclear translocation of p65 in MEF wt cells after X-irradiation or treatment with conditioned medium, TNF- α or LPS

Treatment	Dose / conditioning dose (Gy)	Mean relative translocation \pm SE	p-value vs 0 Gy
X-rays	0	1.00 \pm 0.00	
	4	1.36 \pm 0.00	< 0.001
	8	1.40 \pm 0.00	< 0.001
Cond. medium	0	1.00 \pm 0.00	
	4	1.11 \pm 0.00	< 0.001
	8	1.19 \pm 0.00	< 0.001
Concentration			
TNF- α	20 ng/ml	1.24 \pm 0.00	< 0.001
LPS	2 μ g/ml	1.30 \pm 0.00	< 0.001

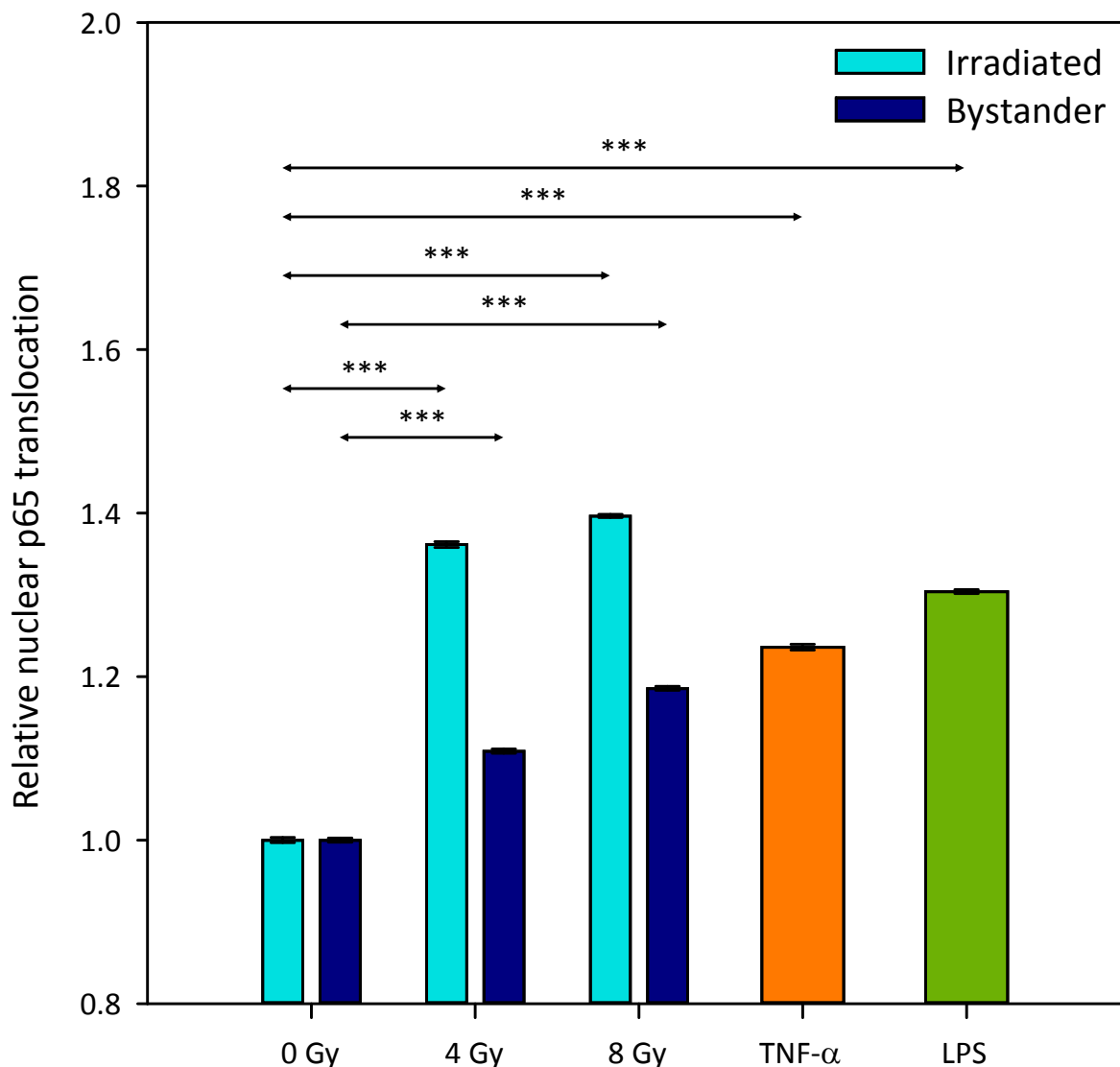


Figure 25 Nuclear translocation of p65 as indicator of NF-κB activation in MEF wt cells after treatment with X-rays, conditioned medium, TNF-α and LPS

Relative nuclear translocation of the NF-κB subunit p65 in MEF wt cells that were either directly exposed to 4 and 8 Gy X-rays (cyan), bystander treated with conditioning doses 4 and 8 Gy (blue) or treated with 20 ng/ml TNF-α (orange) or 2 μg/ml LPS (green, *E. coli* O111:B4). Cells were fixed after 1 h and stained for fluorescence microscopy and analyzed as described above. An asterisk (*) indicates significant difference compared to 0 Gy. A minimum of 2950 cell nuclei were analyzed. Mean ± SE, n = 3-5, *** p < 0.001.

5.2.2. Cellular survival

In order to analyze the relevance of NF- κ B in the bystander response, the clonogenic survival of MEF wt and NEMO ko cells was assessed with the colony forming ability assay. After irradiation with X-ray doses of up to 8 Gy, the culture medium was conditioned by both cell types for 24 h. The conditioned medium was then transferred to non-irradiated cells for 24 h incubation and afterwards plated as described in the section *Colony forming ability* .

Figure 26 shows the relative survival of MEF wt and NEMO ko cells that received conditioned medium from the same cell type. Hence bystander MEF wt cells received conditioned medium from irradiated MEF wt cells and bystander MEF NEMO ko cells from irradiated MEF NEMO ko cells (Table 23). MEF wt cells showed a constant survival up to a conditioning dose of 2 Gy. The survival dropped significantly at a conditioning dose of 4 Gy to 0.69 and stayed at this level at a conditioning dose of 8 Gy (Table 24). MEF NEMO ko cells experienced a significant raise to 1.44 relative survival at 1 Gy conditioning dose. The level of survival decreased significantly at 2 Gy to 1.16 and steadily increased over the range of 4 and 8 Gy conditioning dose back to 1.47 (Table 24). In a comparison between the two cell lines, the differences were significant at 1 Gy conditioning dose, at which point the relative survival of MEF NEMO ko cells showed a peak, as well as at 4 and 8 Gy conditioning dose, at which point the survival of MEF wt cells dropped while the survival level of MEF NEMO ko cells steadily increased (Table 25).

Relative survival after exposure to conditioned medium resulted in completely different dose-effect relationships for cell lines of differing NF- κ B status. This difference indicates a substantial role of the transcription factor in the production and propagation of the bystander signaling.

Table 23 Transfer scheme for conditioned medium

Donor cell type	Recipient cell type	Figure	Symbol
MEF wt	MEF wt	Figure 26	
MEF NEMO ko	MEF NEMO ko		
MEF wt	MEF NEMO ko	Figure 27	
MEF NEMO ko	MEF wt		

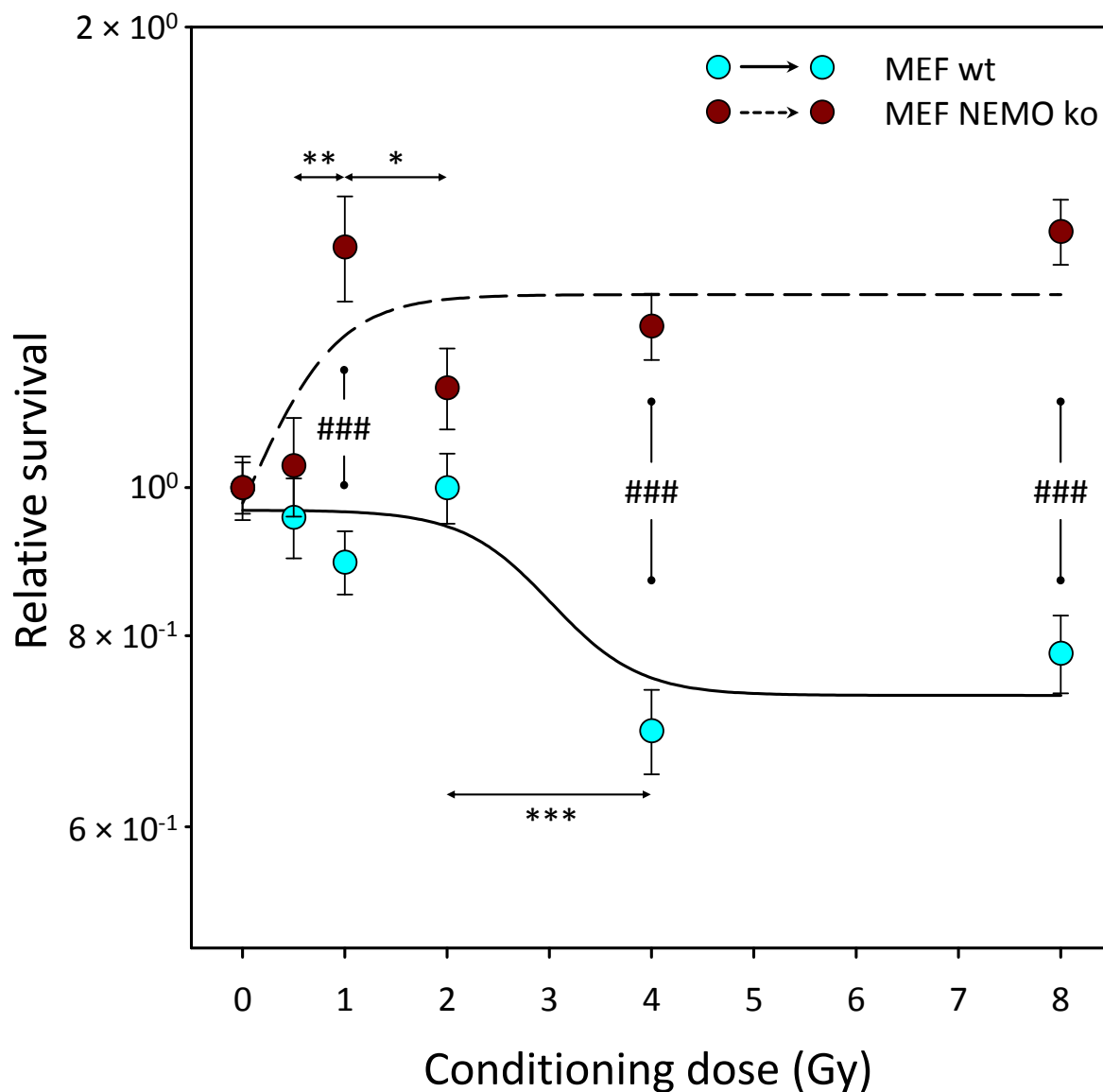


Figure 26 Cellular survival of MEF wt and NEMO ko cells after incubation with conditioned medium

Relative survival of MEF wt (cyan) and NEMO ko (dark red) cells after 24 h incubation with culture medium conditioned by its respective cell line (see Table 23) with X-ray doses up to 8 Gy. Clonogenic colonies were counted after 10 days and the surviving fraction was determined. Sigmoid regression lines (MEF wt: solid, MEF NEMO ko: long dash) are used to support the curve progressions. An asterisk (*) indicates significant difference compared to the preceding dose. A hashtag (#) indicates significant difference between cell lines. A minimum of 900 colonies were analyzed.

Mean \pm SE, n = 5-6 with six technical replicates in each experiment, * p < 0.05, ** p < 0.01, *** / ### p < 0.001.

Table 24 Survival of MEF wt cells after incubation with conditioned medium from X-irradiated MEF wt

Conditioning Dose (Gy)	MEF wt		MEF NEMO ko	
	Mean surviving fraction \pm SE	p-value	Mean surviving fraction \pm SE	p-value
0	1.00 \pm 0.05		1.00 \pm 0.04	
0.5	0.96 \pm 0.06	0.571	1.03 \pm 0.08	0.704
1	0.89 \pm 0.04	0.397	1.44 \pm 0.11	0.006
2	1.00 \pm 0.05	0.127	1.16 \pm 0.07	0.050
4	0.69 \pm 0.04	< 0.001	1.28 \pm 0.06	0.249
8	0.78 \pm 0.05	0.186	1.47 \pm 0.07	0.051

Table 25 Survival statistics for comparison of MEF wt and MEF NEMO ko cells after incubation with conditioned medium from X-irradiated cells of the same origin cell line

Conditioning Dose (Gy)	p-value MEF wt vs. MEF NEMO ko
0	
0.5	0.437
1	< 0.001
2	0.070
4	< 0.001
8	< 0.001

Since the NF- κ B status of the cell appears to play a role in bystander signaling, the survival of MEF wt and MEF NEMO ko cells might be affected depending on the origin of the conditioned medium.

Figure 27 displays the survival of MEF cells after incubation with conditioned medium from the cell line of opposing NF- κ B status. MEF wt cells received conditioned medium from MEF NEMO ko cells, while MEF NEMO ko cells received MEF wt conditioned medium (Table 23). The relative survival of MEF wt cells dropped significantly at 1 Gy conditioning dose to 0.83, stayed at this level at 2 Gy conditioning dose and dropped again significantly to 0.59 at 4 Gy conditioning dose (Table 26). The relative survival of MEF NEMO ko cells increased at 0.5 Gy conditioning dose to 1.22 and stayed at this level up to a conditioning dose of 8 Gy with no significant oscillations (Table 26). The differences in survival between the two cell lines were significant at 1 to 8 Gy conditioning dose, highlighting the strong drop in the survival fraction of MEF wt cells (Table 27).

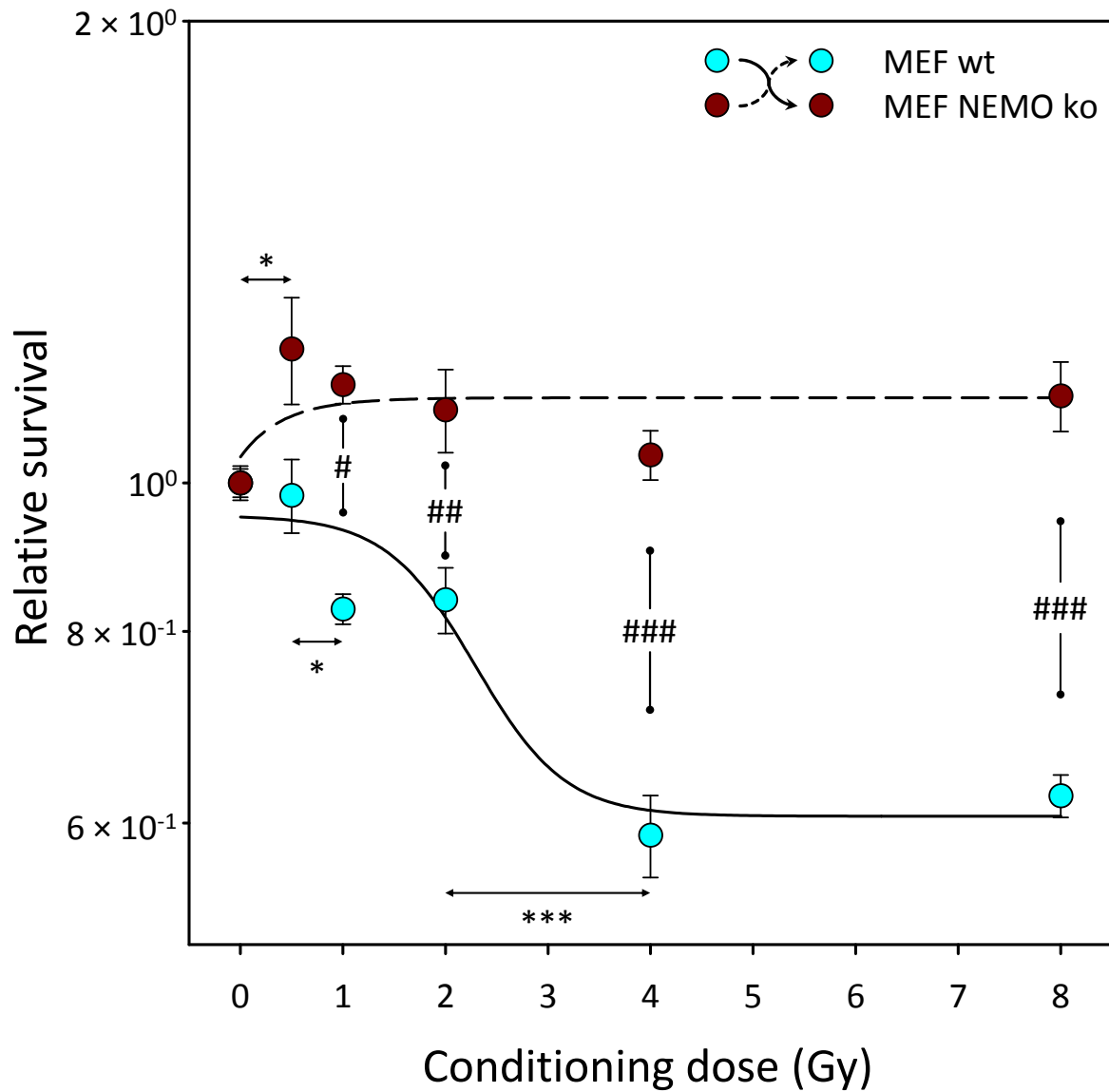


Figure 27 Cellular survival of MEF wt and NEMO ko cells after incubation with conditioned medium from the opposing cell type

Relative survival of MEF wt (cyan) and NEMO ko (dark red) cells after 24 h incubation with culture medium conditioned by the cell line of differing NF- κ B status (see Table 23) that was irradiated with X-ray doses up to 8 Gy. Clonogenic colonies were counted after 10 days and the surviving fraction was determined. Sigmoid regression lines (MEF wt: solid, MEF NEMO ko: long dash) are used to support the curve progressions. An asterisk (*) indicates significant difference compared to the preceding dose. A hashtag (#) indicates significant difference between cell lines. A minimum of 900 colonies were analyzed.

Mean \pm SE, n = 5-6 with six technical replicates in each experiment, * / # p < 0.05, ## p < 0.01, *** / ### p < 0.001.

Table 26 Survival of MEF wt and NEMO ko cells after incubation with conditioned medium from X-irradiated cells of the opposing cell line

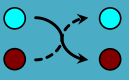
		MEF wt		MEF NEMO ko	
		Mean surviving fraction ± SE	p-value	Mean surviving fraction ± SE	p-value
Conditioning Dose (Gy)					
0	1.00 ± 0.03		1.00 ± 0.02		
0.5	0.98 ± 0.05	0.772	1.22 ± 0.10	0.044	
1	0.83 ± 0.02	0.022	1.16 ± 0.03	0.555	
2	0.84 ± 0.04	0.806	1.12 ± 0.07	0.586	
4	0.59 ± 0.04	< 0.001	1.04 ± 0.04	0.374	
8	0.63 ± 0.01	0.407	1.14 ± 0.06	0.189	

Table 27 Survival statistics for comparison of MEF wt and MEF NEMO ko cells after incubation with conditioned medium from X-irradiated cells of the opposing cell line

Conditioning Dose (Gy)	p-value MEF wt vs. MEF NEMO ko
0	
0.5	0.212
1	< 0.001
2	0.008
4	< 0.001
8	< 0.001

The overall survival curve shapes of MEF wt and MEF NEMO ko cells with alternating origin of conditioned medium were similar to the curves of the cell lines incubated with conditioned medium from the same cell line. Noticeable between those experiments was a shift of both survival curves towards a reduced survival.

The exact direction of the change after incubation with conditioned medium of an alternating origin cell line is given in Table 28 for each conditioning dose. At 0.5 Gy conditioning dose, survival of both cell lines did not significantly rise. At higher conditioning doses the survival was reduced. For MEF wt cells, the reduction in survival was significant only at 8 Gy conditioning dose, while in MEF NEMO ko cells the changes were significant at 1, 4 and 8 Gy conditioning dose. This shift hints at a balancing act between NF-κB-associated signaling and other bystander effect inducing factors regarding the cellular survival of MEF cells.

Table 28 Statistics for the comparison of the transfer schemes of conditioned medium to non-irradiated MEF wt and MEF NEMO ko cells based on the data shown in Table 24 to Table 26.

Conditioning Dose (Gy)	MEF wt		MEF NEMO ko	
	p-value	Direction of change	p-value	Direction of change
0				
0.5	0.772	↑	0.149	↑
1	0.291	↓	0.009	↓
2	0.062	↓	0.651	↓
4	0.354	↓	0.004	↓
8	0.045	↓	0.001	↓

5.2.3. Cellular senescence

As stated before, the nature of the colony forming ability assay permits only evaluation of dividing cells. Therefore, bystander cells that were previously not accounted for could result in the reduced survival of MEF cells, whilst being senescent and mitotically inactive. The stress-induced senescence of MEF wt and NEMO ko bystander cells was investigated by measuring the β -galactosidase activity at a pH of 6.0.

In Figure 28, representative images of brightfield microscopy at 20 \times magnification are shown. A slight blue coloration, signifying β -galactosidase cleavage of X-gal at pH 6.0, was discernable in both cell lines after bystander treatment with a conditioning dose of 8 Gy X-rays.

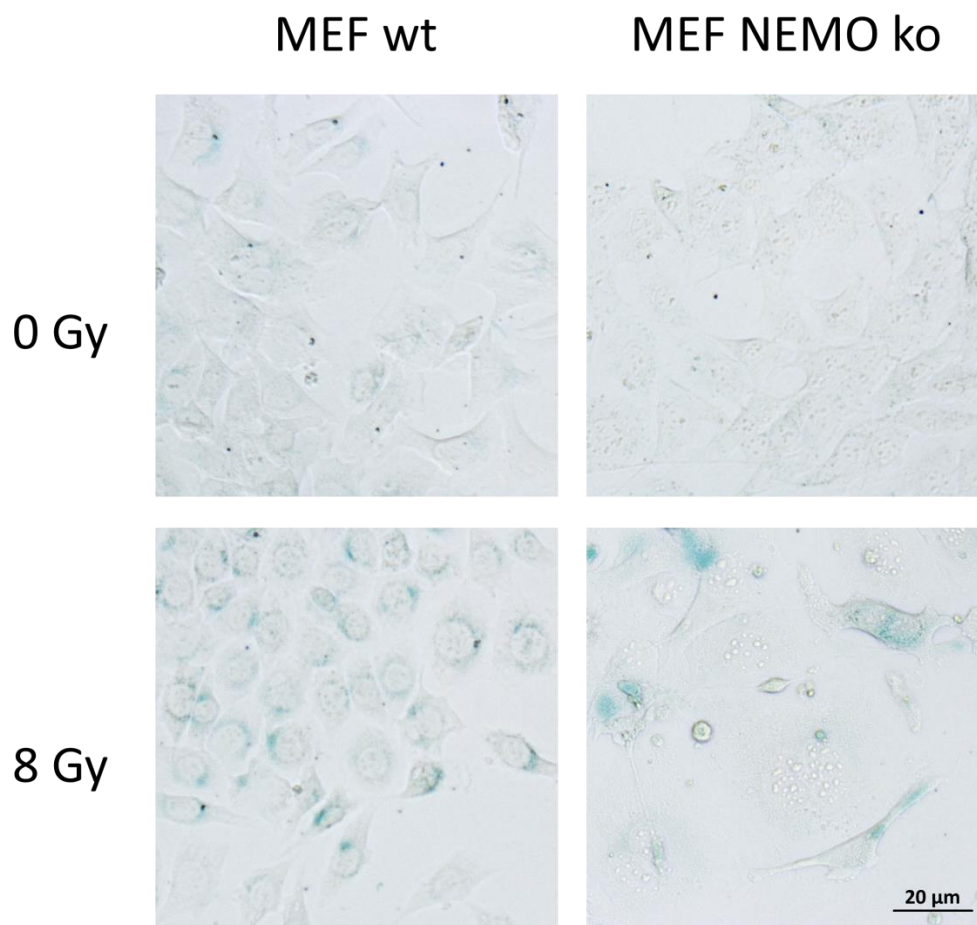


Figure 28 β -galactosidase activity after treatment with conditioned medium

Activity of β -galactosidase in MEF wt (left) and MEF NEMO ko (right) cells after 24 h incubation with culture medium conditioned by its respective cell line with different doses of X-rays. Cells were stained at pH 6.0 after 6 days of recovery in α -medium. Brightfield microscopy at 20 \times magnification.

Figure 29 and Table 29 show the relative activity of β -galactosidase of MEF wt and MEF NEMO ko cells incubated for 24 h with conditioned medium. β -galactosidase activity after exposure to 2 Gy conditioning dose medium did not significantly increase in MEF wt cells – compared to untreated cells. At conditioning doses of 4 and 8 Gy the relative β -galactosidase activity was significantly higher than in untreated cells. Relative β -galactosidase activity of MEF NEMO ko cells was elevated for conditioning doses of 2, 4 and 8 Gy compared to untreated cells. There was a significant difference in β -galactosidase activity for conditioning doses of 2 and 4 Gy but not for 8 Gy.

While the intensity of β -galactosidase activation was similar in both cell lines (MEF wt vs. MEF NEMO ko, 2Gy: $p = 0.32$, 4 Gy: $p = 0.38$, 8 Gy: $p = 0.43$), the signal distribution varied between the cell lines indicating an effect of the NF- κ B status.

Table 29 Relative β -galactosidase activity of MEF wt and MEF NEMO ko after treatment with conditioned medium from X-irradiated cells

Conditioning dose (Gy)	MEF wt		MEF NEMO ko	
	Mean \pm SE	p-value vs 0 Gy	Mean \pm SE	p-value vs 0 Gy
0	1.00 \pm 0.06		1.00 \pm 0.08	
2	1.21 \pm 0.09	0.137	1.54 \pm 0.13	0.003
4	1.46 \pm 0.12	0.019	1.72 \pm 0.15	< 0.001
8	1.40 \pm 0.09	0.004	1.50 \pm 0.16	0.068

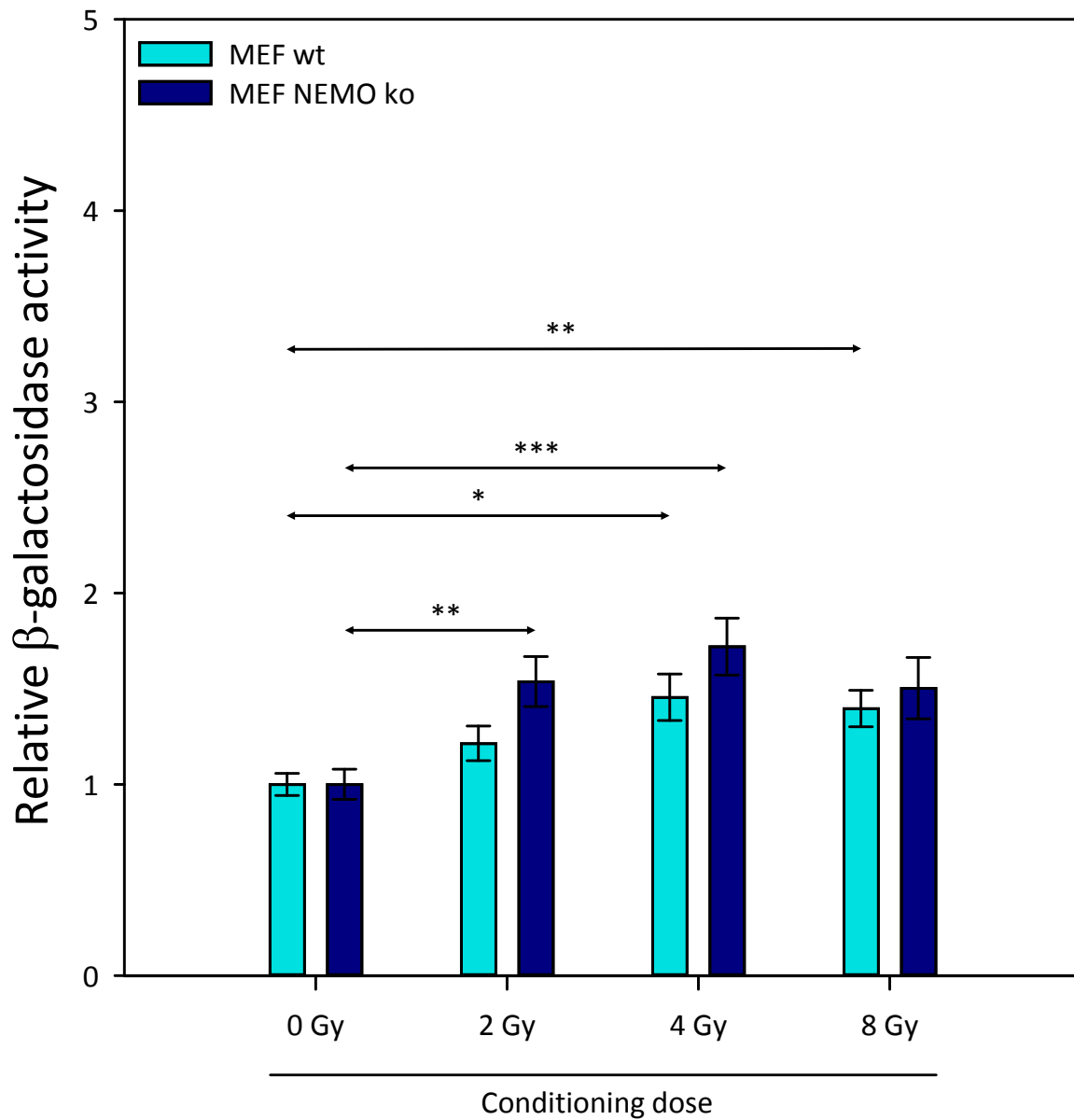


Figure 29 Relative cellular senescence after treatment with conditioned medium

Relative amount of β-galactosidase positive MEF wt (cyan) and MEF NEMO ko (dark blue) cells after 24 h incubation with culture medium conditioned by its respective cell line that was irradiated with different doses of X-rays. Cells were stained at pH 6.0 after 6 days of recovery in α-medium. An asterisk (*) indicates a significant difference compared to 0 Gy.

A minimum of 4300 cells were analyzed. Mean ± SE, n = 6, * p < 0.05, ** p < 0.01, *** p < 0.001.

5.2.4. Apoptosis and cell cycle progression

In order to investigate the nature of the cellular death of MEF cells after incubation with conditioned medium, the cellular DNA content was determined using PI staining and flow cytometric analysis. Induction of apoptosis in the cell is indicated by the amount of cells in sub-G1 portion of the cell cycle.

Figure 30 and Table 30 show the relative amount of MEF wt and NEMO ko cells with a sub-G1 DNA content over a time course of 48 h after incubation with conditioned medium. A conditioning dose of 8 Gy did not significantly change the small amount of sub-G1 cells of both cell lines.

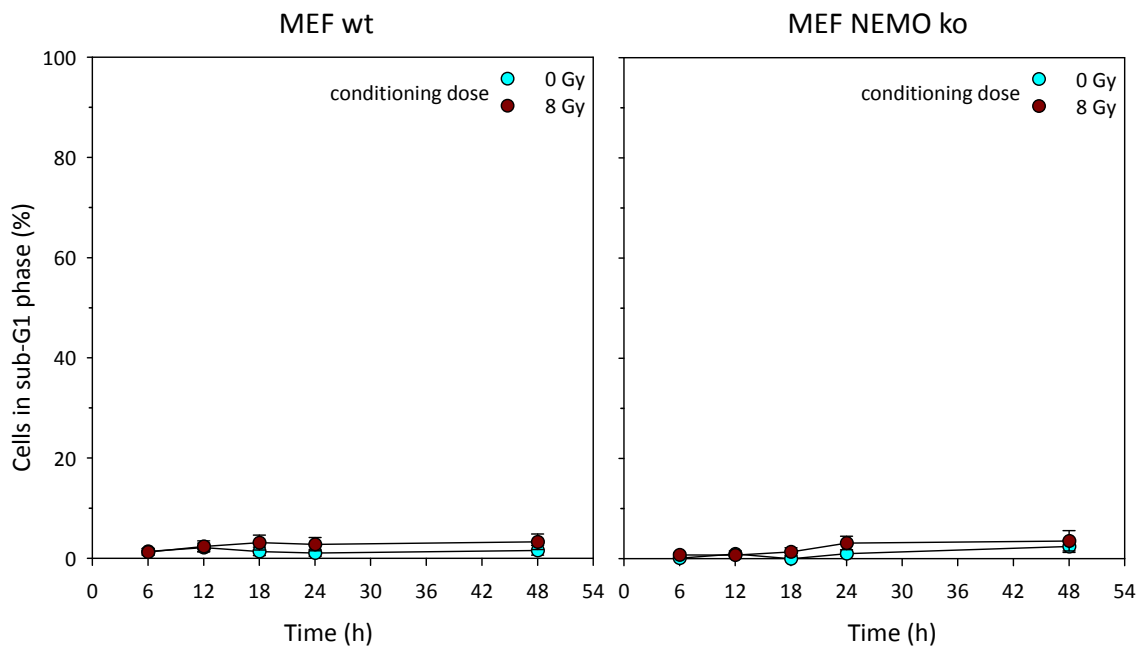


Figure 30 Percentage of cells with a sub-G1 DNA content after treatment with conditioned medium

Amount of MEF wt (left) and MEF NEMO ko (right) cells in sub-G1 cell cycle phase up to 48 h after incubation with conditioned medium at conditioning doses of 0 Gy (cyan) and 8 Gy (dark red). A minimum of 260'000 cells were analyzed. Mean \pm SE, n = 6.

Bystander treatment appeared to have no effect on the number of cells with sub-G1 DNA content indicating that MEF cells did not go into apoptosis after incubation with conditioned medium. Therefore, no further tests on apoptosis were performed.

Table 30 Percentage of MEF wt and MEF NEMO ko cells with sub-G1 DNA content up to 48 h after treatment with conditioned medium at a conditioning dose of 8 Gy.

Time (h)	MEF wt			MEF NEMO ko		
	Conditioning dose 0 Gy	Conditioning dose 8 Gy	p-value	Conditioning dose 0 Gy	Conditioning dose 8 Gy	p-value
6	1.38 ± 0.59	1.26 ± 0.66	0.878	0.12 ± 0.10	0.76 ± 0.44	1.000
12	2.45 ± 0.87	2.37 ± 1.08	0.824	0.95 ± 0.57	0.72 ± 0.39	0.105
18	2.42 ± 0.85	3.14 ± 1.49	0.234	0.01 ± 0.01	1.37 ± 0.78	0.093
24	2.14 ± 0.68	2.81 ± .131	0.076	1.02 ± 0.51	3.12 ± 1.35	0.279
48	2.74 ± 0.97	3.30 ± 1.56	0.397	2.44 ± 1.19	3.55 ± 2.02	0.382

The distribution of the cells in the G1-, S- and G2/M-phase of the cell cycle was analyzed to monitor cell cycle arrest induction as an indication for DNA damage inflicted by the soluble factors in conditioned medium.

Over a time course of 48 h after incubation with conditioned medium of a conditioning dose of 8 Gy, MEF wt and NEMO ko cells showed no significant change in distribution within the cell cycle phases, as seen in Figure 31 and Table 31.

With increasing time, the percentage of cells of both cell lines in G1-phase increased and in S and G2/M-phase decreased irrespective of the treatment modalities. This increase reflected the spatial limitations of the culture vessel and an associated contact growth inhibition.

Treatment of MEF cells with conditioned medium appeared to have no effect on the cell cycle progression, indicating that damage associated with bystander effects did not induce cell cycle arrests between 6 and 48 h after treatment and may have gone unnoticed.

Notably there were significant differences between the cell lines for both conditioning doses of 0 and 8 Gy (Table 32). MEF NEMO ko cells showed significantly less cells in G1-phase (0 Gy: 18 to 48 h, 8 Gy: 12 to 48 h) compared to MEF wt, and more cells in G2/M-phase (0 Gy: 12 and 24 h, 8 Gy: 18 to 48 h) over a time course of 48 h.

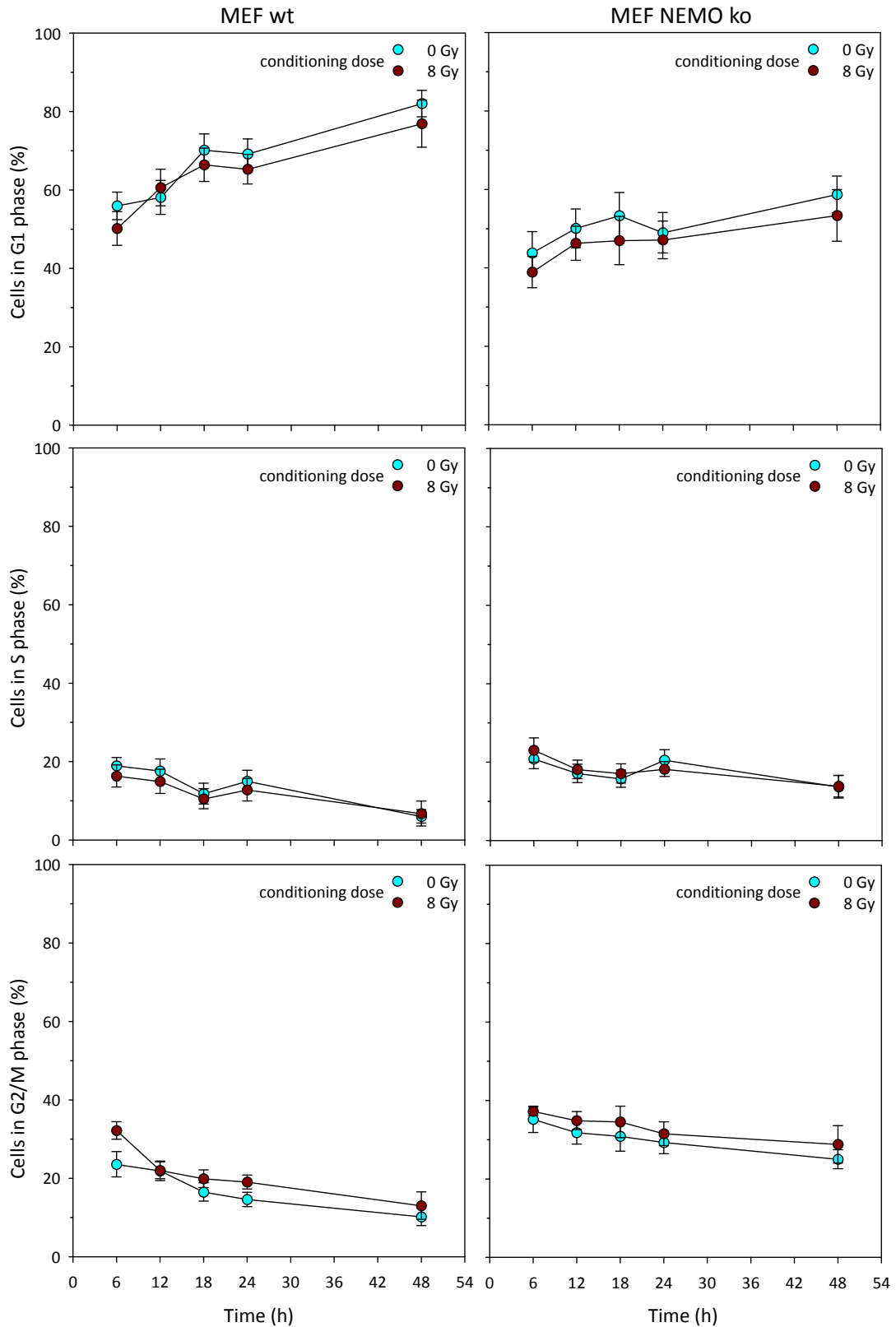


Figure 31 Cell cycle phase distribution after incubation with conditioned medium from X-irradiated cells

Amount of MEF wt (left) and MEF NEMO ko (right) cells in G1, S and G2/M cell cycle phases up to 48 h after incubation with conditioned medium at conditioning doses of 0 Gy (cyan) and 8 Gy (dark red). A minimum of 260'000 cells were analyzed. Mean \pm SE, n = 6.

Table 31 Percentage of MEF wt and MEF NEMO ko cells in G1, S and G2/M cell cycle phase up to 48 h after incubation with conditioned medium from X-irradiated cells (8 Gy).

		MEF wt			MEF NEMO ko		
		G1					
Time (h)	Conditioning dose		p-value	Conditioning dose		p-value	
	0 Gy	8 Gy		0 Gy	8 Gy		
6	55.95 ± 3.51	50.18 ± 4.29	0.340	43.84 ± 5.41	38.94 ± 3.99	0.687	
12	58.11 ± 4.33	60.63 ± 4.66	0.894	50.10 ± 4.94	46.30 ± 4.35	0.061	
18	70.15 ± 4.16	66.42 ± 4.26	0.442	53.33 ± 5.90	46.98 ± 6.18	0.842	
24	69.19 ± 3.85	65.30 ± 3.78	0.503	48.98 ± 5.15	47.15 ± 4.80	0.811	
48	82.03 ± 3.37	76.91 ± 6.02	0.463	58.74 ± 4.67	53.39 ± 6.57	0.505	

		MEF wt			MEF NEMO ko		
		S					
Time (h)	Conditioning dose		p-value	Conditioning dose		p-value	
	0 Gy	8 Gy		0 Gy	8 Gy		
6	18.96 ± 2.07	16.34 ± 2.83	0.505	20.84 ± 2.51	23.06 ± 3.10	0.745	
12	17.63 ± 3.05	14.96 ± 3.09	0.575	17.12 ± 2.35	18.13 ± 2.35	0.214	
18	11.85 ± 2.65	10.53 ± 2.57	0.798	15.78 ± 2.20	17.11 ± 2.44	0.374	
24	15.03 ± 2.76	12.83 ± 2.86	0.623	20.54 ± 2.61	18.22 ± 1.90	0.512	
48	6.02 ± 1.71	6.76 ± 3.18	0.613	13.70 ± 2.89	13.87 ± 2.76	0.974	

		MEF wt			MEF NEMO ko		
		G2/M					
Time (h)	Conditioning dose		p-value	Conditioning dose		p-value	
	0 Gy	8 Gy		0 Gy	8 Gy		
6	23.57 ± 3.22	32.21 ± 2.24	0.059	35.19 ± 3.34	37.24 ± 4.16	0.677	
12	21.90 ± 2.49	22.03 ± 2.16	0.969	31.79 ± 2.92	34.85 ± 2.31	0.190	
18	16.51 ± 2.33	19.90 ± 2.25	0.344	30.86 ± 3.80	34.54 ± 4.00	0.272	
24	14.61 ± 1.82	19.05 ± 1.77	0.114	29.30 ± 2.86	31.52 ± 3.04	0.627	
48	10.18 ± 2.24	13.03 ± 3.48	0.694	25.02 ± 2.41	28.81 ± 4.76	0.639	

Table 32 Error probability (p-value) for comparison of MEF wt and MEF NEMO ko cells in G1, S and G2/M cell cycle phase up to 48 h after incubation with conditioned medium from X-irradiated cells (8 Gy).

		Conditioning dose						
		0 Gy			8 Gy			
Time (h)	G1		S	G2/M		G1	S	G2/M
	0 Gy	8 Gy		0 Gy	8 Gy			
6	0.120	0.853	0.056	0.283	0.320	0.276		
12	0.273	0.904	0.030	0.005	0.398	0.969		
18	0.028	0.770	0.153	0.029	0.120	0.009		
24	0.008	0.198	< 0.001	0.015	0.179	0.007		
48	0.003	0.127	0.065	0.021	0.265	0.109		

5.2.5. DNA damage

As mentioned before, DNA DSB are the most detrimental form of DNA damage, potentially leading to chromosomal aberrations and/or to loss of genomic material.

In order to investigate the damage potential of bystander treatment in view of NF- κ B involvement, the amount of γ H2AX foci in MEF wt and NEMO ko cells was assessed after incubation with conditioned medium from X-irradiated cells of the same cell type as depicted in Table 33 and Figure 32. The statistical evaluation is shown in Table 34 and Table 35.

In MEF wt cells, 1 h after treatment with conditioned medium, the number of γ H2AX foci increased significantly with increasing dose for the conditioning doses 2 and 4 Gy. A conditioning dose of 8 Gy induced a lower amount of foci compared to treatment with 0 Gy conditioning dose medium but the difference was not significant. After 4 h, the γ H2AX foci induced by treatment with 2 Gy conditioning dose medium were not significantly more numerous than the 0 Gy conditioning dose treated control. For 4 and 8 Gy, the amount of foci increased significantly with dose. Bystander treatment resulted in varying amounts of γ H2AX foci after 24 h. Compared to 0 Gy conditioning dose treatment, a 2 Gy conditioning dose induced a significantly increased amount of foci. A conditioning dose of 4 Gy generated a slightly lower number of foci, while a conditioning dose of 8 Gy resulted in a significantly increased γ H2AX response.

The number of γ H2AX foci of each dose showed a general trend towards foci reduction with increasing time, though exceptions were observed. After incubation with medium of 0 Gy conditioning dose, the amount of foci decreased significantly with time. The number of foci after treatment with 2 Gy conditioning dose medium decreased significantly only after 24 h. A conditioning dose of 4 Gy resulted in γ H2AX foci, which decreased with time similarly as after 0 Gy conditioning dose treatment. The amount of foci after 1 h treatment with 8 Gy conditioning dose was significantly lower than at later time points, showing a similar strong increase after 4 h with subsequent foci reduction at 24 h.

The transfer of conditioned medium onto non-irradiated cells appeared to stress the cells. This cellular stress was represented in the amount of DNA DSB at different time points after treatment with a conditioning dose of 0 Gy. The reduction of foci with time indicates that the cells were actively repairing damage during that time. A dilutive effect of proliferating cells can also result in a reduction of the mean foci number over time.

MEF NEMO ko cells showed a fundamentally different behavior than wildtype cells regarding the γ H2AX response after treatment with conditioned medium. One hour after treatment with 4 Gy conditioned medium, the number of γ H2AX foci decreased significantly compared to the 0 Gy

conditioned medium treated control. Treatment with 8 Gy conditioned medium resulted in an amount of foci that was significantly lower than after 4 Gy conditioned medium treatment, yet notably not significantly lower than 0 Gy conditioned medium treatment. The number of γ H2AX foci 4 h after bystander treatment did not differ significantly amongst the applied conditioned doses. After 24 h, the number of foci increased slightly for treatment with 2 Gy conditioning dose and significantly further for treatment with 4 Gy conditioning dose. Treatment with 8 Gy conditioning dose induced foci up to a level not significantly different from 2 Gy conditioning dose treatment at that time point.

For all doses, the amount of foci rose significantly 4 h after treatment and dropped significantly after 24 h. Compared to 1 h, the 24 h time point showed a not significant reduction in foci number for 0 Gy conditioning dose and a significant increase for 4 and 8 Gy conditioning dose.

Numbers of γ H2AX foci between MEF wt and MEF NEMO ko cells showed significant differences for all conditioning doses and time points ($p < 0.001$). This resulted in distinct patterns regarding DNA DSB induction depending on the NF- κ B status of the bystander cell.

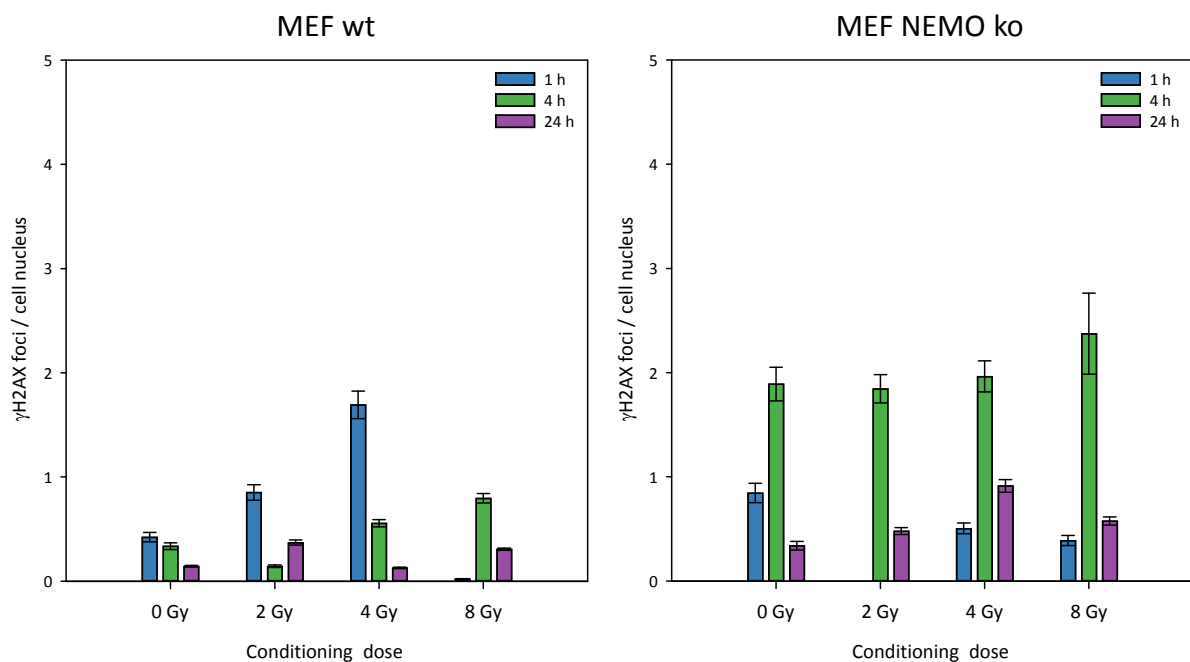


Figure 32 γ H2AX foci per cell nucleus after treatment with conditioned medium from X-irradiated cells

Absolute number of γ H2AX foci per cell nucleus in MEF wt (left) and MEF NEMO ko (right) cells at different time points after bystander treatment with conditioning doses 2, 4 and 8 Gy. Cells on coverslips were fixed after 1 (blue), 4 (green) and 24 hours (purple) then stained for fluorescent. A minimum of 1000 cell nuclei were analyzed. Mean \pm SE, $n = 2-3$.

Table 33 Kinetics of γ H2AX foci (mean \pm SE) in MEF wt and MEF NEMO ko cells after treatment with conditioned medium from X-irradiated cells

		MEF wt				MEF NEMO ko			
		Conditioning dose (Gy)							
Time (h)		0	2	4	8	0	2	4	8
1		0.42 \pm 0.05	0.85 \pm 0.07	1.69 \pm 0.13	0.02 \pm 0.00	0.84 \pm 0.09		0.50 \pm 0.05	0.39 \pm 0.05
		0.34 \pm 0.03	0.14 \pm 0.01	0.56 \pm 0.04	0.80 \pm 0.05	1.89 \pm 0.16	1.84 \pm 0.14	1.96 \pm 0.15	2.37 \pm 0.39
4		0.14 \pm 0.01	0.37 \pm 0.01	0.13 \pm 0.01	0.31 \pm 0.01	0.34 \pm 0.04	0.48 \pm 0.03	0.91 \pm 0.06	0.58 \pm 0.04

Table 34 Error probability (p-value) between conditioning doses at different time points for γ H2AX foci in MEF wt and MEF NEMO ko cells after treatment with conditioned medium from X-irradiated cells

1 h		MEF wt				MEF NEMO ko			
		Conditioning Dose (Gy)							
Dose (Gy)		0	2	4	8	0	2	4	8
0									
2		< 0.001							
4		< 0.001	< 0.001			< 0.001			
8		0.319	< 0.001	< 0.001		0.856		0.026	
4 h		Conditioning Dose (Gy)							
Dose (Gy)		0	2	4	8	0	2	4	8
0									
2		0.087				0.162			
4		< 0.001	< 0.001			0.670	0.319		
8		< 0.001	< 0.001	< 0.001		0.608	0.370	0.932	
24 h		Conditioning Dose (Gy)							
Dose (Gy)		0	2	4	8	0	2	4	8
0									
2		< 0.001				< 0.001			
4		0.008	< 0.001			< 0.001	< 0.001		
8		< 0.001	< 0.001	< 0.001		< 0.001	0.288	< 0.001	

Table 35 Error probability (p-value) between time points for different conditioning doses regarding γ H2AX foci in MEF wt and MEF NEMO ko cells after treatment with conditioned medium from X-irradiated cells

0 Gy		MEF wt			MEF NEMO ko		
		Time (h)					
Time (h)		1	4	24	1	4	24
1							
4		< 0.001			< 0.001		
24		< 0.001	0.013		0.938	< 0.001	
2 Gy		Time (h)					
Time (h)		1	4	24	1	4	24
1							
4		0.639					
24		< 0.001	< 0.001			< 0.001	
4 Gy		Time (h)					
Time (h)		1	4	24	1	4	24
1							
4		< 0.001			< 0.001		
24		< 0.001	< 0.001		< 0.001	< 0.001	
8 Gy		Time (h)					
Time (h)		1	4	24	1	4	24
1							
4		< 0.001			< 0.001		
24		< 0.001	< 0.001		< 0.001	< 0.001	

6. Discussion

6.1. Scientific approach

This work investigated the role of the transcription factor NF- κ B in the radiation response of directly irradiated cells and of cells treated with conditioned medium of radiation exposed cells. Genetically impeding NF- κ B activation by removal of NEMO enables a mechanistic analysis of the NF- κ B signaling pathway (SCHMIDT-SUPPRIAN et al., 2000). For that reason a knock-out cell culture model was chosen. MEF NEMO ko cells are NF- κ B (-) due to the removal of NEMO, one of the main components of the NF- κ B signaling cascade (ADHIKARI et al., 2007; COURTOIS, FAUVARQUE, 2018; MAUBACH et al., 2017; MCCOOL, MIYAMOTO, 2012; WANG et al., 2017b). Studies of molecular mechanisms using pharmacological inhibition suffer a series of limitations: degree of inhibition efficiency, specificity to the target protein, potential interactions with secondary targets, and toxicity of the compound (KNIGHT, SHOKAT, 2007). Several inhibitors of NF- κ B have been tested for efficiency and cytotoxicity before (HELLWEG et al., 2009). The most promising of those substances was MG-132, a proteasome inhibitor that enables NF- κ B cytoplasmic retention through I κ B. The target specificity on the other hand made MG-132 unsuitable for investigation of NF- κ B-dependent mechanisms, as the proteasome plays a role in many cellular processes. Another substance, BMS-345541, inhibits IKK and thereby blocks NF- κ B activity similar to the NEMO ko model (BURKE et al., 2003; WU et al., 2011; YANG et al., 2006). Preliminary tests showed effective inhibition of NF- κ B at 10 μ M BMS-345541, but long incubation times, necessary for the study of the radiation-induced bystander effect, increased the cytotoxicity of the compound to levels that rendered the use of BMS-345541 in future experiments inapplicable (data not shown).

6.2. The role of NF- κ B in the cellular radiation response

6.2.1. Survival after exposure to X-rays

A first assessment of the cellular response to direct radiation exposure was the study of clonogenic survival after X-irradiation. The time point of plating for the colony forming assay determines the duration of DNA repair after damage induction, as only successfully repaired cells will form colonies (FRANKEN et al., 2004; VAN OORSCHOT et al., 2014).

In this work, the survival was compared for MEF wt and NEMO ko cells, plated immediately and 24 h after X-irradiation. MEF wt cells have been previously shown to exhibit a similar survival after radiation injury as seen in Figure 16, with no difference between the plating times (DONG et al., 2018; TOKUYAMA et al., 2015; VEUGER et al., 2009; VON HOLZEN et al., 2007). Clonogenic survival of

MEF NEMO ko cells (Figure 17) appeared to be unaffected by repair times, similar to MEF wt. When comparing both cell lines, a difference became apparent for the samples immediately plated after X-irradiation (Figure 18) and samples plated 24 h post-irradiation (Figure 19). MEF NEMO ko cells were more sensitive to low radiation doses than the wildtype as previously shown in a MEF p65^{-/-} model (VEUGER et al., 2009), but were less susceptible to a high dose of 8 Gy compared with wildtype. Knock-down, knock-out and chemical inhibition of NF-κB was reported to sensitize cells to IR (DONG et al., 2015; ESTABROOK et al., 2011; HELLWEG et al., 2018; MENDONCA et al., 2017; REN et al., 2017; RUSSO et al., 2001; TSOLOU et al., 2017; VEUGER et al., 2009; WANG et al., 1996; WATSON et al., 2009; WU et al., 2011). The improved survival of MEF NEMO ko cells at 8 Gy may be attributed to the mesenchymal heritage of MEF cells, which appeared to be generally more resistant to X-irradiation than epithelial cells. This dissent cannot be fully resolved as earlier studies assessed survival only at lower doses (DONG et al., 2018; DONG et al., 2015; MENDONCA et al., 2017; RUSSO et al., 2001; VEUGER et al., 2009; VON HOLZEN et al., 2007; WANG et al., 1996; WATSON et al., 2009; WU et al., 2011).

6.2.2. Premature senescence induction by X-irradiation

Cellular survival assessment using the colony forming assay established by Puck et al. (PUCK, MARCUS, 1956; PUCK et al., 1957) does not reflect on the manner of the loss of further mitotic divisions. Therefore, not only cell death but also other cell fates such as premature senescence need to be taken into account.

In this work, the induction of premature senescence was assessed by measuring the increase in β-galactosidase activity at pH 6.0 (DEBACQ-CHAINIAUX et al., 2010; LEE et al., 2006). As described before, the chemical topoisomerase II inhibitor etoposide increased β-galactosidase activity in MEF cells (YANG et al., 2017a). Loss of NF-κB sensitized cells to senesce due to etoposide treatment as shown in Figure 21 and Figure 20, which confirms results that have been achieved using chemical inhibition of NF-κB. In that study, the transcription factor was surmised to counteract DNA damage-induced cytotoxicity by expressing anti-apoptotic signaling molecules (LI et al., 2017).

Exposure to X-rays induced premature cellular senescence measured by β-galactosidase staining as well as expression of p16^{INK4a} (CORREIA-MELO et al., 2016; PALACIO et al., 2017; ZHANG et al., 2016). Mechanistically, IR induces DNA damage that lead to the stabilization and subsequent activation of the tumor suppressor p53. Downstream of p53 activation, the arrest of the cell cycle involves p21 for the inactivation of cell cycle regulators such as cyclin E-CDK2 complexes (LI et al., 2018; RODIER et al., 2009). This transient arrest can become permanent and is marked by increasing levels of p16^{INK4a} and

β -galactosidase while levels of p21 and p53 decline (JONES et al., 2005; LI et al., 2018; MAIER et al., 2016; WANG et al., 2016b). A dose-dependent increase of senescence-associated parameters follows the rationale that more DNA damage increases the amount of activated p53 and downstream targets. Such dose dependence of premature senescence has been reported before in epithelial cell lines A549 and H460 (HE et al., 2017). In MCR-5, HCA-2 cells and WI-38 human fibroblasts, an increase in senescence induction has been found that was absent at lower doses similar to the results achieved with the wildtype MEF in this work (Figure 21 and Figure 20) (KOLLAROVIC et al., 2016; MARTHANDAN et al., 2016; RODIER et al., 2009; SAKAI et al., 2018).

A stronger and dose-dependent increase in senescence induction after exposure to X-rays and etoposide was found for NF- κ B (-) cells (Figure 21 and Figure 20). Genetic knock-out of *nfkb1* has been reported to increase senescence after exposure to 10 Gy X-rays in mouse fibroblasts as well as a SASP that was linked to COX-2-induced ROS production (JURK et al., 2014). Another study showed decreased radiation-induced senescence in HUVEC treated with the NEMO inhibitor PS1145, which is able to block I κ B phosphorylation (DONG et al., 2015; YEMELYANOV et al., 2006). This indicates a cell type specific involvement of NF- κ B in the induction of premature senescence in response to radiation exposure.

Senescent cells are metabolically active and can secrete signaling factors. Increased glycolysis as well as SASP have been linked to NF- κ B and downstream targets such as the cytokines IL-6 and TNF- α (FERRAND et al., 2015; FREUND et al., 2011; LI et al., 2018; LIAO et al., 2014; ORJALO et al., 2009). The activity of NF- κ B and subsequent secretion of SASP-associated factors can be regulated by p38MAPK and the transcription factor GATA binding protein 4 (GATA4) (KANG et al., 2015). Senescence induced by exposure to 10 Gy X-rays was accompanied by activation of p38MAPK in fibroblasts (FREUND et al., 2011). The activation of the kinase is sufficient to induce SASP and was found to regulate NF- κ B activation in radiation-induced senescent cells (FREUND et al., 2011; KANG et al., 2015). Activation of p38MAPK is linked to p21 signaling, which is initiated via DNA damage and leads to mitochondrial dysfunction and ROS production. These ROS are part of a continuous DDR-signaling furthering the activation of p21 and henceforth p38MAPK, creating a signaling loop that causes a sustained growth arrest (NELSON et al., 2018; PASSOS et al., 2010). This feedback loop could lead to a continuous activation of NF- κ B via p38MAPK and therefore sustain a secretory phenotype in senescent cells. Additionally, GATA4 can induce senescence and the NF- κ B-associated SASP independent of p21 or p16 (KANG et al., 2015).

Besides the ubiquitin-proteasome pathway, autophagy is one of the major eukaryotic pathways for protein degradation (KANG et al., 2015). The highly conserved protein p62 binds damaged cell organelles such as dysfunctional mitochondria and targets them for degradation via the autophagy-

lysosome, a process termed mitophagy. NF- κ B activation leads to an upregulation of p62 and the associated mitophagy (ZHONG et al., 2016), and depletion of p62 has been found to increase senescence (KANG et al., 2015). Incapacitating NF- κ B activation in this work resulted in increased senescence (Figure 16 and 17). Mechanistically, the lack of NF- κ B activation might have disturbed the removal of dysfunctional mitochondria via the p62-associated autophagy pathway. Accumulating damaged mitochondria would have led to ROS production and DDR-signaling that could have resulted in perpetual senescence via the above mentioned p21/p38MAPK feedback loop. GATA4 was shown to be degraded in a p62-associated manner (KANG et al., 2015). In NF- κ B (-) cells, the signaling via GATA4 is unimpeded may additionally have strengthened the senescence response.

6.2.3. Apoptosis after exposure to X-rays

Apoptotic cells with cleaved DNA can be distinguished via flow cytometry measuring DNA content in form of a subpopulation with sub-G1 DNA content (KAJSTURA et al., 2007; LI, YAN, 2018). Other methods for apoptosis detection include Annexin V staining of phosphatidylserine on the surface of apoptotic cells and TUNEL staining (terminal deoxynucleotidyl transferase dUTP nick end labeling) of fragmented DNA (XIONG et al., 2015; YANG et al., 2017b).

The apoptotic response to IR is highly dependent on cell type. Hematopoietic (U973, IM-9) and umbilical vein endothelial cells (HUVEC) showed a strong apoptotic response to IR (EOM et al., 2017; KIM et al., 2015b; PARK et al., 2009; WU et al., 2019; WU et al., 2014). A weak radiation-apoptosis response has been observed in hepatocytes. Epithelial cells (A549, MCF7 and ARPE) were shown to respond even weaker than hepatocytes *in vitro* (JIANG et al., 2004; LIU et al., 2017; MARTINEL LAMAS et al., 2015; WANG et al., 2017a; YANG et al., 2017b).

MEF cells in this work showed a lacking sub-G1 faction (Figure 22), which indicates absence of apoptosis. This result agrees with previous literature as MEF cells have been reported not to show apoptosis after exposure to doses below 10 Gy (BANERJEE et al., 2016; KASHIWAGI et al., 2018; KOLLAROVIC et al., 2016; PARK et al., 2000). It has been implied that fibroblasts and other non-hematopoietic cells such as epithelial cells go into senescence rather than undergoing apoptosis after exposure to moderate doses (up to 8 Gy) of IR (MIRZAYANS et al., 2013).

6.2.4. Cell cycle arrest after exposure to X-rays

Cells assess damage to the genome at DNA integrity checkpoints (VERMEULEN et al., 2003). Recognition of damage leads to the arrest of the cell cycle to enable DNA repair. Arrest at the G2/M checkpoint of the cell cycle is a prominent response to radiation exposure (CHEN et al., 2017; DONG et al., 2017; FURUSAWA et al., 2012; KIM et al., 2015a; QIAO et al., 2013; SMITH et al., 2016; YOU et al., 2014). In this work, MEF wt and MEF NEMO ko cells arrested at the G2/M checkpoint between 6 and 18 h post-irradiation and resume cell cycle progression 24 h after irradiation (Figure 23). These findings are supported by other studies, showing similar cell cycle arrest of MEF cells after irradiation (DONG et al., 2017).

Compared to MEF wt cells, the knockout of NEMO in MEF cells led to a stronger and earlier G2/M-arrest in response to IR (Figure 23). This supports reported evidence of NF- κ B involvement in cell cycle arrest induction stating that chemical inhibition of NF- κ B increased G2/M-arrest in human lymphoma cells (QIAO et al., 2013).

As described before, NF- κ B regulates cell cycle progression via expression of several proteins (see *NF- κ B-associated regulation of cell cycle progression*). Cyclin D, a NF- κ B target responsible for progression through G1-phase, was previously hypothesized not to affect a radiation-associated cell cycle response (SMITH et al., 2016). This notion is supported in this study by an early and increased G2/M-arrest in NF- κ B (-) cells (Figure 23). Rather, the cell cycle progression of NF- κ B dysfunctional MEF NEMO ko cells may be affected by cyclin A, and CDK, NF- κ B targets crucial for S-phase entry.

Furthermore, the CDK inhibitor p27, when bound to the cyclin A/CDK2 complex, blocks progression into S-phase. Upon radiation exposure, protein levels of p27 reportedly increased (CHEN et al., 2016), which coincides with radiation-induced G2/M-arrest observed in many cell lines (CHEN et al., 2017; DONG et al., 2017; FURUSAWA et al., 2012; KIM et al., 2015a; QIAO et al., 2013; SMITH et al., 2016; YOU et al., 2014). Increased expression of p27 can thus be associated with cell cycle arrest (CHEN et al., 2016). Proteasomal degradation of p27 releases the cyclin A/CDK2 complex and may be initiated by SKP2, which can be expressed in a NF- κ B-dependent manner (LEDOUX, PERKINS, 2014). Positive regulation of SKP2 protein levels thus promotes cell cycle progression. In response to IR SKP2 levels were found to be decreased, resulting in increased p27 levels and a subsequent G2/M-arrest (CHEN et al., 2016). MEF NEMO ko cells may lack a NF- κ B driven SKP2 expression limiting p27 degradation, which may have resulted in a stronger G2/M-arrest.

6.2.5. X-ray-induced DNA damage

DNA DSB were detected by immunofluorescence staining of the histone H2AX phosphorylated at S139, termed γ H2AX. Phosphorylation of H2AX is one of the first cellular responses to IR by ATM or DNA-PK at a range of 2Mbp around the DSB site (GOODWIN, KNUDSEN, 2014; JEZKOVA et al., 2018; LEE et al., 2018). Microscopically, γ H2AX manifests as foci within the cell nucleus that can be used as a marker for detection of DNA DSB after exposure to IR (ROGAKOU et al., 1998). Quantification of γ H2AX foci formation kinetics is an elegant assessment of cellular DSB repair capabilities: The decrease of γ H2AX foci after radiation exposure in a time-dependent manner indicates repair of the lesions (BEE et al., 2013; SUETENS et al., 2016; ZHANG et al., 2016).

The amount of DSB varies strongly between cell types, and detection via immunofluorescence reveals ranges between 1 and 40 foci per cell after 0.5 – 4 h post 1 Gy X-irradiation (ACHEVA et al., 2014; AHMED et al., 2017; BASELET et al., 2017; BEE et al., 2013; BOCK et al., 2013; COSTES et al., 2010; DI FRANCESCO et al., 2013; DONG et al., 2018; DONG et al., 2015; HERNANDEZ et al., 2013; IWABUCHI et al., 2006; KONG et al., 2018; LARGE et al., 2014; SUETENS et al., 2016; TEMELIE et al., 2018; WU et al., 2011).

In studies using MEF cells, the damage foci frequency was below 15 foci per Gy (AHMED et al., 2017; BOCK et al., 2013; DONG et al., 2018; TEMELIE et al., 2018). One study showed 10 foci per cell 1 h after radiation exposure with 5 Gy (DONG et al., 2018) which is similar to results from this work (Figure 24). A dose-dependent increase in γ H2AX foci in MEF wt cells as observed in this study has been reported before. The damage was repaired within 24 h, but high doses resulted in residual damage (BASELET et al., 2017; DONG et al., 2018).

Several studies found that inhibition of NF- κ B by chemical or genetic modulation impedes DSB repair. These studies showed retention of unrepaired damage for longer periods of time compared to the mock-inhibited controls (DE LAVAL et al., 2014; ESTABROOK et al., 2011; KRAFT et al., 2015; VOLCIC et al., 2012; WANG et al., 2009; WU et al., 2011). Similarly, MEF NEMO ko cells showed increased DSB foci formation after exposure to X-rays, which were repaired after 24 h (Figure 24). This indicates that DNA repair is only partially affected by NF- κ B inactivation and that a delayed repair of the damage is accomplished via alternative repair mechanisms.

In general, the homologous recombination repair pathway is strongly affected by NF- κ B modulation. NF- κ B-dependent transcription of BRCA2 and ATM stimulates the HR pathway, whereas direct interaction of p65 with the CtIP/BRCA1 complex promotes DNA end processing necessary for successful HR repair (VOLCIC et al., 2012). While NF- κ B can transcriptionally regulate Ku70 and Ku80

expression, thereby promoting NHEJ repair as well as HR, inhibition of NF- κ B resulted in stronger suppression of HR repair (LIM et al., 2002; VOLCIC et al., 2012).

6.2.6. The role of NF- κ B after direct exposure to ionizing radiation

The transcription factor NF- κ B is a prominent regulator in the DDR. Cells lacking NF- κ B were more sensitive to radiation-induced effects like reduction of clonogenic survival, induction of premature senescence, cell cycle arrest and DNA damage repair. The mechanistic connection of these endpoints can be further analyzed with the MEF NEMO ko *in vitro* model.

Residual DSB seen in MEF wt and NEMO ko cells after 24 h may correlate with the induction of cellular senescence as a consequence of irreparable damage and therefore constitutive induction of cell cycle arrest signaling (RODIER et al., 2009).

NF- κ B and p53 co-regulate cell cycle-associated signaling and senescence induction (LOWE et al., 2014; RUFINI et al., 2013; WEBSTER, PERKINS, 1999). Enhanced senescence induction in NF- κ B (-) cells and the effect of NF- κ B inhibition on cell cycle regulation and repair response may be attributed to an increased role of p53 signaling.

Furthermore, the role of NF- κ B in the SASP highlights the importance of the transcription factor in intercellular signaling. Therefore NF- κ B is a potential candidate to modulate or even induce RIBE.

6.3. The role of NF- κ B in the radiation-induced bystander response

The effects of radiation-induced signaling in non-irradiated cells can be elicited via secretion of soluble factors and extracellular vesicles into the surrounding environment. Surface receptors on neighboring cells can bind the appropriate ligands and induce a humoral response, while extracellular vesicles can be taken up via endocytosis and modulate the bystander cells depending on their composition. In this work, non-irradiated MEF wt and MEF NEMO ko cells were treated with culture medium conditioned by irradiated cells for 24 h in order to study the effect of NF- κ B on the radiation-induced bystander response.

6.3.1. Activation of NF- κ B in irradiated and bystander cells

The transcription factor NF- κ B is a dimeric complex with DNA binding activity to κ B-response-elements on target genes that encode proteins for regulation of intracellular processes and intercellular communication. The NF- κ B target gene products acting within the cell affect processes including the cell cycle, senescence, oxidative metabolism and DNA repair. Cytokines under NF- κ B control like IL-1, IL-6 and TNF- α are essential for communication with surrounding cells. The inactive cytoplasmic NF- κ B dimer is bound to I κ B, which masks the nuclear translocation sequence. Upon stimulation, I κ B is phosphorylated and subsequently marked with poly-ubiquitination for proteasomal degradation. Without I κ B, the transcription factor is free to translocate into the nucleus and bind to target gene promoters (DIDONATO et al., 2012; FERRAND et al., 2015; HEI et al., 2008; HELLWEG, 2015; HELLWEG et al., 2011; HELLWEG et al., 2018; KRAFT et al., 2015; LEDOUX, PERKINS, 2014; LI, VERMA, 2002; LI et al., 2017; ORJALO et al., 2009; VOLCIC et al., 2012; YU et al., 2017; ZHONG et al., 2016).

The activating NF- κ B subunit p65 is associated with transcription of pro-inflammatory target genes (HELLWEG et al., 2018). Immunofluorescence-based detection of p65 in the nucleus can be used for measurement of NF- κ B activity (ZHU et al., 2015).

In this work, MEF wt cells were treated with X-rays, conditioned medium and the NF- κ B activators TNF- α and LPS in order to analyze the NF- κ B response. MEF wt cells showed an increase in NF- κ B activation upon chemical stimulation via TNF- α and LPS (Figure 25). Activation of NF- κ B by TNF- α and LPS has been reported to occur via the canonical pathway (BANNERMAN et al., 2004; BANNERMAN et al., 2002; HELLWEG et al., 2018; JANUS et al., 2018; MARTINCUKS et al., 2017; O'DEA, HOFFMANN, 2009; WU et al., 2015; ZHU et al., 2015). Exposure to X-rays activated NF- κ B to a higher degree than chemical stimulation (Figure 25). IR was reported to activate NF- κ B via the genotoxic stress-induced pathway (HELLWEG et al., 2016; HELLWEG et al., 2018; JANUS et al., 2018; VEUGER et al., 2009).

The X-ray-induced increase of NF- κ B activation implies a stronger response of MEF wt cells to genotoxic stimulation compared to canonical activation of the signaling pathway. Moreover treatment of MEF wt cells with conditioned medium also increased NF- κ B activation, proving the *in vitro* model to be applicable for investigation of RIBE (Figure 25).

It has been shown that transfer of conditioned medium as well as co-culture with irradiated cells activates NF- κ B in a bystander-associated manner in several cell types including A549, H460, MCF7, HCT116 cells, HUVECs, MDA-MB-231 breast cancer cells, normal human lung fibroblasts, human skin fibroblasts and AG1522 fibroblasts. After irradiating these cells with 3 - 30 mGy alpha-particles or 0 - 8 Gy X-rays, NF- κ B activation was assessed via DNA-binding of NF- κ B, p65 translocation and I κ B α phosphorylation (AZZAM et al., 2002; IVANOV et al., 2010; LIAO et al., 2014; SHAREEF et al., 2007; WIDEL et al., 2015; YU et al., 2017; ZHOU et al., 2008). The NF- κ B response of MEF wt cells to conditioned medium was weaker compared to chemical or X-ray stimulation of the cell (Figure 25).

Conditioning by irradiated cells adds a mixture of factors to the culture medium that can induce the NF- κ B bystander response via both humoral and genotoxic pathways. After exposure to IR, NF- κ B is involved in regulating the release of pro-inflammatory cytokines such as IL-6, IL-1 β , IL-8 and TNF- α , which subsequently can stimulate NF- κ B activation in non-irradiated cells. Additionally, the composition of conditioned medium includes DAMPs and extracellular vesicle contents, which are regulated by NF- κ B and moreover can themselves activate NF- κ B (BOTT et al., 2017; KOSTJUK et al., 2012; KWAK et al., 2015; WANG et al., 2016a; WEI et al., 2014; WU et al., 2018; YANG, WANG, 2016; YE et al., 2017; ZHANG et al., 2014). Extracellular vesicles may also contain miRNA and oxidative metabolites that produce DNA damage, which in turn can activate NF- κ B via the genotoxic pathway (AL-MAYAH et al., 2012; CHISHTI et al., 2018; DESAI et al., 2013; DIEGELER, HELLWEG, 2017; ERMAKOV et al., 2013; HELLWEG et al., 2018; JANUS et al., 2018; KONG et al., 2018; MO et al., 2018; NELSON et al., 2018; PASI et al., 2010; RASTOGI et al., 2018; SCHAUE et al., 2012; SHAN et al., 2007; SHAO et al., 2003; SHAREEF et al., 2007; WANG et al., 2016a; WIDEL et al., 2015).

Activation of NF- κ B in bystander cells creates a feedback loop, which further activates NF- κ B and therefore regulates the strength of the bystander response.

6.3.2. Survival after treatment with conditioned medium from irradiated cells

The study of cellular survival is not only highly relevant for cells directly exposed to IR, but also for cells subjected to conditioned medium from irradiated cells. A reduction in cellular survival is a hallmark for the cytotoxicity of any treatment. Studies investigating the RIBE on cellular survival *in vitro* found cytotoxic effects on bystander cells based on the intercellular communication between irradiated and non-irradiated cells (BELLONI et al., 2011; HANU et al., 2017; JELLA et al., 2013; LEWIS et al., 2001; LIU et al., 2006; SHAREEF et al., 2007; WIDEL et al., 2015; YOKOTA et al., 2015).

In order to understand the role of radiation dose in bystander cells, downstream consequences of direct radiation exposure need to be elucidated. While high dose irradiation is associated with cytotoxicity that correspond to a linear-quadratic dose-effect relationship, different studies indicated both beneficial and harmful effects of low dose irradiation (SHIBAMOTO, NAKAMURA, 2018). In case of beneficial effects of radiation exposure, termed radiation hormesis, low doses of ionizing radiation stimulate cells and tissues towards increased anti-oxidative responses, DNA repair and elimination of genomically damaged cells. This results in a radio-adaptive response, which is able to diminish cytotoxic effects of subsequent radiation exposure (SHARMA et al., 2019; SHIBAMOTO, NAKAMURA, 2018; SZUMIEL, 2012). On the other hand, reports of radiation hypersensitivity indicate increased cytotoxicity after exposure to low dose irradiation (MATSUYA et al., 2018; OLOBATUYI et al., 2017; PIOTROWSKI et al., 2017). Both radiation hormesis and hypersensitivity are suggested to depend on the genetic background of the cells and their inherent radiosensitivity (SHIBAMOTO, NAKAMURA, 2018).

The induction of RIBE relies on signaling factors produced by irradiated cells, which likely depends on both radiation dose and time after exposure. Pro-inflammatory cytokines such as IL-6 and TNF- α have been shown to increase in a dose-dependent manner and accumulation of the protein increases with time, but full scale dose-response curves and kinetics for all secreted factors have not yet been established (DESAI et al., 2013; JANUS et al., 2018; MARIOTTI et al., 2011; PASI et al., 2010; SCHAUE et al., 2012; WIDEL et al., 2015; YOKOTA et al., 2015). In this work, all cells were treated with medium that had been conditioned for 24 h, a time used by others for bystander induction (SHAREEF et al., 2007). Similar to previous reports, cellular survival of bystander MEF wt cells in this work has been found to correlate with a dose-threshold response (JELLA et al., 2013; LEWIS et al., 2001; LIU et al., 2006; MARIOTTI et al., 2012; MATSUYA et al., 2018; RYAN et al., 2008). A reduced survival of MEF wt cells was observed after treatment with conditioned medium of a conditioning dose above 2 Gy (Figure 26), which supports the notion that a certain dose is necessary for producing enough factors to induce a bystander response.

On the other hand, MEF NEMO ko bystander cells show a significantly improved survival compared to MEF wt cells (Figure 26). The difference in survival data implies a role of NF- κ B in the bystander response as a mediator of the release or the reception of the bystander signal. Soluble downstream targets of NF- κ B, such as TNF- α , IL-6, IL-8 and IL-33 expressed after radiation exposure are implicated in the induction of RIBE (DESAI et al., 2013; IVANOV et al., 2010; MARIOTTI et al., 2012; PASI et al., 2010; SHAREEF et al., 2007). The NF- κ B-regulated production of ROS via increased expression of COX-2 has also been associated with the induction of RIBE (CHAI et al., 2013; FARDID et al., 2017; FARHOOD et al., 2019; ZHOU et al., 2005). NF- κ B can additionally regulate intracellular signaling by transcription of surface receptors like CD40 and TNF receptor 1b or receptor-associated proteins like TRAF1/2 and cIAP1/2 (HINZ et al., 2001; SANTEE, OWEN-SCHAUB, 1996; WANG et al., 1998).

In order to test the importance of the NF- κ B status of irradiated and recipient cells, survival of bystander cells in this work was analyzed for MEF wt cells treated with conditioned medium of NF- κ B (-) cells and for MEF NEMO ko cells incubated with conditioned medium from irradiated wildtype MEF. Notably, the survival of bystander cells appeared to be independent of the NF- κ B status of the conditioning cells. Similar to previously mentioned results (Figure 26), MEF wt bystander cells in this work showed a threshold-associated reduction in survival, while a significantly better survival of MEF NEMO ko cells was observed after treatment with conditioned medium of NF- κ B (+) cells (Figure 27). This implies that NF- κ B-independent factors induce the detrimental RIBE. Oxidative stress or miRNA transmitted via extracellular vesicles might introduce DNA damage leading to the demise of bystander cells (FARHOOD et al., 2019; JELLA et al., 2014; KLAMMER et al., 2015; MO et al., 2018; RASTOGI et al., 2018; XU et al., 2015).

As one explanation for better survival of MEF NEMO ko versus wt bystander cells, cells without functional NF- κ B may not be able to amplify and propagate the signal. As mentioned before, RIBE-inducing factors can trigger NF- κ B activation in bystander cells via extracellular vesicle-mediated, receptor-associated and genotoxic pathways, which altogether leads to the production of more NF- κ B activating factors establishing a positive feedback loop. In contrast, NF- κ B (-) cells, receiving NF- κ B activating signals, might be unable to contribute to NF- κ B-associated signal propagation.

The NF- κ B-regulated autophagic cell death provides another possible explanation for increased survival of NF- κ B (-) bystander cells. While autophagy is an intracellular process to remove damaged organelles, excessive autophagy can lead to non-apoptotic cell death (YUAN et al., 2017). NF- κ B has been shown to regulate the expression of the autophagy marker p62 (ZHONG et al., 2016). Induction of RIBE may trigger an autophagic response that exceeds the mitigating role of autophagy. Without NF- κ B-regulated activation of autophagy, cells may thus be able to withstand excessive autophagy

and the resulting cell death. Autophagy has been shown to alleviate RIBE-induced damage at doses below a conditioning dose of 3 Gy (KONG et al., 2018; SONG et al., 2016; WANG et al., 2015). The reduced survival in NF- κ B (+) cells in this study manifested at 4 Gy (Figure 26 and Figure 27), so a higher conditioning dose may be necessary to induce excessive autophagy and the associated cell death.

The survival curves of MEF NEMO ko cells showed a slight increase after treatment with radiation-conditioned medium irrespective of the NF- κ B status of the conditioning cells (Figure 26 and Figure 27). An increase in survival most likely results from an increased plating efficiency caused by growth factors secreted into the conditioned medium. Moreover it may be accompanied by an increased seeding cell density, which would lead to a higher production of soluble factors (ADRIAN et al., 2018; TAKAHASHI, OKADA, 1970). The increase of survival in NF- κ B (-) bystander cells implies that the detrimental RIBE are antagonized by secreted survival-promoting factors. Radiation-associated exosomes as well as extracellular miR-1246 have been found to stimulate proliferation (MUTSCHELKNAUS et al., 2016; YUAN et al., 2016).

6.3.3. Senescence induction after treatment with conditioned medium from irradiated cells

The cellular demise after treatment with conditioned medium cannot be fully explored with clonogenic survival measurements, as the colony forming assay does not differentiate between non-proliferating live cells and dead cells.

Premature stress-induced senescence is induced in cells that undergo a prolonged cell cycle arrest, initiated via stress-induced p53 stabilization and subsequent upregulation of p16^{INK4}. These cells are metabolically active and secrete factors into the surrounding milieu for signaling and growth (MAIER et al., 2016). Senescence has been correlated with intracellular ROS production and ROS-associated DNA damage, which can initiate a p21/p16-mediated permanent cell cycle arrest and moreover modulate NF- κ B activation and production of downstream pro-inflammatory cytokines such as IL-6 and IL-8 (NELSON et al., 2018; SAWAL et al., 2017; WANG et al., 2016b). The SASP includes not only cytokines and soluble mediators, but also extracellular vesicles (KADOTA et al., 2018).

Signaling via secreted factors and oxidative stress factors produced after exposure to IR has been shown to induce senescence as a RIBE (POLESZCZUK et al., 2015; SAWAL et al., 2017; WIDEL et al., 2015). These findings are supported by this work, showing a slight senescence induction in MEF wt cells after treatment with conditioned medium of conditioning doses higher than 4 Gy (Figure 29).

NF- κ B is a regulator of the SASP (FERRAND et al., 2015). Activation of NF- κ B, in both irradiated and bystander cells, can initiate production of downstream targets of NF- κ B including pro-inflammatory cytokines like IL-6, IL-8, TNF- α . These factors are considered to be part of the SASP secretome and have been shown to induce senescence in bystander cells. The SASP factors are thought to initiate a ROS-induced DDR that results in premature senescence of bystander cells (HODNY et al., 2013; NELSON et al., 2018; NELSON et al., 2012; SAWAL et al., 2017). Besides cytokines, extracellular vesicles have been found to be secreted in response to senescence induction (KADOTA et al., 2018). Constituents of extracellular vesicles, like miRNA, can also modulate senescence induction by targeting various cell cycle-regulating proteins. Some miRNAs such as miR-34a, miR-22 or miR-128a can facilitate senescence induction by promoting the p53-pathway and the p16-pathway or interfering with the CDK/cyclin complexes. Other miRNAs such as miR24 or miR20a/b suppress senescence induction by inhibition of p21 or p16 (XU, TAHARA, 2013). Radiation exposure leads to increased expression of miR-34a, which has been reported to promote radiation-induced senescence induction (HE et al., 2017; LACOMBE, ZENHAUSERN, 2017).

MEF NEMO ko cells, in this work, showed a slight increase in senescence induction at conditioning doses higher than 2 Gy, similar in strength to MEF wt cells (Figure 29). The senescence response of bystander cells at a lower conditioning dose indicates that NF- κ B (-) cells were more sensitive to senescence induction. The cells that produced the RIBE-inducing factors were NF- κ B (-). Thus the factors inducing senescence in bystander cells such as the contents of extracellular vesicles or ROS were independent of NF- κ B.

After entry into a cell via endocytosis, extracellular vesicles can be incorporated in autolysosomes and be degraded in an autophagy-mediated manner (KADOTA et al., 2018). Autophagy via p62 can reportedly be regulated by NF- κ B (ZHONG et al., 2016). Cells with dysfunctional NF- κ B therefore lack p62-associated autophagy and cannot remove extracellular vesicles in such a manner. In bystander cells this lack of p62-associated autophagy may affect the induction of senescence via extracellular vesicles.

The transcription factor GATA4 can modify senescence independent of p21 or p16 signaling and has been shown to activate NF- κ B. Additionally GATA4 has been reported to be degraded via p62-mediated autophagy (KANG et al., 2015). GATA4 may therefore have contributed to RIBE-induced senescence in NF- κ B (-) cells.

6.3.4. Apoptosis in bystander cells

The stress-induced initiation of programmed cell death, apoptosis, is a protective mechanism for the cell-population. The removal of a potentially neoplastic cell from the population prevents formation of a tumor.

As mentioned before, the apoptotic response to cellular stresses depends on the particular cell type. Epithelial cells such as the A549, H460 and HCT116 cell lines show RIBE-associated induction of apoptosis (SHAREEF et al., 2007; WIDEL et al., 2015). MEF cells in this work did not show any indication of apoptosis after treatment with conditioned medium (Figure 30). Likewise, MEF cells were resistant to apoptosis induction even after exposure to high doses of IR and rather showed senescence as reported before (BANERJEE et al., 2016; KASHIWAGI et al., 2018; KOLLAROVIC et al., 2016; MIRZAYANS et al., 2013; PARK et al., 2000).

6.3.5. Cell cycle arrest in bystander cells

Changes in the distribution of cell cycle phases after stress induction indicate an arrest at one of the DNA damage checkpoints, necessary for repair of DNA lesions. Arrest at the G2/M checkpoint was observed after exposure to IR (VERMEULEN et al., 2003). Treatment with radiation-conditioned medium has been shown to induce a slight increase in the G2/M fraction of HaCaT and A549 cells. HaCaT cells showed a return to baseline distribution after 12 h, while the arrest in A549 lasted up to 72 h (JELLA et al., 2013; YANG et al., 2015). A549 cells exposed to IR remained arrested at the G2/M checkpoint longer than HaCaT cells (CHEN et al., 2017; JELLA et al., 2013). This implies that the cell cycle response to stresses is cell type-dependent. This work and others show that MEF cells resolved a cell cycle arrest within 24 h after direct exposure to doses of IR above 5 Gy (DONG et al., 2017). Damage induced before the G1 checkpoint is being repaired via fast repair pathways such as the NHEJ. A single DNA DSB has been shown to be sufficient to induce a transient G2/M-arrest that can be resolved within 6 h (VAN DEN BERG et al., 2018). In this work treatment with conditioned medium had no effect on cell cycle distribution of MEF cells (Figure 31). Data for cell cycle arrest were obtained 6 h after addition of conditioned medium. Detrimental RIBE factors may induce damage at a low frequency, which might be repaired faster than assessed in this work.

6.3.6. RIBE-induced DNA damage

The induction of DNA damage via factors transmitted from irradiated cells emphasizes the danger of RIBE. Mutations, chromosomal aberrations, formation of micronuclei with loss of genetic information can lead to neoplastic transformation of bystander cells (JELLA et al., 2018; SOKOLOV et al., 2007). DNA DSB are difficult to repair and imply that sections of DNA from the genome can be lost. Several studies found γ H2AX foci in bystander cells, indicating DNA DSB (JEZKOVA et al., 2018), as well as differential kinetics of foci persistence in different cell types (BURDAK-ROTHKAMM et al., 2015; KOBAYASHI et al., 2017; MO et al., 2018; SOKOLOV et al., 2005; WANG et al., 2017c; YANG et al., 2005). In T98G glioma cells and WI38 fibroblasts, γ H2AX foci increased steadily over 24 h. A549 bystander cells showed a time-dependent increase until 8 h after treatment that returned to a basal level after 16 h (BURDAK-ROTHKAMM et al., 2015; KOBAYASHI et al., 2017). MEF cells in this work showed different patterns of γ H2AX foci formation (Figure 32). The foci induced by treatment with conditioned medium were less frequent than those induced by X-irradiation (Figure 24), but a linear dose-response relationship for foci increase was not evident.

In MEF wt cells, conditioning doses up to 4 Gy led to an increased foci formation after 1 h but a conditioning dose of 8 Gy did not change the γ H2AX level (Figure 32). A dose-dependent response for 4 Gy and 8 Gy was observed 4 h after treatment similar to other studies (BURDAK-ROTHKAMM et al., 2015; KOBAYASHI et al., 2017). This implies a delay of the γ H2AX response at higher conditioning doses.

A study showed that the composition of extracellular vesicles, isolated 24 h after irradiation, was modified by radiation doses up to 8 Gy (ABRAMOWICZ et al., 2019). MEF wt bystander cells in this work were treated with conditioned medium for 24 h as well. This may indicate an effect of extracellular vesicles on the γ H2AX response.

After 1 h treatment MEF NEMO ko cells showed a reduction of γ H2AX foci at higher doses compared to a conditioning dose of 0 Gy (Figure 32). Because the conditioning medium requires a prolonged culture of cells, the culture medium gradually suffers nutrient depletion as well as accumulation of metabolic waste products including ROS (SPINELLI, HAIGIS, 2018). Bystander cells receiving the conditioned medium may thus have experienced stress from the medium transfer that may have led to the formation of DSB. On the other hand, high conditioning doses increased the cellular survival of MEF NEMO ko cells (Figure 26 and Figure 27), which may be ascribed to a reduced production of transmittable NF- κ B-dependent ROS in NF- κ B (-) donor cells (FARHOOD et al., 2019).

MEF NEMO ko cells showed no difference in γ H2AX foci formation at all conditioning doses 4 h after treatment (Figure 32). While at this time point the cells showed an increased amount of foci for all

the conditioning doses, the lack of a dose-dependent effect implies that NF- κ B-dependent damaging agents such as ROS were absent in MEF NEMO ko bystander cells.

For both MEF wt and MEF NEMO ko bystander cells, the temporal-pattern of γ H2AX foci formation is irregular for each dose (Figure 32), possibly due to factors secreted after treatment with the respective IR doses that induced temporally delayed damage in the target cells. Exosome composition can change as a function of the applied dose (ABRAMOWICZ et al., 2019; MUTSCHELKNAUS et al., 2017). Extracellular vesicle contents including miR-21, miR-1246 and miR-34c have been shown to induce DNA damage in bystander cells 24 h after incubation with radiation-modified extracellular vesicles (MO et al., 2018; RASTOGI et al., 2018; XU et al., 2015).

Differences in the response may also have been caused by varying distribution of damaged cells. Some studies show the DSB response as a percentage of γ H2AX-positive cells rather than foci/cell, because the bystander response is not affecting the cells uniformly, both in co-culture and medium transfer experimental setups (SOKOLOV et al., 2005; YANG et al., 2005). In this work the minimum amount of 1000 analyzed nuclei included cells with a high number of γ H2AX foci as well as undamaged cells as exemplary shown in Figure 33 for MEF wt bystander cells. The results display the arithmetic mean of those numbers. An analytic approach with regard to the distribution of damaged cells may provide further insight on the formation of bystander DSB in this cell model.

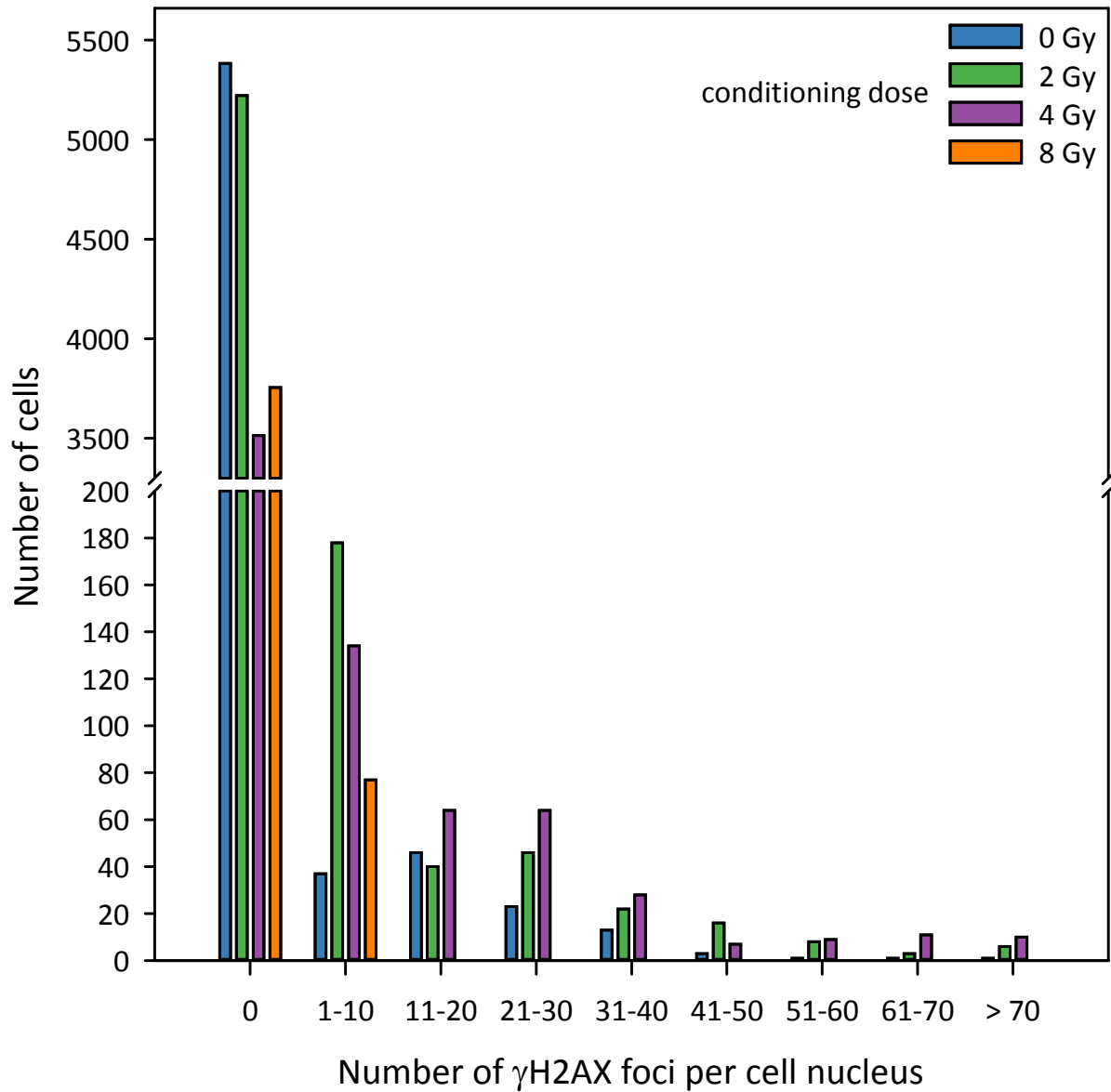


Figure 33 Distribution of γ H2AX foci per cell nucleus after treatment with conditioned medium from X-irradiated cells

Histogram of the number of cells as a function of the number of γ H2AX foci per nucleus for MEF wt cells one hour after bystander treatment with conditioning doses 0, 2, 4 and 8 Gy. Data were taken Figure 32 (left).

6.3.7. Summary of the role of NF- κ B in the radiation-induced bystander response

The transcription factor NF- κ B is involved in the regulation of many intra- and intercellular processes, like cell cycle regulation, DNA repair and inflammation. It is activated in irradiated cells and controls the radiation-associated secretome including cytokines, miRNAs, extracellular vesicles, and ROS.

Consequently, NF- κ B is also activated in bystander cells by the factors secreted in response to direct radiation exposure, including factors downstream of a NF- κ B radiation response. Because the factors initiated by NF- κ B are able to induce NF- κ B, a feedback loop is created that amplifies and propagates the bystander signal, which is shown schematically in Figure 34. In this work, it has been shown that NF- κ B-independent signaling factors can reduce the survival in cells with an intact NF- κ B pathway. Cells with dysfunctional NF- κ B on the other hand did not show bystander-associated cell death, which may be caused by dysregulated signal propagation or intracellular processes.

Additionally, NF- κ B has been shown to cause the induction of SIPS of bystander cells in this thesis. Treatment of bystander cells increased senescence irrespective of their NF- κ B status, but NF- κ B (-) cells were slightly sensitized to senescence induction. Of the other endpoints analyzed in this work, the cell cycle was not altered by treatment with conditioned medium, while DNA damage was induced in bystander cells. More work is required to understand the DNA damage in NF- κ B (-) bystander cells.

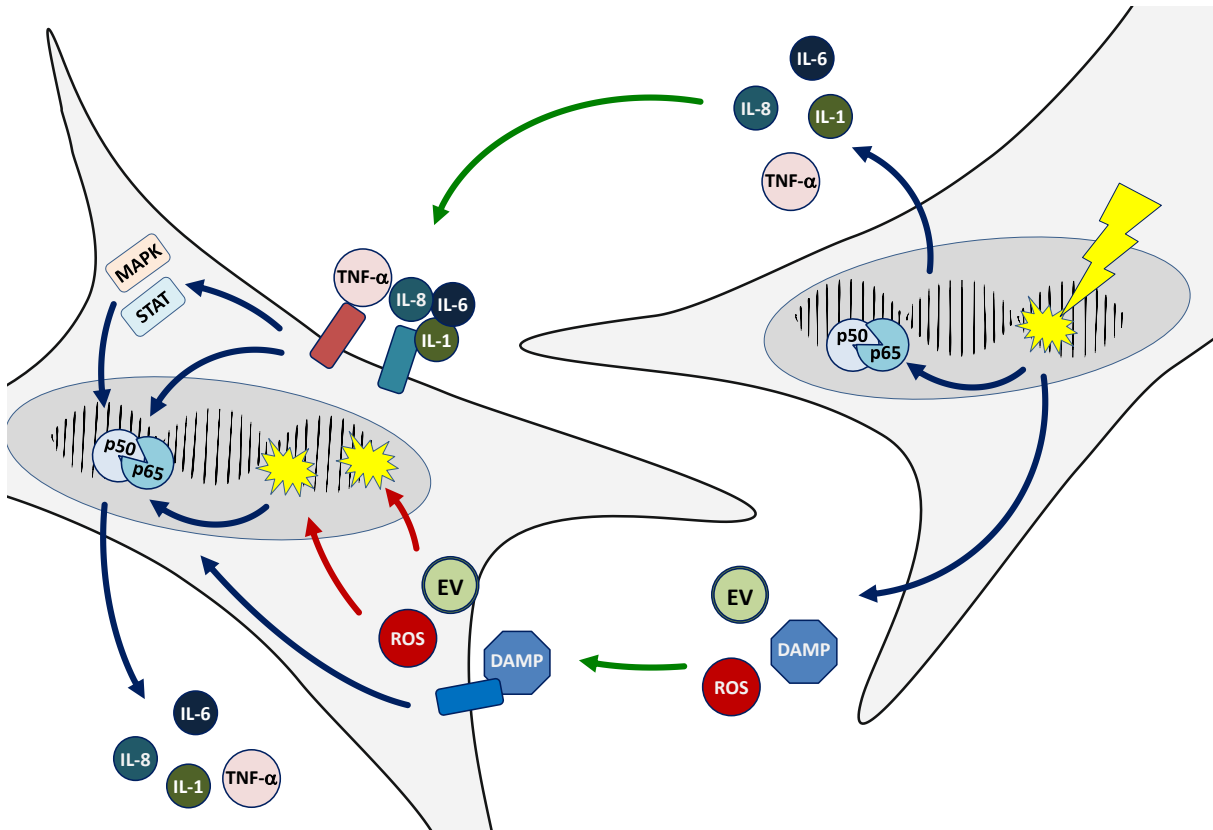


Figure 34 Scheme of the radiation-induced bystander signaling

DNA damage (yellow star) induced by ionizing radiation (yellow lightning) can lead to the production and secretion of signaling factors in an immediate or delayed manner. Immediate signals are damage-associated molecular patterns (DAMPs, light blue), reactive oxygen species (ROS, red) and extracellular vesicles (EV, light green). Damage-induced activation of transcription factors, such as NF- κ B (p65/p50 dimer), lead to a delayed expression and secretion of cytokines such as TNF- α (light pink) and interleukins (IL, blue and green). Green arrows indicate action of signaling factors onto bystander cells. DAMPs and extracellular vesicles bind to TLR (blue) or enter the cells like ROS. These factors may induce DNA damage (red arrow) or change responses to transcription factors. Cytokines bind to surface receptors of the bystander cell and trigger signaling pathways that lead to direct or indirect activation of transcription factors (via MAPK or STAT). In turn the transcription factors produce more cytokines to amplify the bystander signal.

6.4. Conclusion

The radiation-induced bystander effect can be generally viewed as an effect of the communication between radiation-damaged and healthy cells.

Damage in untreated cells is a risk factor for the formation of secondary tumors and other therapy-associated adverse effects like tissue necrosis and functional deficiencies. Induction of DNA DSB, senescence and of replicative cell death in bystander MEFs makes such risks plausible.

On the other hand, signaling factors secreted by the irradiated cells can recruit and activate immune cells, leading to immune responses. The amplification of bystander signals enhances the communication with the immune system and is partially responsible for the success of radiation therapies.

Elucidating the mechanisms behind intercellular communication is therefore an important goal in order to optimize therapies with immunogenic approaches for better protection of healthy tissue and more efficient elimination of tumors and metastases.

6.5. Outlook

Future research should focus on the distribution of damaged bystander cells within the population and include mechanistic models for DNA damage induction and repair involved in bystander signaling. Genetic knock-out of genes coding for proteins involved in repair pathways will highlight the pathway choice in damaged bystander cells whereas ROS-scavenging agents could narrow down the origin of detrimental bystander factors.

The exact nature of bystander inducing factors remains obscure. Secretome analyses of irradiated cells should include cytokines, chemokines, DAMPs as well as extracellular vesicles and their compositions in order to identify the variety of RIBE in tissues. Genetic ablation of receptors and chemical blockade of endocytosis in recipient cells will clarify the mechanisms of the bystander response.

Furthermore, cell models sensitive for apoptosis and bystander-induced cell cycle arrest should be implemented for mechanistic studies to fully elucidate the role of NF- κ B in RIBE.

7. Abbreviations

Description	Abbreviation
4',6-Diamidin-2-phenylindol	DAPI
5-bromo-4-chloro-3-indoyl-b-D-galactopyranoside	X-gal
Abasic sites	AP sites
Alexa Fluor 488	AF488
Alternate end-joining	Alt-EJ
AP endonuclease 1	APE1
Aprataxin	APTX
Acute radiation syndrome	ARS
Ataxia telangiectasia mutated	ATM
Base excision repair	BER
B-cell activation factor receptor	BAFFR
Bloom's syndrome helicase	BLM
Bovine serum albumin	BSA
Breast cancer type-1 susceptibility protein	BRCA1
Breast cancer type-2 susceptibility protein	BRCA2
β -transducing repeat-containing protein	β -TrCP
Cell-division-cycle 25	cdc25
Cellular inhibitor of apoptosis protein	ciAP
Checkpoint kinase	CHK
C-terminal binding protein 1 interacting protein	CtIP
Cyclin-dependent kinases	CDKs
Cyclooxygenase 2	COX-2
Damage-associated molecular pattern	DAMP
DEATH domain	DD
Deoxyribonucleic acid	DNA
Dimethyl sulfoxide	DMSO
Displacement loop	D-loop
DNA damage response	DDR
DNA polymerase β	pol β
DNA polymerase λ	pol λ
DNA polymerase μ	pol μ
DNA polymerase θ	pol θ

DNA synthesis phase	S-phase
DNA-dependent protein kinase	DNA-PK
DNA-PK catalytic subunit	DNA-PKcs
Double strand breaks	DSB
Double strand DNA	dsDNA
DSBR	DSB repair
Electron Volt	eV
Ethylenediaminetetraacetic acid	EDTA
Exonuclease 1	EXO1
Flap endonuclease 1	FEN1
Forward scatter	FSC
Galactic cosmic rays	GCR
GATA binding protein 4	GATA4
Glutamic acid	E
Gray	Gy
High charge and high energy	HZE
High mobility group box 1	HMGB1
Homologous recombination	HR
Hour	h
Hue / saturation / brightness	HSB
I κ B kinase	IKK
IL-1R-associated kinase	IRAK
Importin 3	IPO3
Inducible nitric oxide synthase	iNOS
Inhibitor of NF- κ B	I κ B
Interleukin	IL
Ionizing radiation	IR
Knock-out	ko
KRAB-associated protein 1	KAP-1
Leucine	L
Ligase	Lig
Linear energy transfer	LET
Lipopolysaccharide	LPS
Lysine	K
Meiotic recombination 11	MRE11

MicroRNA	miRNA
Mitogen-activated protein kinase 14	MAPK14
Mitosis	M-phase
Murine embryonic fibroblasts	MEF
Myeloid differentiation primary response gene 88	MyD88
National Aeronautics and Space Administration	NASA
NF- κ B essential modulator	NEMO
NF- κ B inducing kinase	NIK
Nijmegen breakage syndrome protein 1	NBS1
Nitric oxide	NO
Non-homologous end-joining	NHEJ
Northern lights 557	NL557
Nuclear factor κ B	NF- κ B
p53 binding protein 1	53BP1
p53-induced death domain protein	PIDD
Pathogen-associated molecular pattern	PAMP
Phosphate buffered saline	PBS
Phosphatidylinositol 3 lipid kinase	PI3K
PI3K-like protein kinase	PIKK
Plating efficiency	PE
Poly(ADP-ribose)	PAR
poly(ADP-ribose) glycohydrolase	PARG
Poly(ADP-ribose) polymerase-1	PARP1
Poly(ADP-ribosyl)ation	PARylation
Polynucleotide kinase 3'-phosphatase	PNKP
Proliferating cell nuclear antigen	PCNA
Propidium iodide	PI
Protein inhibitor of activated STATy	PIASy
Radiation-induced bystander effects	RIBE
Reactive oxygen species	ROS
Receptor activator of NF- κ B	RANK
Receptor-interacting serine/threonine-protein-1	RIP1
Relative biological effectiveness	RBE
Replicating factor C	RFC
Replication protein A	RPA

Replication timing regulatory factor 1	RIF1
Retinoblastoma protein	pRb
Senescence-associated secretory phenotype	SASP
Serine	S
Side scatter	SSC
Sievert	Sv
Signal transducer and activator of transcription	STAT
Single strand breaks	SSB
Single strand DNA	ssDNA
Small ubiquitin like modifier 1	SUMO
Solar particle events	SPE
S-phase kinase-associated protein 2	SKP2
Standard error	SE
Stress-induced premature senescence	SIPS
Survival fraction	S
Synthesis-dependent strand annealing	SDSA
TGF β activated kinase 1	TAK1
Threonine	T
TIR-containing adapter protein	TIRAP
TIR-domain-containing adapter inducing IFN- β	TRIF
TIR-domain-containing adapter molecule	TRAM
TNFR1-associated DEATH domain	TRADD
TNFR-associated factor family	TRAF
Toll/IL-1 receptor	TIR
Toll-like receptor	TLR
Topoisomerase 3a	Top3a
Transcriptional activating domain	TAD
Tris-buffered saline containing Tween 20	TBST
Tumor necrosis factor	TNF
Tumor necrosis factor receptor-1	TNFR1
Weighting factor	W
Werner syndrome helicase	WRN
Wildtype	wt
X-linked inhibitor of apoptosis	XIAP
X-ray repair cross-complementing protein 1	XRCC1

8. List of Figures

Figure 1	Initiation of the HR repair pathway	16
Figure 2	Resolution of the HR repair pathway	18
Figure 3	Non-homologous end-joining pathway of DNA DSB repair	19
Figure 4	The cell cycle and DNA damage checkpoints	22
Figure 5	TNF- α initiated activation of NF- κ B via the canonical pathway.	28
Figure 6	PAMP / IL-1 initiated activation of NF- κ B via the canonical pathway.....	29
Figure 7	Non-canonical activation of NF- κ B.	31
Figure 8	Genotoxic pathway of NF- κ B activation – Model 1.	33
Figure 9	Genotoxic pathway of NF- κ B activation – Model 2.	34
Figure 10	Genotoxic pathway of NF- κ B activation – Model 3.	35
Figure 11	Gating scheme for cell cycle analysis	49
Figure 12	Histogram of DNA content	50
Figure 13	Angular display of color hue in the hue / saturation / brightness (HSB) color space	52
Figure 14	The linear-quadratic model.....	55
Figure 15	The single-hit multi-target model.....	57
Figure 16	Cellular survival of MEF wt cells after direct exposure to X-rays – Immediate Plating vs. Late Plating	60
Figure 17	Cellular survival of MEF NEMO ko cells after direct exposure to X-rays – Immediate Plating vs. Late Plating	62
Figure 18	Cellular survival of immediately plated MEF wt and NEMO ko cells after direct exposure to X-rays	64
Figure 19	Cellular survival of late plated MEF wt and NEMO ko cells after direct exposure to X-rays.....	65
Figure 20	β -galactosidase activity after direct X-rays exposure	67
Figure 21	Relative cellular senescence after direct X-rays exposure	69
Figure 22	Percentage of cells with a sub-G1 DNA content after direct X-rays exposure.....	70
Figure 23	Cell cycle phase distribution after direct X-rays exposure	72
Figure 24	γ H2AX foci per cell nucleus after direct X-rays exposure.....	75
Figure 25	Nuclear translocation of p65 as indicator of NF- κ B activation in MEF wt cells after treatment with X-rays, conditioned medium, TNF- α and LPS.....	79
Figure 26	Cellular survival of MEF wt and NEMO ko cells after incubation with conditioned medium.....	81
Figure 27	Cellular survival of MEF wt and NEMO ko cells after incubation with conditioned medium from the opposing cell type.....	83

Figure 28	β -galactosidase activity after treatment with conditioned medium	86
Figure 29	Relative cellular senescence after treatment with conditioned medium.....	88
Figure 30	Percentage of cells with a sub-G1 DNA content after treatment with conditioned medium.....	89
Figure 31	Cell cycle phase distribution after incubation with conditioned medium from X-irradiated cells	91
Figure 32	γ H2AX foci per cell nucleus after treatment with conditioned medium from X-irradiated cells	94
Figure 33	Distribution of γ H2AX foci per cell nucleus after treatment with conditioned medium from X-irradiated cells	113
Figure 34	Schematics for radiation-induced bystander signaling	115

9. List of Tables

Table 1	Cell culture medium supplements	41
Table 2	Composition of phosphate-buffered saline (PBS)	42
Table 3	NF- κ B activators and senescence inducers	42
Table 4	Composition of Tris-buffered saline with Tween-20 (TBST).....	44
Table 5	Specifications of DAPI.....	45
Table 6	Antibodies for p65 immunofluorescence staining	45
Table 7	Antibodies for γ H2AX immunofluorescence staining.....	46
Table 8	Specifications of propidium iodide.....	48
Table 9	Survival data for X-irradiated MEF wt (Immediate Plating and Late Plating).....	61
Table 10	Parameters of the survival curves determined by the linear-quadratic model and statistics for X-irradiation of MEF wt (Immediate vs. Late Plating)	61
Table 11	Survival data for X-irradiated MEF NEMO ko (Immediate Plating and Late Plating)	63
Table 12	Parameters of the survival curves determined by the linear-quadratic model and statistics for X-irradiation of MEF NEMO ko (Immediate vs. Late Plating)	63
Table 13	Parameters of the survival curves determined by the linear-quadratic model and statistics for X-irradiation and Immediate Plating (MEF wt vs. MEF NEMO ko).....	66
Table 14	Parameters of the survival curves determined by the linear-quadratic model and statistics for X-irradiation and Late Plating (MEF wt vs. MEF NEMO ko).....	66
Table 15	Relative β -galactosidase activity of MEF wt and MEF NEMO ko after X-irradiation and etoposide treatment.....	68
Table 16	Percentage of MEF wt and MEF NEMO ko cells with sub-G1 DNA content (mean \pm SE) up to 48 h after X-irradiation with 8 Gy.....	71
Table 17	Percentage of MEF wt and MEF NEMO ko cells in G1, S and G2/M cell cycle phases up to 48 h after X-irradiation with 8 Gy.	73
Table 18	Error probability (p-value) for comparison of MEF wt and MEF NEMO ko cells G1, S and G2/M cell cycle phases up to 48 h after X-irradiation with 8 Gy.....	73
Table 19	Kinetics of γ H2AX foci (mean \pm SE) in MEF wt vs. MEF NEMO ko after X-irradiation	76
Table 20	Error probability (p-value) between doses at different time points for γ H2AX foci in MEF wt vs. MEF NEMO ko after X-irradiation.....	76
Table 21	Error probability (p-value) between time points for different doses regarding γ H2AX foci in MEF wt vs. MEF NEMO ko after X-irradiation.....	77
Table 22	Nuclear translocation of p65 in MEF wt cells after X-irradiation or treatment with conditioned medium, TNF- α or LPS.....	78
Table 23	Transfer scheme for conditioned medium.....	80

Table 24	Survival of MEF wt cells after incubation with conditioned medium from X-irradiated MEF wt	82
Table 25	Survival statistics for comparison of MEF wt and MEF NEMO ko cells after incubation with conditioned medium from X-irradiated cells of the same origin cell line	82
Table 26	Survival of MEF wt and NEMO ko cells after incubation with conditioned medium from X-irradiated cells of the opposing cell line.....	84
Table 27	Survival statistics for comparison of MEF wt and MEF NEMO ko cells after incubation with conditioned medium from X-irradiated cells of the opposing cell line	84
Table 28	Statistics for the comparison of the transfer schemes of conditioned medium to non-irradiated MEF wt and MEF NEMO ko cells based on the data shown in Table 24 to Table 26.	85
Table 29	Relative β -galactosidase activity of MEF wt and MEF NEMO ko after treatment with conditioned medium from X-irradiated cells.....	87
Table 30	Percentage of MEF wt and MEF NEMO ko cells with sub-G1 DNA content up to 48 h after treatment with conditioned medium at a conditioning dose of 8 Gy.....	90
Table 31	Percentage of MEF wt and MEF NEMO ko cells in G1, S and G2/M cell cycle phase up to 48 h after incubation with conditioned medium from X-irradiated cells (8 Gy).	92
Table 32	Error probability (p-value) for comparison of MEF wt and MEF NEMO ko cells in G1, S and G2/M cell cycle phase up to 48 h after incubation with conditioned medium from X-irradiated cells (8 Gy).....	92
Table 33	Kinetics of γ H2AX foci (mean \pm SE) in MEF wt and MEF NEMO ko cells after treatment with conditioned medium from X-irradiated cells.....	95
Table 34	Error probability (p-value) between conditioning doses at different time points for γ H2AX foci in MEF wt and MEF NEMO ko cells after treatment with conditioned medium from X-irradiated cells	95
Table 35	Error probability (p-value) between time points for different conditioning doses regarding γ H2AX foci in MEF wt and MEF NEMO ko cells after treatment with conditioned medium from X-irradiated cells.....	96

10. References

1. Abramowicz A, Wojakowska A, Marczak L, Lysek-Gladysinska M, Smolarz M, Story MD, Polanska J, Widlak P, Pietrowska M (2019) Ionizing radiation affects the composition of the proteome of extracellular vesicles released by head-and-neck cancer cells in vitro. *J Radiat Res* 60:289-297
2. Acheva A, Ghita M, Patel G, Prise KM, Schettino G (2014) Mechanisms of DNA damage response to targeted irradiation in organotypic 3D skin cultures. *PLoS One* 9:e86092
3. Adhikari A, Xu M, Chen ZJ (2007) Ubiquitin-mediated activation of TAK1 and IKK. *Oncogene* 26:3214-3226
4. Adrian G, Ceberg C, Carneiro A, Ekblad L (2018) Rescue Effect Inherited in Colony Formation Assays Affects Radiation Response. *Radiat Res* 189:44-52
5. Ahmed EA, Velaz E, Rosemann M, Gilbertz KP, Scherthan H (2017) DNA repair kinetics in SCID mice Sertoli cells and DNA-PKcs-deficient mouse embryonic fibroblasts. *Chromosoma* 126:287-298
6. Al-Mayah AH, Irons SL, Pink RC, Carter DR, Kadhim MA (2012) Possible role of exosomes containing RNA in mediating nontargeted effect of ionizing radiation. *Radiat Res* 177:539-545
7. Aravindan S, Natarajan M, Ramraj SK, Pandian V, Khan FH, Herman TS, Aravindan N (2014) Abscopal effect of low-LET gamma-radiation mediated through Rel protein signal transduction in a mouse model of nontargeted radiation response. *Cancer Gene Ther* 21:54-59
8. Autsavapromporn N, Suzuki M, Funayama T, Usami N, Plante I, Yokota Y, Mutou Y, Ikeda H, Kobayashi K, Kobayashi Y, Uchihori Y, Hei TK, Azzam EI, Murakami T (2013) Gap junction communication and the propagation of bystander effects induced by microbeam irradiation in human fibroblast cultures: the impact of radiation quality. *Radiat Res* 180:367-375
9. Autsavapromporn N, Liu C, Konishi T (2017) Impact of Co-Culturing with Fractionated Carbon-Ion-Irradiated Cancer Cells on Bystander Normal Cells and Their Progeny. *Radiat Res* 188:335-341
10. Azzam EI, De Toledo SM, Spitz DR, Little JB (2002) Oxidative metabolism modulates signal transduction and micronucleus formation in bystander cells from alpha-particle-irradiated normal human fibroblast cultures. *Cancer Res* 62:5436-5442
11. Azzam EI, de Toledo SM, Little JB (2003) Expression of CONNEXIN43 is highly sensitive to ionizing radiation and other environmental stresses. *Cancer Res* 63:7128-7135
12. Banerjee S, Aykin-Burns N, Krager KJ, Shah SK, Melnyk SB, Hauer-Jensen M, Pawar SA (2016) Loss of C/EBPdelta enhances IR-induced cell death by promoting oxidative stress and mitochondrial dysfunction. *Free Radic Biol Med* 99:296-307
13. Bannerman DD, Tupper JC, Kelly JD, Winn RK, Harlan JM (2002) The Fas-associated death domain protein suppresses activation of NF-kappa B by LPS and IL-1 beta. *J Clin Invest* 109:419-425
14. Bannerman DD, Eiting KT, Winn RK, Harlan JM (2004) FLICE-like inhibitory protein (FLIP) protects against apoptosis and suppresses NF-kappaB activation induced by bacterial lipopolysaccharide. *Am J Pathol* 165:1423-1431
15. Barascu A, Le Chalony C, Pennarun G, Genet D, Imam N, Lopez B, Bertrand P (2012) Oxidative stress induces an ATM-independent senescence pathway through p38 MAPK-mediated lamin B1 accumulation. *Embo j* 31:1080-1094
16. Baselet B, Belmans N, Coninx E, Lowe D, Janssen A, Michaux A, Tabury K, Raj K, Quintens R, Benotmane MA, Baatout S, Sonveaux P, Aerts A (2017) Functional Gene Analysis Reveals Cell Cycle Changes and Inflammation in Endothelial Cells Irradiated with a Single X-ray Dose. *Front Pharmacol* 8:213
17. Beaujean R, Kopp J, Burmeister S, Petersen F, Reitz G (2002) Dosimetry inside MIR station using a silicon detector telescope (DOSTEL). *Radiat Meas* 35:433-438

18. Bee L, Fabris S, Cherubini R, Mognato M, Celotti L (2013) The efficiency of homologous recombination and non-homologous end joining systems in repairing double-strand breaks during cell cycle progression. *PLoS One* 8:e69061
19. Begalli F, Bennett J, Capece D, Verzella D, D'Andrea D, Tornatore L, Franzoso G (2017) Unlocking the NF-kappaB Conundrum: Embracing Complexity to Achieve Specificity. *Biomedicines* 5
20. Belloni P, Latini P, Palitti F (2011) Radiation-induced bystander effect in healthy G(o) human lymphocytes: biological and clinical significance. *Mutat Res* 713:32-38
21. Berger T, Bilski P, Hajek M, Puchalska M, Reitz G (2013) The MATROSHKA experiment: results and comparison from extravehicular activity (MTR-1) and intravehicular activity (MTR-2A/2B) exposure. *Radiat Res* 180:622-637
22. Bertoli C, Skotheim JM, de Bruin RA (2013) Control of cell cycle transcription during G1 and S phases. *Nat Rev Mol Cell Biol* 14:518-528
23. Bhargava R, Carson CR, Lee G, Stark JM (2017) Contribution of canonical nonhomologous end joining to chromosomal rearrangements is enhanced by ATM kinase deficiency. *Proc Natl Acad Sci U S A* 114:728-733
24. Bledsoe TJ, Nath SK, Decker RH (2017) Radiation Pneumonitis. *Clin Chest Med* 38:201-208
25. Bock FJ, Krumschnabel G, Manzl C, Peintner L, Tanzer MC, Hermann-Kleiter N, Baier G, Llacuna L, Yelamos J, Villunger A (2013) Loss of PIDD limits NF-kappaB activation and cytokine production but not cell survival or transformation after DNA damage. *Cell Death Differ* 20:546-557
26. Bogliolo M, Lyakhovich A, Callen E, Castella M, Cappelli E, Ramirez MJ, Creus A, Marcos R, Kalb R, Neveling K, Schindler D, Surralles J (2007) Histone H2AX and Fanconi anemia FANCD2 function in the same pathway to maintain chromosome stability. *EMBO J* 26:1340-1351
27. Bott A, Erdem N, Lerrer S, Hotz-Wagenblatt A, Breunig C, Abnaof K, Worner A, Wilhelm H, Munstermann E, Ben-Baruch A, Wiemann S (2017) miRNA-1246 induces pro-inflammatory responses in mesenchymal stem/stromal cells by regulating PKA and PP2A. *Oncotarget* 8:43897-43914
28. Boutros R, Lobjois V, Ducommun B (2007) CDC25 phosphatases in cancer cells: key players? Good targets? *Nat Rev Cancer* 7:495-507
29. Brown NR, Lowe ED, Petri E, Skamnaki V, Antrobus R, Johnson LN (2007) Cyclin B and cyclin A confer different substrate recognition properties on CDK2. *Cell Cycle* 6:1350-1359
30. Bryant J, Shields L, Hynes C, Howe O, McClean B, Lyng F (2019) DNA Damage and Cytokine Production in Non-Target Irradiated Lymphocytes. *Radiat Res*
31. Buonanno M, de Toledo SM, Azzam EI (2011a) Increased frequency of spontaneous neoplastic transformation in progeny of bystander cells from cultures exposed to densely ionizing radiation. *PLoS One* 6:e21540
32. Buonanno M, de Toledo SM, Pain D, Azzam EI (2011b) Long-term consequences of radiation-induced bystander effects depend on radiation quality and dose and correlate with oxidative stress. *Radiat Res* 175:405-415
33. Burdak-Rothkamm S, Rothkamm K, Prise KM (2008) ATM acts downstream of ATR in the DNA damage response signaling of bystander cells. *Cancer Res* 68:7059-7065
34. Burdak-Rothkamm S, Rothkamm K, McClelland K, Al Rashid ST, Prise KM (2015) BRCA1, FANCD2 and Chk1 are potential molecular targets for the modulation of a radiation-induced DNA damage response in bystander cells. *Cancer Lett* 356:454-461
35. Burke JR, Pattoli MA, Gregor KR, Brassil PJ, MacMaster JF, McIntyre KW, Yang X, Iotzova VS, Clarke W, Strnad J, Qiu Y, Zusi FC (2003) BMS-345541 is a highly selective inhibitor of I kappa B kinase that binds at an allosteric site of the enzyme and blocks NF-kappa B-dependent transcription in mice. *J Biol Chem* 278:1450-1456
36. Caldecott KW (2008) Single-strand break repair and genetic disease. *Nat Rev Genet* 9:619-631
37. Castedo M, Perfettini JL, Roumier T, Andreau K, Medema R, Kroemer G (2004) Cell death by mitotic catastrophe: a molecular definition. *Oncogene* 23:2825-2837

38. Chai Y, Calaf GM, Zhou H, Ghandhi SA, Elliston CD, Wen G, Nohmi T, Amundson SA, Hei TK (2013) Radiation induced COX-2 expression and mutagenesis at non-targeted lung tissues of gpt delta transgenic mice. *Br J Cancer* 108:91-98
39. Chapman JR, Barral P, Vannier JB, Borel V, Steger M, Tomas-Loba A, Sartori AA, Adams IR, Batista FD, Boulton SJ (2013) RIF1 is essential for 53BP1-dependent nonhomologous end joining and suppression of DNA double-strand break resection. *Mol Cell* 49:858-871
40. Chatterjee N, Walker GC (2017) Mechanisms of DNA damage, repair, and mutagenesis. *Environ Mol Mutagen* 58:235-263
41. Chen CF, Dou XW, Liang YK, Lin HY, Bai JW, Zhang XX, Wei XL, Li YC, Zhang GJ (2016) Notch3 overexpression causes arrest of cell cycle progression by inducing Cdh1 expression in human breast cancer cells. *Cell Cycle* 15:432-440
42. Chen J (2016) The Cell-Cycle Arrest and Apoptotic Functions of p53 in Tumor Initiation and Progression. *Cold Spring Harb Perspect Med* 6:a026104
43. Chen S, Zhao Y, Han W, Chiu SK, Zhu L, Wu L, Yu KN (2011) Rescue effects in radiobiology: unirradiated bystander cells assist irradiated cells through intercellular signal feedback. *Mutat Res* 706:59-64
44. Chen X, Zhuang X, Zhang Q, Luo Y, Yuan S, Qiao T (2017) Analgesic enhances the anti-tumor response of radiotherapy by increasing apoptosis and cell cycle arrest in non-small cell lung cancer. *Oncotarget* 8:80730-80740
45. Chen ZJ (2012) Ubiquitination in signaling to and activation of IKK. *Immunol Rev* 246:95-106
46. Chishti AA, Baumstark-Khan C, Koch K, Kolanus W, Feles S, Konda B, Azhar A, Spitta LF, Henschenmacher B, Diegeler S, Schmitz C, Hellweg CE (2018) Linear Energy Transfer Modulates Radiation-Induced NF-kappa B Activation and Expression of its Downstream Target Genes. *Radiat Res* 189:354-370
47. Correia-Melo C, Marques FD, Anderson R, Hewitt G, Hewitt R, Cole J, Carroll BM, Miwa S, Birch J, Merz A, Rushton MD, Charles M, Jurk D, Tait SW, Czapiewski R, Greaves L, Nelson G, Bohlooly YM, Rodriguez-Cuenca S, Vidal-Puig A, Mann D, Saretzki G, Quarato G, Green DR, Adams PD, von Zglinicki T, Korolchuk VI, Passos JF (2016) Mitochondria are required for pro-ageing features of the senescent phenotype. *EMBO J* 35:724-742
48. Costes SV, Chiolo I, Pluth JM, Barcellos-Hoff MH, Jakob B (2010) Spatiotemporal characterization of ionizing radiation induced DNA damage foci and their relation to chromatin organization. *Mutat Res* 704:78-87
49. Courtois G, Fauvarque MO (2018) The Many Roles of Ubiquitin in NF-kappaB Signaling. *Biomedicine* 6
50. Crickard JB, Greene EC (2018) Biochemical attributes of mitotic and meiotic presynaptic complexes. *DNA Repair (Amst)* 71:148-157
51. Cuadrado A, Nebreda AR (2010) Mechanisms and functions of p38 MAPK signalling. *Biochem J* 429:403-417
52. Cucinotta FA, To K, Cacao E (2017) Predictions of space radiation fatality risk for exploration missions. *Life Sci Space Res (Amst)* 13:1-11
53. Darzynkiewicz Z, Zhao H, Zhang S, Lee MY, Lee EY, Zhang Z (2015) Initiation and termination of DNA replication during S phase in relation to cyclins D1, E and A, p21WAF1, Cdt1 and the p12 subunit of DNA polymerase delta revealed in individual cells by cytometry. *Oncotarget* 6:11735-11750
54. de Laval B, Pawlikowska P, Barbieri D, Besnard-Guerin C, Cico A, Kumar R, Gaudry M, Baud V, Porteu F (2014) Thrombopoietin promotes NHEJ DNA repair in hematopoietic stem cells through specific activation of Erk and NF-kappaB pathways and their target, IEX-1. *Blood* 123:509-519
55. de Toledo SM, Buonanno M, Harris AL, Azzam EI (2017) Genomic instability induced in distant progeny of bystander cells depends on the connexins expressed in the irradiated cells. *Int J Radiat Biol* 93:1182-1194

56. Debacq-Chainiaux F, Erusalimsky JD, Campisi J, Toussaint O (2009) Protocols to detect senescence-associated beta-galactosidase (SA-beta-gal) activity, a biomarker of senescent cells in culture and in vivo. *Nat Protoc* 4:1798-1806
57. Debacq-Chainiaux F, Boilan E, Dedessus Le Moutier J, Weemaels G, Toussaint O (2010) p38(MAPK) in the senescence of human and murine fibroblasts. *Adv Exp Med Biol* 694:126-137
58. Desai S, Kumar A, Laskar S, Pandey BN (2013) Cytokine profile of conditioned medium from human tumor cell lines after acute and fractionated doses of gamma radiation and its effect on survival of bystander tumor cells. *Cytokine* 61:54-62
59. Desai S, Kumar A, Laskar S, Pandey BN (2014) Differential roles of ATF-2 in survival and DNA repair contributing to radioresistance induced by autocrine soluble factors in A549 lung cancer cells. *Cell Signal* 26:2424-2435
60. Di Francesco A, De Pitta C, Moret F, Barbieri V, Celotti L, Mognato M (2013) The DNA-damage response to gamma-radiation is affected by miR-27a in A549 cells. *Int J Mol Sci* 14:17881-17896
61. Di Meo S, Reed TT, Venditti P, Victor VM (2016) Role of ROS and RNS Sources in Physiological and Pathological Conditions. *Oxid Med Cell Longev* 2016:1245049
62. DiDonato JA, Mercurio F, Karin M (2012) NF-kappaB and the link between inflammation and cancer. *Immunol Rev* 246:379-400
63. Diegeler S, Hellweg CE (2017) Intercellular Communication of Tumor Cells and Immune Cells after Exposure to Different Ionizing Radiation Qualities. *Front Immunol* 8:664
64. Dong J, Zhang T, Ren Y, Wang Z, Ling CC, He F, Li GC, Wang C, Wen B (2017) Inhibiting DNA-PKcs in a non-homologous end-joining pathway in response to DNA double-strand breaks. *Oncotarget* 8:22662-22673
65. Dong J, Ren Y, Zhang T, Wang Z, Ling CC, Li GC, He F, Wang C, Wen B (2018) Inactivation of DNA-PK by knockdown DNA-PKcs or NU7441 impairs non-homologous end-joining of radiation-induced double strand break repair. *Oncol Rep* 39:912-920
66. Dong X, Tong F, Qian C, Zhang R, Dong J, Wu G, Hu Y (2015) NEMO modulates radiation-induced endothelial senescence of human umbilical veins through NF-kappaB signal pathway. *Radiat Res* 183:82-93
67. El-Deiry WS (2016) p21(WAF1) Mediates Cell-Cycle Inhibition, Relevant to Cancer Suppression and Therapy. *Cancer Res* 76:5189-5191
68. Elmore S (2007) Apoptosis: a review of programmed cell death. *Toxicol Pathol* 35:495-516
69. Eom HS, Park HS, You GE, Kim JY, Nam SY (2017) Identification of cellular responses to low-dose radiation by the profiling of phosphorylated proteins in human B-lymphoblast IM-9 cells. *Int J Radiat Biol* 93:1207-1216
70. Eriksson D, Stigbrand T (2010) Radiation-induced cell death mechanisms. *Tumour Biol* 31:363-372
71. Ermakov AV, Konkova MS, Kostyuk SV, Izevskaya VL, Baranova A, Veiko NN (2013) Oxidized extracellular DNA as a stress signal in human cells. *Oxid Med Cell Longev* 2013:649747
72. Escribano-Diaz C, Orthwein A, Fradet-Turcotte A, Xing M, Young JT, Tkac J, Cook MA, Rosebrock AP, Munro M, Canny MD, Xu D, Durocher D (2013) A cell cycle-dependent regulatory circuit composed of 53BP1-RIF1 and BRCA1-CtIP controls DNA repair pathway choice. *Mol Cell* 49:872-883
73. Estabrook NC, Chin-Sinex H, Borgmann AJ, Dhaemers RM, Shapiro RH, Gilley D, Huda N, Crooks P, Sweeney C, Mendonca MS (2011) Inhibition of NF-kappaB and DNA double-strand break repair by DMAPT sensitizes non-small-cell lung cancers to X-rays. *Free Radic Biol Med* 51:2249-2258
74. Fang L, Choudhary S, Zhao Y, Edeh CB, Yang C, Boldogh I, Brasier AR (2014) ATM regulates NF-kappaB-dependent immediate-early genes via RelA Ser 276 phosphorylation coupled to CDK9 promoter recruitment. *Nucleic Acids Res* 42:8416-8432

75. Fardid R, Salajegheh A, Mosleh-Shirazi MA, Sharifzadeh S, Okhovat MA, Najafi M, Rezaeyan A, Abaszadeh A (2017) Melatonin Ameliorates The Production of COX-2, iNOS, and The Formation of 8-OHdG in Non-Targeted Lung Tissue after Pelvic Irradiation. *Cell J* 19:324-331
76. Farhood B, Goradel NH, Mortezaee K, Khanlarkhani N, Salehi E, Nashtaei MS, Shabeeb D, Musa AE, Fallah H, Najafi M (2019) Intercellular communications-redox interactions in radiation toxicity; potential targets for radiation mitigation. *J Cell Commun Signal* 13:3-16
77. Fernandez-Capetillo O, Nussenzweig A (2008) ATM breaks into heterochromatin. *Mol Cell* 31:303-304
78. Fernandez-Palomo C, Schultke E, Brauer-Krisch E, Laissue JA, Blattmann H, Seymour C, Mothersill C (2016) Investigation of Abscopal and Bystander Effects in Immunocompromised Mice After Exposure to Pencilbeam and Microbeam Synchrotron Radiation. *Health Phys* 111:149-159
79. Ferrand M, Kirsh O, Griveau A, Vindrieux D, Martin N, Defossez PA, Bernard D (2015) Screening of a kinase library reveals novel pro-senescence kinases and their common NF-kappaB-dependent transcriptional program. *Aging (Albany NY)* 7:986-1003
80. Franken NA, Ten Cate R, Van Bree C, Haveman J (2004) Induction of the early response protein EGR-1 in human tumour cells after ionizing radiation is correlated with a reduction of repair of lethal lesions and an increase of repair of sublethal lesions. *Int J Oncol* 24:1027-1031
81. Freund A, Patil CK, Campisi J (2011) p38MAPK is a novel DNA damage response-independent regulator of the senescence-associated secretory phenotype. *Embo j* 30:1536-1548
82. Frey B, Ruckert M, Deloch L, Ruhle PF, Derer A, Fietkau R, Gaipl US (2017) Immunomodulation by ionizing radiation-impact for design of radio-immunotherapies and for treatment of inflammatory diseases. *Immunol Rev* 280:231-248
83. Furusawa Y, Wei ZL, Sakurai H, Tabuchi Y, Li P, Zhao QL, Nomura T, Saiki I, Kondo T (2012) TGF-beta-activated kinase 1 promotes cell cycle arrest and cell survival of X-ray irradiated HeLa cells dependent on p21 induction but independent of NF-kappaB, p38 MAPK and ERK phosphorylations. *Radiat Res* 177:766-774
84. Giacinti C, Giordano A (2006) RB and cell cycle progression. *Oncogene* 25:5220-5227
85. Godwin P, Baird AM, Heavey S, Barr MP, O'Byrne KJ, Gately K (2013) Targeting nuclear factor-kappa B to overcome resistance to chemotherapy. *Front Oncol* 3:120
86. Goodwin JF, Knudsen KE (2014) Beyond DNA repair: DNA-PK function in cancer. *Cancer Discov* 4:1126-1139
87. Goto H, Izawa I, Li P, Inagaki M (2012) Novel regulation of checkpoint kinase 1: Is checkpoint kinase 1 a good candidate for anti-cancer therapy? *Cancer Sci* 103:1195-1200
88. Goto H, Kasahara K, Inagaki M (2015) Novel insights into Chk1 regulation by phosphorylation. *Cell Struct Funct* 40:43-50
89. Grammaticos P, Giannoula E, Fountos GP (2013) Acute radiation syndrome and chronic radiation syndrome. *Hell J Nucl Med* 16:56-59
90. Guo J, Zeitlin C, Wimmer-Schweingruber RF, Hassler DM, Ehresmann B, Kohler J, Bohm E, Bottcher S, Brinza D, Burmeister S, Cucinotta F, Martin C, Posner A, Rafkin S, Reitz G (2015) MSL-RAD radiation environment measurements. *Radiat Prot Dosimetry* 166:290-294
91. Guo X, Bai Y, Zhao M, Zhou M, Shen Q, Yun CH, Zhang H, Zhu WG, Wang J (2018) Acetylation of 53BP1 dictates the DNA double strand break repair pathway. *Nucleic Acids Res* 46:689-703
92. Habets TH, Oth T, Houben AW, Huijskens MJ, Senden-Gijsbers BL, Schnijderberg MC, Brans B, Dubois LJ, Lambin P, De Saint-Hubert M, Germeraad WT, Tilanus MG, Mottaghy FM, Bos GM, Vanderlocht J (2016) Fractionated Radiotherapy with 3 x 8 Gy Induces Systemic Anti-Tumour Responses and Abscopal Tumour Inhibition without Modulating the Humoral Anti-Tumour Response. *PLoS One* 11:e0159515
93. Habraken Y, Jolios O, Piette J (2003) Differential involvement of the hMRE11/hRAD50/NBS1 complex, BRCA1 and MLH1 in NF-kappaB activation by camptothecin and X-ray. *Oncogene* 22:6090-6099

94. Hagelstrom RT, Askin KF, Williams AJ, Ramaiah L, Desaintes C, Goodwin EH, Ullrich RL, Bailey SM (2008) DNA-PKcs and ATM influence generation of ionizing radiation-induced bystander signals. *Oncogene* 27:6761-6769
95. Hamada N, Matsumoto H, Hara T, Kobayashi Y (2007) Intercellular and intracellular signaling pathways mediating ionizing radiation-induced bystander effects. *J Radiat Res* 48:87-95
96. Hanu C, Wong R, Sur RK, Hayward JE, Seymour C, Mothersill C (2017) Low-dose non-targeted radiation effects in human esophageal adenocarcinoma cell lines. *Int J Radiat Biol* 93:165-173
97. He X, Yang A, McDonald DG, Riemer EC, Vanek KN, Schulte BA, Wang GY (2017) MiR-34a modulates ionizing radiation-induced senescence in lung cancer cells. *Oncotarget* 8:69797-69807
98. Hei TK, Persaud R, Zhou H, Suzuki M (2004) Genotoxicity in the eyes of bystander cells. *Mutat Res* 568:111-120
99. Hei TK (2006) Cyclooxygenase-2 as a signaling molecule in radiation-induced bystander effect. *Mol Carcinog* 45:455-460
100. Hei TK, Zhou H, Ivanov VN, Hong M, Lieberman HB, Brenner DJ, Amundson SA, Geard CR (2008) Mechanism of radiation-induced bystander effects: a unifying model. *J Pharm Pharmacol* 60:943-950
101. Hei TK, Zhou H, Chai Y, Ponnaiya B, Ivanov VN (2011) Radiation induced non-targeted response: mechanism and potential clinical implications. *Curr Mol Pharmacol* 4:96-105
102. Hellweg CE, Baumstark-Khan C (2007) Getting ready for the manned mission to Mars: the astronauts' risk from space radiation. *Naturwissenschaften* 94:517-526
103. Hellweg CE, Langen B, Klimow G, Ruscher R, Schmitz C, Baumstark-Khan C, Reitz G (2009) Upstream events in the nuclear factor κ B activation cascade in response to sparsely ionizing radiation. *Adv Space Res* 44:907-916
104. Hellweg CE, Baumstark-Khan C, Schmitz C, Lau P, Meier MM, Testard I, Berger T, Reitz G (2011) Carbon-ion-induced activation of the NF- κ B pathway. *Radiat Res* 175:424-431
105. Hellweg CE (2015) The Nuclear Factor κ B pathway: A link to the immune system in the radiation response. *Cancer Lett* 368:275-289
106. Hellweg CE, Spitta LF, Henschenmacher B, Diegeler S, Baumstark-Khan C (2016) Transcription Factors in the Cellular Response to Charged Particle Exposure. *Front Oncol* 6:61
107. Hellweg CE, Spitta LF, Koch K, Chishti AA, Henschenmacher B, Diegeler S, Konda B, Feles S, Schmitz C, Berger T, Baumstark-Khan C (2018) The Role of the Nuclear Factor κ B Pathway in the Cellular Response to Low and High Linear Energy Transfer Radiation. *Int J Mol Sci* 19
108. Hengartner MO (2000) The biochemistry of apoptosis. *Nature* 407:770-776
109. Hernandez L, Terradas M, Martin M, Tusell L, Genesca A (2013) Highly sensitive automated method for DNA damage assessment: gamma-H2AX foci counting and cell cycle sorting. *Int J Mol Sci* 14:15810-15826
110. Hinz M, Loser P, Mathas S, Krappmann D, Dorken B, Scheidereit C (2001) Constitutive NF- κ B maintains high expression of a characteristic gene network, including CD40, CD86, and a set of antiapoptotic genes in Hodgkin/Reed-Sternberg cells. *Blood* 97:2798-2807
111. Hinz M, Stilmann M, Arslan SC, Khanna KK, Dittmar G, Scheidereit C (2010) A cytoplasmic ATM-TRAF6-clAP1 module links nuclear DNA damage signaling to ubiquitin-mediated NF- κ B activation. *Mol Cell* 40:63-74
112. Hodny Z, Hubackova S, Bartek J (2013) Cytokine-induced 'bystander' senescence in DDR and immuno-surveillance. *Oncotarget* 4:1552-1553
113. Hoesel B, Schmid JA (2013) The complexity of NF- κ B signaling in inflammation and cancer. *Mol Cancer* 12:86
114. Hwang B, McCool K, Wan J, Wuerzberger-Davis SM, Young EW, Choi EY, Cingolani G, Weaver BA, Miyamoto S (2015) IPO3-mediated Nonclassical Nuclear Import of NF- κ B Essential Modulator (NEMO) Drives DNA Damage-dependent NF- κ B Activation. *J Biol Chem* 290:17967-17984

115. ICRP (2007) The 2007 Recommendations of the International Commission on Radiological Protection. ICRP publication 103. *Ann ICRP* 37:1-332
116. Iliakis G, Murmann T, Soni A (2015) Alternative end-joining repair pathways are the ultimate backup for abrogated classical non-homologous end-joining and homologous recombination repair: Implications for the formation of chromosome translocations. *Mutat Res Genet Toxicol Environ Mutagen* 793:166-175
117. Imbert V, Peyron JF (2017) NF-kappaB in Hematological Malignancies. *Biomedicines* 5
118. Ivanov VN, Zhou H, Ghandhi SA, Karasic TB, Yaghoubian B, Amundson SA, Hei TK (2010) Radiation-induced bystander signaling pathways in human fibroblasts: a role for interleukin-33 in the signal transmission. *Cell Signal* 22:1076-1087
119. Iwabuchi K, Hashimoto M, Matsui T, Kurihara T, Shimizu H, Adachi N, Ishiai M, Yamamoto K, Tauchi H, Takata M, Koyama H, Date T (2006) 53BP1 contributes to survival of cells irradiated with X-ray during G1 without Ku70 or Artemis. *Genes Cells* 11:935-948
120. Iyer DR, Rhind N (2017) The Intra-S Checkpoint Responses to DNA Damage. *Genes (Basel)* 8
121. Jaccard N, Griffin LD, Keser A, Macown RJ, Super A, Veraitch FS, Szita N (2014) Automated method for the rapid and precise estimation of adherent cell culture characteristics from phase contrast microscopy images. *Biotechnol Bioeng* 111:504-517
122. Jackson SP, Bartek J (2009) The DNA-damage response in human biology and disease. *Nature* 461:1071-1078
123. Janus P, Szoltysek K, Zajac G, Stokowy T, Walaszczyk A, Widlak W, Wojtas B, Gielniewski B, Iwanaszko M, Braun R, Cockell S, Perkins ND, Kimmel M, Widlak P (2018) Pro-inflammatory cytokine and high doses of ionizing radiation have similar effects on the expression of NF-kappaB-dependent genes. *Cell Signal* 46:23-31
124. Jasin M, Rothstein R (2013) Repair of strand breaks by homologous recombination. *Cold Spring Harb Perspect Biol* 5:a012740
125. Jella KK, Garcia A, McClean B, Byrne HJ, Lyng FM (2013) Cell death pathways in directly irradiated cells and cells exposed to medium from irradiated cells. *Int J Radiat Biol* 89:182-190
126. Jella KK, Rani S, O'Driscoll L, McClean B, Byrne HJ, Lyng FM (2014) Exosomes are involved in mediating radiation induced bystander signaling in human keratinocyte cells. *Radiat Res* 181:138-145
127. Jella KK, Moriarty R, McClean B, Byrne HJ, Lyng FM (2018) Reactive oxygen species and nitric oxide signaling in bystander cells. *PLoS One* 13:e0195371
128. Jezkova L, Zadneprianetc M, Kulikova E, Smirnova E, Bulanova T, Depes D, Falkova I, Boreyko A, Krasavin E, Davidkova M, Kozubek S, Valentova O, Falk M (2018) Particles with similar LET values generate DNA breaks of different complexity and reparability: a high-resolution microscopy analysis of gammaH2AX/53BP1 foci. *Nanoscale* 10:1162-1179
129. Jiang YL, Escano MF, Sasaki R, Fujii S, Kusuhara S, Matsumoto A, Sugimura K, Negi A (2004) Ionizing radiation induces a p53-dependent apoptotic mechanism in ARPE-19 cells. *Jpn J Ophthalmol* 48:106-114
130. Jin HS, Lee DH, Kim DH, Chung JH, Lee SJ, Lee TH (2009) cIAP1, cIAP2, and XIAP act cooperatively via nonredundant pathways to regulate genotoxic stress-induced nuclear factor-kappaB activation. *Cancer Res* 69:1782-1791
131. Jones KR, Elmore LW, Jackson-Cook C, Demasters G, Povirk LF, Holt SE, Gewirtz DA (2005) p53-Dependent accelerated senescence induced by ionizing radiation in breast tumour cells. *Int J Radiat Biol* 81:445-458
132. Jurk D, Wilson C, Passos JF, Oakley F, Correia-Melo C, Greaves L, Saretzki G, Fox C, Lawless C, Anderson R, Hewitt G, Pender SL, Fullard N, Nelson G, Mann J, van de Sluis B, Mann DA, von Zglinicki T (2014) Chronic inflammation induces telomere dysfunction and accelerates ageing in mice. *Nat Commun* 2:4172
133. Kadota T, Fujita Y, Yoshioka Y, Araya J, Kuwano K, Ochiya T (2018) Emerging role of extracellular vesicles as a senescence-associated secretory phenotype: Insights into the pathophysiology of lung diseases. *Mol Aspects Med* 60:92-103

134. Kajstura M, Halicka HD, Pryjma J, Darzynkiewicz Z (2007) Discontinuous fragmentation of nuclear DNA during apoptosis revealed by discrete "sub-G1" peaks on DNA content histograms. *Cytometry A* 71:125-131
135. Kamiya K, Ozasa K, Akiba S, Niwa O, Kodama K, Takamura N, Zaharieva EK, Kimura Y, Wakeford R (2015) Long-term effects of radiation exposure on health. *Lancet* 386:469-478
136. Kang C, Xu Q, Martin TD, Li MZ, Demaria M, Aron L, Lu T, Yankner BA, Campisi J, Elledge SJ (2015) The DNA damage response induces inflammation and senescence by inhibiting autophagy of GATA4. *Science* 349:aaa5612
137. Kaplan-Turkoz B, Koelblen T, Felix C, Candusso MP, O'Callaghan D, Vergunst AC, Terradot L (2013) Structure of the Toll/interleukin 1 receptor (TIR) domain of the immunosuppressive *Brucella* effector BtpA/Btp1/TcpB. *FEBS Lett* 587:3412-3416
138. Karthik K, Rajan V, Pandey BN, Sivasubramanian K, Paul SFD, Venkatachalam P (2019) Direct and bystander effects in human blood lymphocytes exposed to (241)Am alpha particles and the relative biological effectiveness using chromosomal aberration and micronucleus assay. *Int J Radiat Biol*:1-12
139. Kashiwagi H, Shiraishi K, Sakaguchi K, Nakahama T, Kodama S (2018) Repair kinetics of DNA double-strand breaks and incidence of apoptosis in mouse neural stem/progenitor cells and their differentiated neurons exposed to ionizing radiation. *J Radiat Res* 59:261-271
140. Kawai T, Akira S (2007) Signaling to NF-kappaB by Toll-like receptors. *Trends Mol Med* 13:460-469
141. Khan DZ, Lacasse MC, Khan R, Murphy KJ (2017) Radiation Cataractogenesis: The Progression of Our Understanding and Its Clinical Consequences. *J Vasc Interv Radiol* 28:412-419
142. Khoronenkova SV, Dianov GL (2015) ATM prevents DSB formation by coordinating SSB repair and cell cycle progression. *Proc Natl Acad Sci U S A* 112:3997-4002
143. Kim MY, Park SJ, Shim JW, Yang K, Kang HS, Heo K (2015a) Naphthazarin enhances ionizing radiation-induced cell cycle arrest and apoptosis in human breast cancer cells. *Int J Oncol* 46:1659-1666
144. Kim SY, Lee HJ, Nam JW, Seo EK, Lee YS (2015b) Coniferyl aldehyde reduces radiation damage through increased protein stability of heat shock transcriptional factor 1 by phosphorylation. *Int J Radiat Oncol Biol Phys* 91:807-816
145. Kinner A, Wu W, Staudt C, Iliakis G (2008) Gamma-H2AX in recognition and signaling of DNA double-strand breaks in the context of chromatin. *Nucleic Acids Res* 36:5678-5694
146. Klammer H, Mladenov E, Li F, Iliakis G (2015) Bystander effects as manifestation of intercellular communication of DNA damage and of the cellular oxidative status. *Cancer Lett* 356:58-71
147. Knight ZA, Shokat KM (2007) Chemical genetics: where genetics and pharmacology meet. *Cell* 128:425-430
148. Kobayashi A, Tengku Ahmad TAF, Autsavapromporn N, Oikawa M, Homma-Takeda S, Furusawa Y, Wang J, Konishi T (2017) Enhanced DNA double-strand break repair of microbeam targeted A549 lung carcinoma cells by adjacent WI38 normal lung fibroblast cells via bi-directional signaling. *Mutat Res* 803-805:1-8
149. Kobayashi A, Konishi T (2018) Radiation quality effects alteration in COX-2 pathway to trigger radiation-induced bystander response in A549 lung carcinoma cells. *J Radiat Res* 59:754-759
150. Kollarovic G, Studencka M, Ivanova L, Lauenstein C, Heinze K, Lapytsko A, Talemi SR, Figueiredo AS, Schaber J (2016) To senesce or not to senesce: how primary human fibroblasts decide their cell fate after DNA damage. *Aging (Albany NY)* 8:158-177
151. Kong EY, Cheng SH, Yu KN (2018) Induction of autophagy and interleukin 6 secretion in bystander cells: metabolic cooperation for radiation-induced rescue effect? *J Radiat Res* 59:129-140
152. Kostjuk S, Loseva P, Chvartatskaya O, Ershova E, Smirnova T, Malinovskaya E, Roginko O, Kuzmin V, Izhevskaya V, Baranova A, Ginter E, Veiko N (2012) Extracellular GC-rich DNA activates TLR9- and NF-kB-dependent signaling pathways in human adipose-derived mesenchymal stem cells (haMSCs). *Expert Opin Biol Ther* 12 Suppl 1:S99-111

153. Kraft D, Rall M, Volcic M, Metzler E, Groo A, Stahl A, Bauer L, Nasonova E, Salles D, Taucher-Scholz G, Bonig H, Fournier C, Wiesmuller L (2015) NF-kappaB-dependent DNA damage-signaling differentially regulates DNA double-strand break repair mechanisms in immature and mature human hematopoietic cells. *Leukemia* 29:1543-1554
154. Kwak MS, Lim M, Lee YJ, Lee HS, Kim YH, Youn JH, Choi JE, Shin JS (2015) HMGB1 Binds to Lipoteichoic Acid and Enhances TNF-alpha and IL-6 Production through HMGB1-Mediated Transfer of Lipoteichoic Acid to CD14 and TLR2. *J Innate Immun* 7:405-416
155. Lacombe J, Zenhausern F (2017) Emergence of miR-34a in radiation therapy. *Crit Rev Oncol Hematol* 109:69-78
156. Large M, Reichert S, Hehlhans S, Fournier C, Rodel C, Rodel F (2014) A non-linear detection of phospho-histone H2AX in EA.hy926 endothelial cells following low-dose X-irradiation is modulated by reactive oxygen species. *Radiat Oncol* 9:80
157. Lea DE, Catchside DG (1942) The mechanism of the induction by radiation of chromosome aberrations in *Tradescantia*. *Journal of Genetics* 44:216-245
158. Ledoux AC, Perkins ND (2014) NF-kappaB and the cell cycle. *Biochem Soc Trans* 42:76-81
159. Lee BY, Han JA, Im JS, Morrone A, Johung K, Goodwin EC, Kleijer WJ, DiMaio D, Hwang ES (2006) Senescence-associated beta-galactosidase is lysosomal beta-galactosidase. *Aging Cell* 5:187-195
160. Lee NS, Kim S, Jung YW, Kim H (2018) Eukaryotic DNA damage responses: Homologous recombination factors and ubiquitin modification. *Mutat Res* 809:88-98
161. Leontieva OV, Natarajan V, Demidenko ZN, Burdelya LG, Gudkov AV, Blagosklonny MV (2012) Hypoxia suppresses conversion from proliferative arrest to cellular senescence. *Proc Natl Acad Sci U S A* 109:13314-13318
162. Lewis DA, Mayhugh BM, Qin Y, Trott K, Mendonca MS (2001) Production of delayed death and neoplastic transformation in CGL1 cells by radiation-induced bystander effects. *Radiat Res* 156:251-258
163. Li M, You L, Xue J, Lu Y (2018) Ionizing Radiation-Induced Cellular Senescence in Normal, Non-transformed Cells and the Involved DNA Damage Response: A Mini Review. *Front Pharmacol* 9:522
164. Li Q, Verma IM (2002) NF-kappaB regulation in the immune system. *Nat Rev Immunol* 2:725-734
165. Li TH, Yan HX (2018) Antitumor and apoptosis-inducing effects of pomolic acid against SKMEL2 human malignant melanoma cells are mediated via inhibition of cell migration and subG1 cell cycle arrest. *Mol Med Rep* 17:1035-1040
166. Li X, Wu Z, An X, Mei Q, Bai M, Hanski L, Li X, Ahola T, Han W (2017) Blockade of the LRP16-PKR-NF-kappaB signaling axis sensitizes colorectal carcinoma cells to DNA-damaging cytotoxic therapy. *Elife* 6
167. Liao EC, Hsu YT, Chuah QY, Lee YJ, Hu JY, Huang TC, Yang PM, Chiu SJ (2014) Radiation induces senescence and a bystander effect through metabolic alterations. *Cell Death Dis* 5:e1255
168. Lilley DMJ (2017) Holliday junction-resolving enzymes-structures and mechanisms. *FEBS Lett* 591:1073-1082
169. Lim JW, Kim H, Kim KH (2002) Expression of Ku70 and Ku80 mediated by NF-kappa B and cyclooxygenase-2 is related to proliferation of human gastric cancer cells. *J Biol Chem* 277:46093-46100
170. Lindqvist A (2010) Cyclin B-Cdk1 activates its own pump to get into the nucleus. *J Cell Biol* 189:197-199
171. Liu R, Zhao D, Zhang X, Han S, Yang Y, Ma J, Meng D (2017) A20 enhances the radiosensitivity of hepatocellular carcinoma cells to (60)Co-gamma ionizing radiation. *Oncotarget* 8:93103-93116
172. Liu T, Huang J (2016) DNA End Resection: Facts and Mechanisms. *Genomics Proteomics Bioinformatics* 14:126-130

173. Liu Z, Mothersill CE, McNeill FE, Lyng FM, Byun SH, Seymour CB, Prestwich WV (2006) A dose threshold for a medium transfer bystander effect for a human skin cell line. *Radiat Res* 166:19-23
174. Lobrich M, Jeggo P (2017) A Process of Resection-Dependent Nonhomologous End Joining Involving the Goddess Artemis. *Trends Biochem Sci* 42:690-701
175. Logvinenko AD (2015) The geometric structure of color. *J Vis* 15:15 11 16
176. Lopez M, Martin M (2011) Medical management of the acute radiation syndrome. *Rep Pract Oncol Radiother* 16:138-146
177. Lowe JM, Menendez D, Bushel PR, Shatz M, Kirk EL, Troester MA, Garantziotis S, Fessler MB, Resnick MA (2014) p53 and NF-kappaB coregulate proinflammatory gene responses in human macrophages. *Cancer Res* 74:2182-2192
178. Lozano-Gerona J, Garcia-Otin AL (2018) ImageJ-based semiautomatic method to analyze senescence in cell culture. *Anal Biochem* 543:30-32
179. Maia J, Caja S, Strano Moraes MC, Couto N, Costa-Silva B (2018) Exosome-Based Cell-Cell Communication in the Tumor Microenvironment. *Front Cell Dev Biol* 6:18
180. Maier P, Hartmann L, Wenz F, Herskind C (2016) Cellular Pathways in Response to Ionizing Radiation and Their Targetability for Tumor Radiosensitization. *Int J Mol Sci* 17
181. Makale MT, King GL (1993) Plasticity of autonomic control of emesis in irradiated ferrets. *Am J Physiol* 265:R1092-1099
182. Mariotti L, Facchetti A, Bertolotti A, Ranza E, Alloni D, Ottolenghi A (2011) Radiation-induced perturbation of cell-to-cell signalling and communication. *Radiat Prot Dosimetry* 143:294-300
183. Mariotti LG, Bertolotti A, Ranza E, Babini G, Ottolenghi A (2012) Investigation of the mechanisms underpinning IL-6 cytokine release in bystander responses: the roles of radiation dose, radiation quality and specific ROS/RNS scavengers. *Int J Radiat Biol* 88:751-762
184. Marthandan S, Menzel U, Priebe S, Groth M, Guthke R, Platzer M, Hemmerich P, Kaether C, Diekmann S (2016) Conserved genes and pathways in primary human fibroblast strains undergoing replicative and radiation induced senescence. *Biol Res* 49:34
185. Martincuks A, Andryka K, Kuster A, Schmitz-Van de Leur H, Komorowski M, Muller-Newen G (2017) Nuclear translocation of STAT3 and NF-kappaB are independent of each other but NF-kappaB supports expression and activation of STAT3. *Cell Signal* 32:36-47
186. Martinel Lamas DJ, Cortina JE, Ventura C, Sterle HA, Valli E, Balestrasse KB, Blanco H, Cremaschi GA, Rivera ES, Medina VA (2015) Enhancement of ionizing radiation response by histamine in vitro and in vivo in human breast cancer. *Cancer Biol Ther* 16:137-148
187. Matsuya Y, Sasaki K, Yoshii Y, Okuyama G, Date H (2018) Integrated Modelling of Cell Responses after Irradiation for DNA-Targeted Effects and Non-Targeted Effects. *Sci Rep* 8:4849
188. Maubach G, Schmadicke AC, Naumann M (2017) NEMO Links Nuclear Factor-kappaB to Human Diseases. *Trends Mol Med* 23:1138-1155
189. McCool KW, Miyamoto S (2012) DNA damage-dependent NF-kappaB activation: NEMO turns nuclear signaling inside out. *Immunol Rev* 246:311-326
190. McMahon SJ (2018) The linear quadratic model: usage, interpretation and challenges. *Phys Med Biol* 64:01TR01
191. Mehta A, Haber JE (2014) Sources of DNA double-strand breaks and models of recombinational DNA repair. *Cold Spring Harb Perspect Biol* 6:a016428
192. Mendonca MS, Turchan WT, Alpuche ME, Watson CN, Estabrook NC, Chin-Sinex H, Shapiro JB, Imasuen-Williams IE, Rangel G, Gilley DP, Huda N, Crooks PA, Shapiro RH (2017) DMAPT inhibits NF-kappaB activity and increases sensitivity of prostate cancer cells to X-rays in vitro and in tumor xenografts in vivo. *Free Radic Biol Med* 112:318-326
193. Menon V, Povirk L (2014) Involvement of p53 in the repair of DNA double strand breaks: multifaceted Roles of p53 in homologous recombination repair (HRR) and non-homologous end joining (NHEJ). *Subcell Biochem* 85:321-336
194. Micheau O, Tschopp J (2003) Induction of TNF receptor I-mediated apoptosis via two sequential signaling complexes. *Cell* 114:181-190

195. Mirzayans R, Andrais B, Scott A, Wang YW, Murray D (2013) Ionizing radiation-induced responses in human cells with differing TP53 status. *Int J Mol Sci* 14:22409-22435
196. Mladenov E, Magin S, Soni A, Iliakis G (2013) DNA double-strand break repair as determinant of cellular radiosensitivity to killing and target in radiation therapy. *Front Oncol* 3:113
197. Mladenov E, Magin S, Soni A, Iliakis G (2016) DNA double-strand-break repair in higher eukaryotes and its role in genomic instability and cancer: Cell cycle and proliferation-dependent regulation. *Semin Cancer Biol* 37-38:51-64
198. Mladenov E, Li F, Zhang L, Klammer H, Iliakis G (2018) Intercellular communication of DNA damage and oxidative status underpin bystander effects. *Int J Radiat Biol* 94:719-726
199. Mo LJ, Song M, Huang QH, Guan H, Liu XD, Xie DF, Huang B, Huang RX, Zhou PK (2018) Exosome-packaged miR-1246 contributes to bystander DNA damage by targeting LIG4. *Br J Cancer* 119:492-502
200. Mutschelknaus L, Peters C, Winkler K, Yentrapalli R, Heider T, Atkinson MJ, Moertl S (2016) Exosomes Derived from Squamous Head and Neck Cancer Promote Cell Survival after Ionizing Radiation. *PLoS One* 11:e0152213
201. Mutschelknaus L, Azimzadeh O, Heider T, Winkler K, Vetter M, Kell R, Tapio S, Merl-Pham J, Huber SM, Edalat L, Radulovic V, Anastasov N, Atkinson MJ, Moertl S (2017) Radiation alters the cargo of exosomes released from squamous head and neck cancer cells to promote migration of recipient cells. *Sci Rep* 7:12423
202. Nagano T, Nakano M, Nakashima A, Onishi K, Yamao S, Enari M, Kikkawa U, Kamada S (2016) Identification of cellular senescence-specific genes by comparative transcriptomics. *Sci Rep* 6:31758
203. Nagasawa H, Little JB (1992) Induction of sister chromatid exchanges by extremely low doses of alpha-particles. *Cancer Res* 52:6394-6396
204. Najafi M, Fardid R, Hadadi G, Fardid M (2014) The mechanisms of radiation-induced bystander effect. *J Biomed Phys Eng* 4:163-172
205. Nakayama KI, Hatakeyama S, Nakayama K (2001) Regulation of the cell cycle at the G1-S transition by proteolysis of cyclin E and p27Kip1. *Biochem Biophys Res Commun* 282:853-860
206. Nassour J, Martien S, Martin N, Deruy E, Tomellini E, Malaquin N, Bouali F, Sabatier L, Wernert N, Pinte S, Gilson E, Pourtier A, Pluquet O, Abbadie C (2016) Defective DNA single-strand break repair is responsible for senescence and neoplastic escape of epithelial cells. *Nat Commun* 7:10399
207. Nelson G, Wordsworth J, Wang C, Jurk D, Lawless C, Martin-Ruiz C, von Zglinicki T (2012) A senescent cell bystander effect: senescence-induced senescence. *Aging Cell* 11:345-349
208. Nelson G, Kucheryavenko O, Wordsworth J, von Zglinicki T (2018) The senescent bystander effect is caused by ROS-activated NF-kappaB signalling. *Mech Ageing Dev* 170:30-36
209. Nikolettou V, Markaki M, Palikaras K, Tavernarakis N (2013) Crosstalk between apoptosis, necrosis and autophagy. *Biochim Biophys Acta* 1833:3448-3459
210. Norbury JW, Schimmerling W, Slaba TC, Azzam EI, Badavi FF, Baiocco G, Benton E, Bindi V, Blakely EA, Blattnig SR, Boothman DA, Borak TB, Britten RA, Curtis S, Dingfelder M, Durante M, Dynan WS, Eisch AJ, Robin Elgart S, Goodhead DT, Guida PM, Heilbronn LH, Hellweg CE, Huff JL, Kronenberg A, La Tessa C, Lowenstein DI, Miller J, Morita T, Narici L, Nelson GA, Norman RB, Ottolenghi A, Patel ZS, Reitz G, Rusek A, Schreurs AS, Scott-Carnell LA, Semones E, Shay JW, Shurshakov VA, Sihver L, Simonsen LC, Story MD, Turker MS, Uchihori Y, Williams J, Zeitlin CJ (2016) Galactic cosmic ray simulation at the NASA Space Radiation Laboratory. *Life Sci Space Res (Amst)* 8:38-51
211. O'Dea E, Hoffmann A (2009) NF-kappaB signaling. *Wiley Interdiscip Rev Syst Biol Med* 1:107-115
212. Olobatuyi O, de Vries G, Hillen T (2017) A reaction-diffusion model for radiation-induced bystander effects. *J Math Biol* 75:341-372
213. Orjalo AV, Bhaumik D, Gengler BK, Scott GK, Campisi J (2009) Cell surface-bound IL-1alpha is an upstream regulator of the senescence-associated IL-6/IL-8 cytokine network. *Proc Natl Acad Sci U S A* 106:17031-17036

214. Palacio L, Krishnan V, Le NL, Sharpless NE, Beausejour CM (2017) Sustained p16(INK4a) expression is required to prevent IR-induced tumorigenesis in mice. *Oncogene* 36:1309-1314
215. Park HJ, Lyons JC, Ohtsubo T, Song CW (2000) Cell cycle progression and apoptosis after irradiation in an acidic environment. *Cell Death Differ* 7:729-738
216. Park HS, Yun Y, Kim CS, Yang KH, Jeong M, Ahn SK, Jin YW, Nam SY (2009) A critical role for AKT activation in protecting cells from ionizing radiation-induced apoptosis and the regulation of acinus gene expression. *Eur J Cell Biol* 88:563-575
217. Pascal JM (2018) The comings and goings of PARP-1 in response to DNA damage. *DNA Repair (Amst)*
218. Pasi F, Facchetti A, Nano R (2010) IL-8 and IL-6 bystander signalling in human glioblastoma cells exposed to gamma radiation. *Anticancer Res* 30:2769-2772
219. Passos JF, Nelson G, Wang C, Richter T, Simillion C, Proctor CJ, Miwa S, Olijslagers S, Hallinan J, Wipat A, Saretzki G, Rudolph KL, Kirkwood TB, von Zglinicki T (2010) Feedback between p21 and reactive oxygen production is necessary for cell senescence. *Mol Syst Biol* 6:347
220. Pawlik TM, Keyomarsi K (2004) Role of cell cycle in mediating sensitivity to radiotherapy. *Int J Radiat Oncol Biol Phys* 59:928-942
221. Piotrowski I, Kulcenty K, Suchorska WM, Skrobala A, Skorska M, Kruszyna-Mochalska M, Kowalik A, Jackowiak W, Malicki J (2017) Carcinogenesis Induced by Low-dose Radiation. *Radiol Oncol* 51:369-377
222. Poleszczuk J, Krzywon A, Forys U, Widel M (2015) Connecting radiation-induced bystander effects and senescence to improve radiation response prediction. *Radiat Res* 183:571-577
223. Prise KM, Folkard M, Michael BD (2003) Bystander responses induced by low LET radiation. *Oncogene* 22:7043-7049
224. Puck TT, Marcus PI (1956) Action of x-rays on mammalian cells. *J Exp Med* 103:653-666
225. Puck TT, Morkovin D, Marcus PI, Cieciora SJ (1957) Action of x-rays on mammalian cells. II. Survival curves of cells from normal human tissues. *J Exp Med* 106:485-500
226. Qiao Q, Jiang Y, Li G (2013) Curcumin enhances the response of non-Hodgkin's lymphoma cells to ionizing radiation through further induction of cell cycle arrest at the G2/M phase and inhibition of mTOR phosphorylation. *Oncol Rep* 29:380-386
227. Raghunathan D, Khilji MI, Hassan SA, Yusuf SW (2017) Radiation-Induced Cardiovascular Disease. *Curr Atheroscler Rep* 19:22
228. Rastogi S, Hwang A, Chan J, Wang JYJ (2018) Extracellular vesicles transfer nuclear Abl-dependent and radiation-induced miR-34c into unirradiated cells to cause bystander effects. *Mol Biol Cell* 29:2228-2242
229. Ren K, Li Z, Li Y, Zhang W, Han X (2017) Sulforaphene enhances radiosensitivity of hepatocellular carcinoma through suppression of the NF-kappaB pathway. *J Biochem Mol Toxicol* 31
230. Rodier F, Coppe JP, Patil CK, Hoeijmakers WA, Munoz DP, Raza SR, Freund A, Campeau E, Davalos AR, Campisi J (2009) Persistent DNA damage signalling triggers senescence-associated inflammatory cytokine secretion. *Nat Cell Biol* 11:973-979
231. Rogakou EP, Pilch DR, Orr AH, Ivanova VS, Bonner WM (1998) DNA double-stranded breaks induce histone H2AX phosphorylation on serine 139. *J Biol Chem* 273:5858-5868
232. Roos WP, Kaina B (2006) DNA damage-induced cell death by apoptosis. *Trends Mol Med* 12:440-450
233. Roy P, Sarkar UA, Basak S (2018) The NF-kappaB Activating Pathways in Multiple Myeloma. *Biomedicines* 6
234. Rufini A, Tucci P, Celardo I, Melino G (2013) Senescence and aging: the critical roles of p53. *Oncogene* 32:5129-5143
235. Russo SM, Tepper JE, Baldwin AS, Jr., Liu R, Adams J, Elliott P, Cusack JC, Jr. (2001) Enhancement of radiosensitivity by proteasome inhibition: implications for a role of NF-kappaB. *Int J Radiat Oncol Biol Phys* 50:183-193
236. Ryan LA, Smith RW, Seymour CB, Mothersill CE (2008) Dilution of irradiated cell conditioned medium and the bystander effect. *Radiat Res* 169:188-196

237. Sabatel H, Pirlot C, Piette J, Habraken Y (2011) Importance of PIKKs in NF-kappaB activation by genotoxic stress. *Biochem Pharmacol* 82:1371-1383
238. Sage E, Shikazono N (2017) Radiation-induced clustered DNA lesions: Repair and mutagenesis. *Free Radic Biol Med* 107:125-135
239. Sahraneshin Samani F, Moore JK, Khosravani P, Ebrahimi M (2014) Features of free software packages in flow cytometry: a comparison between four non-commercial software sources. *Cytotechnology* 66:555-559
240. Sakai Y, Yamamori T, Yoshikawa Y, Bo T, Suzuki M, Yamamoto K, Ago T, Inanami O (2018) NADPH oxidase 4 mediates ROS production in radiation-induced senescent cells and promotes migration of inflammatory cells. *Free Radic Res* 52:92-102
241. Santee SM, Owen-Schaub LB (1996) Human tumor necrosis factor receptor p75/80 (CD120b) gene structure and promoter characterization. *J Biol Chem* 271:21151-21159
242. Santivasi WL, Xia F (2014) Ionizing radiation-induced DNA damage, response, and repair. *Antioxid Redox Signal* 21:251-259
243. Sastre-Moreno G, Pryor JM, Moreno-Onate M, Herrero-Ruiz AM, Cortes-Ledesma F, Blanco L, Ramsden DA, Ruiz JF (2017) Regulation of human pollambda by ATM-mediated phosphorylation during non-homologous end joining. *DNA Repair (Amst)* 51:31-45
244. Sawal HA, Asghar K, Bureik M, Jalal N (2017) Bystander signaling via oxidative metabolism. *Onco Targets Ther* 10:3925-3940
245. Schafer KA (1998) The cell cycle: a review. *Vet Pathol* 35:461-478
246. Schae D, Kachikwu EL, McBride WH (2012) Cytokines in radiobiological responses: a review. *Radiat Res* 178:505-523
247. Schmidt-Suppran M, Bloch W, Courtois G, Addicks K, Israel A, Rajewsky K, Pasparakis M (2000) NEMO/IKK gamma-deficient mice model incontinentia pigmenti. *Mol Cell* 5:981-992
248. Shaker A, Rubin DC (2010) Intestinal stem cells and epithelial-mesenchymal interactions in the crypt and stem cell niche. *Transl Res* 156:180-187
249. Shan YX, Jin SZ, Liu XD, Liu Y, Liu SZ (2007) Ionizing radiation stimulates secretion of pro-inflammatory cytokines: dose-response relationship, mechanisms and implications. *Radiat Environ Biophys* 46:21-29
250. Shao AW, Sun H, Geng Y, Peng Q, Wang P, Chen J, Xiong T, Cao R, Tang J (2016) Bclaf1 is an important NF-kappaB signaling transducer and C/EBPbeta regulator in DNA damage-induced senescence. *Cell Death Differ* 23:865-875
251. Shao C, Stewart V, Folkard M, Michael BD, Prise KM (2003) Nitric oxide-mediated signaling in the bystander response of individually targeted glioma cells. *Cancer Res* 63:8437-8442
252. Shareef MM, Cui N, Burikhanov R, Gupta S, Satishkumar S, Shajahan S, Mohiuddin M, Rangnekar VM, Ahmed MM (2007) Role of tumor necrosis factor-alpha and TRAIL in high-dose radiation-induced bystander signaling in lung adenocarcinoma. *Cancer Res* 67:11811-11820
253. Sharma S, Singla N, Chadha VD, Dhawan DK (2019) A concept of radiation hormesis: stimulation of antioxidant machinery in rats by low dose ionizing radiation. *Hell J Nucl Med* 22:43-48
254. Shi JH, Sun SC (2018) Tumor Necrosis Factor Receptor-Associated Factor Regulation of Nuclear Factor kappaB and Mitogen-Activated Protein Kinase Pathways. *Front Immunol* 9:1849
255. Shibamoto Y, Nakamura H (2018) Overview of Biological, Epidemiological, and Clinical Evidence of Radiation Hormesis. *Int J Mol Sci* 19
256. Shlush LI, Itzkovitz S, Cohen A, Rutenberg A, Berkovitz R, Yehezkel S, Shahar H, Selig S, Skorecki K (2011) Quantitative digital in situ senescence-associated beta-galactosidase assay. *BMC Cell Biol* 12:16
257. Sihver L, Ploc O, Puchalska M, Ambrozova I, Kubancak J, Kyselova D, Shurshakov V (2015) Radiation environment at aviation altitudes and in space. *Radiat Prot Dosimetry* 164:477-483

258. Smith D, Mann D, Yong K (2016) Cyclin D type does not influence cell cycle response to DNA damage caused by ionizing radiation in multiple myeloma tumours. *Br J Haematol* 173:693-704
259. Smith TA, Kirkpatrick DR, Smith S, Smith TK, Pearson T, Kailasam A, Herrmann KZ, Schubert J, Agrawal DK (2017) Radioprotective agents to prevent cellular damage due to ionizing radiation. *J Transl Med* 15:232
260. Sokolov MV, Smilenov LB, Hall EJ, Panyutin IG, Bonner WM, Sedelnikova OA (2005) Ionizing radiation induces DNA double-strand breaks in bystander primary human fibroblasts. *Oncogene* 24:7257-7265
261. Sokolov MV, Dickey JS, Bonner WM, Sedelnikova OA (2007) gamma-H2AX in bystander cells: not just a radiation-triggered event, a cellular response to stress mediated by intercellular communication. *Cell Cycle* 6:2210-2212
262. Sollazzo A, Shakeri-Manesh S, Fotouhi A, Czub J, Haghdoost S, Wojcik A (2016) Interaction of low and high LET radiation in TK6 cells-mechanistic aspects and significance for radiation protection. *J Radiol Prot* 36:721-735
263. Song M, Wang Y, Shang ZF, Liu XD, Xie DF, Wang Q, Guan H, Zhou PK (2016) Bystander autophagy mediated by radiation-induced exosomal miR-7-5p in non-targeted human bronchial epithelial cells. *Sci Rep* 6:30165
264. Soubannier V, Stifani S (2017) NF-kappaB Signalling in Glioblastoma. *Biomedicines* 5
265. Spinelli JB, Haigis MC (2018) The multifaceted contributions of mitochondria to cellular metabolism. *Nat Cell Biol* 20:745-754
266. Sprung CN, Ivashkevich A, Forrester HB, Redon CE, Georgakilas A, Martin OA (2015) Oxidative DNA damage caused by inflammation may link to stress-induced non-targeted effects. *Cancer Lett* 356:72-81
267. Stilmann M, Hinz M, Arslan SC, Zimmer A, Schreiber V, Scheidereit C (2009) A nuclear poly(ADP-ribose)-dependent signalosome confers DNA damage-induced I kappaB kinase activation. *Mol Cell* 36:365-378
268. Stubblefield MD (2017) Clinical Evaluation and Management of Radiation Fibrosis Syndrome. *Phys Med Rehabil Clin N Am* 28:89-100
269. Suetens A, Konings K, Moreels M, Quintens R, Verslegers M, Soors E, Tabury K, Gregoire V, Baatout S (2016) Higher Initial DNA Damage and Persistent Cell Cycle Arrest after Carbon Ion Irradiation Compared to X-irradiation in Prostate and Colon Cancer Cells. *Front Oncol* 6:87
270. Sun B, Ross SM, Rowley S, Adeleye Y, Clewell RA (2017) Contribution of ATM and ATR kinase pathways to p53-mediated response in etoposide and methyl methanesulfonate induced DNA damage. *Environ Mol Mutagen* 58:72-83
271. Sur S, Agrawal DK (2016) Phosphatases and kinases regulating CDC25 activity in the cell cycle: clinical implications of CDC25 overexpression and potential treatment strategies. *Mol Cell Biochem* 416:33-46
272. Suzuki M, Tsuruoka C (2004) Heavy charged particles produce a bystander effect via cell-cell junctions. *Biol Sci Space* 18:241-246
273. Szatmari T, Persa E, Kis E, Benedek A, Hargitai R, Safrany G, Lumniczky K (2019) Extracellular vesicles mediate low dose ionizing radiation-induced immune and inflammatory responses in the blood. *Int J Radiat Biol* 95:12-22
274. Szumiel I (2012) Radiation hormesis: Autophagy and other cellular mechanisms. *Int J Radiat Biol* 88:619-628
275. Takahashi K, Okada TS (1970) An analysis of the effect of "conditioned medium" upon the cell culture at low density. *Dev Growth Differ* 12:65-77
276. Takeda DY, Dutta A (2005) DNA replication and progression through S phase. *Oncogene* 24:2827-2843
277. Tang FR, Loganovsky K (2018) Low dose or low dose rate ionizing radiation-induced health effect in the human. *J Environ Radioact* 192:32-47

278. Tang TT, Rendon DA, Zawaski JA, Afshar SF, Kaffes CK, Sabek OM, Gaber MW (2017) Imaging Radiation-Induced Gastrointestinal, Bone Marrow Injury and Recovery Kinetics Using ¹⁸F-FDG PET. *PLoS One* 12:e0169082
279. Tegowski M, Baldwin A (2018) Noncanonical NF-kappaB in Cancer. *Biomedicines* 6
280. Telford WG (2011) Lasers in flow cytometry. *Methods Cell Biol* 102:375-409
281. Temelie M, Savu DI, Moiso N (2018) Intracellular and Intercellular Signalling Mechanisms following DNA Damage Are Modulated By PINK1. *Oxid Med Cell Longev* 2018:1391387
282. Tokuyama Y, Furusawa Y, Ide H, Yasui A, Terato H (2015) Role of isolated and clustered DNA damage and the post-irradiating repair process in the effects of heavy ion beam irradiation. *J Radiat Res* 56:446-455
283. Tomita M, Matsumoto H, Funayama T, Yokota Y, Otsuka K, Maeda M, Kobayashi Y (2015) Nitric oxide-mediated bystander signal transduction induced by heavy-ion microbeam irradiation. *Life Sci Space Res (Amst)* 6:36-43
284. Tsolou A, Lioucia M, Kalamida D, Pouliliou S, Giatromanolaki A, Koukourakis M (2017) Inhibition of IKK-NFkappaB pathway sensitizes lung cancer cell lines to radiation. *Cancer Biol Med* 14:293-301
285. Tu W, Dong C, Konishi T, Kobayashi A, Furusawa Y, Uchihori Y, Xie Y, Dang B, Li W, Shao C (2016) G(2)-M phase-correlative bystander effects are co-mediated by DNA-PKcs and ATM after carbon ion irradiation. *Mutat Res Genet Toxicol Environ Mutagen* 795:1-6
286. Tu W, Dong C, Fu J, Pan Y, Kobayashi A, Furusawa Y, Konishi T, Shao C (2019) Both irradiated and bystander effects link with DNA repair capacity and the linear energy transfer. *Life Sci* 222:228-234
287. Vallabhapurapu S, Karin M (2009) Regulation and function of NF-kappaB transcription factors in the immune system. *Annu Rev Immunol* 27:693-733
288. van den Berg J, A GM, Kielbassa K, Feringa FM, Freire R, Medema RH (2018) A limited number of double-strand DNA breaks is sufficient to delay cell cycle progression. *Nucleic Acids Res*
289. Van Oorschot B, Oei AL, Nuijens AC, Rodermond H, Hoeben R, Stap J, Stalpers LJ, Franken NA (2014) Decay of gamma-H2AX foci correlates with potentially lethal damage repair and P53 status in human colorectal carcinoma cells. *Cell Mol Biol Lett* 19:37-51
290. Vermeulen K, Van Bockstaele DR, Berneman ZN (2003) The cell cycle: a review of regulation, deregulation and therapeutic targets in cancer. *Cell Prolif* 36:131-149
291. Veuger SJ, Hunter JE, Durkacz BW (2009) Ionizing radiation-induced NF-kappaB activation requires PARP-1 function to confer radioresistance. *Oncogene* 28:832-842
292. Volcic M, Karl S, Baumann B, Salles D, Daniel P, Fulda S, Wiesmuller L (2012) NF-kappaB regulates DNA double-strand break repair in conjunction with BRCA1-CtIP complexes. *Nucleic Acids Res* 40:181-195
293. von Holzen U, Pataer A, Raju U, Bocangel D, Vorburger SA, Liu Y, Lu X, Roth JA, Aggarwal BB, Barber GN, Keyomarsi K, Hunt KK, Swisher SG (2007) The double-stranded RNA-activated protein kinase mediates radiation resistance in mouse embryo fibroblasts through nuclear factor kappaB and Akt activation. *Clin Cancer Res* 13:6032-6039
294. Wang CY, Mayo MW, Baldwin AS, Jr. (1996) TNF- and cancer therapy-induced apoptosis: potentiation by inhibition of NF-kappaB. *Science* 274:784-787
295. Wang CY, Mayo MW, Korneluk RG, Goeddel DV, Baldwin AS, Jr. (1998) NF-kappaB antiapoptosis: induction of TRAF1 and TRAF2 and c-IAP1 and c-IAP2 to suppress caspase-8 activation. *Science* 281:1680-1683
296. Wang J, Jacob NK, Ladner KJ, Beg A, Perko JD, Tanner SM, Liyanarachchi S, Fishel R, Guttridge DC (2009) RelA/p65 functions to maintain cellular senescence by regulating genomic stability and DNA repair. *EMBO Rep* 10:1272-1278
297. Wang JZ, Huang Z, Lo SS, Yuh WT, Mayr NA (2010) A generalized linear-quadratic model for radiosurgery, stereotactic body radiation therapy, and high-dose rate brachytherapy. *Sci Transl Med* 2:39ra48

298. Wang L, He L, Bao G, He X, Fan S, Wang H (2016a) Ionizing Radiation Induces HMGB1 Cytoplasmic Translocation and Extracellular Release. *Guo Ji Fang She Yi Xue He Yi Xue Za Zhi* 40:91-99
299. Wang M, Meng B, Liu Y, Yu J, Chen Q, Liu Y (2017a) MiR-124 Inhibits Growth and Enhances Radiation-Induced Apoptosis in Non-Small Cell Lung Cancer by Inhibiting STAT3. *Cell Physiol Biochem* 44:2017-2028
300. Wang W, Mani AM, Wu ZH (2017b) DNA damage-induced nuclear factor-kappa B activation and its roles in cancer progression. *J Cancer Metastasis Treat* 3:45-59
301. Wang X, Zhang J, Fu J, Wang J, Ye S, Liu W, Shao C (2015) Role of ROS-mediated autophagy in radiation-induced bystander effect of hepatoma cells. *Int J Radiat Biol* 91:452-458
302. Wang XC, Zhang TJ, Guo ZJ, Xiao CY, Ding XW, Fang F, Sheng WT, Shu X, Li J (2017c) Overexpression of SKP2 Inhibits the Radiation-Induced Bystander Effects of Esophageal Carcinoma. *Int J Environ Res Public Health* 14
303. Wang Y, Liu L, Zhou D (2011) Inhibition of p38 MAPK attenuates ionizing radiation-induced hematopoietic cell senescence and residual bone marrow injury. *Radiat Res* 176:743-752
304. Wang Y, Boerma M, Zhou D (2016b) Ionizing Radiation-Induced Endothelial Cell Senescence and Cardiovascular Diseases. *Radiat Res* 186:153-161
305. Watson C, Miller DA, Chin-Sinex H, Losch A, Hughes W, Sweeney C, Mendonca MS (2009) Suppression of NF-kappaB activity by parthenolide induces X-ray sensitivity through inhibition of split-dose repair in TP53 null prostate cancer cells. *Radiat Res* 171:389-396
306. Webb GJ, Brooke R, De Silva AN (2013) Chronic radiation enteritis and malnutrition. *J Dig Dis* 14:350-357
307. Webster GA, Perkins ND (1999) Transcriptional cross talk between NF-kappaB and p53. *Mol Cell Biol* 19:3485-3495
308. Wei C, Li L, Kim IK, Sun P, Gupta S (2014) NF-kappaB mediated miR-21 regulation in cardiomyocytes apoptosis under oxidative stress. *Free Radic Res* 48:282-291
309. Werner E, Wang H, Doetsch PW (2014) Opposite roles for p38MAPK-driven responses and reactive oxygen species in the persistence and resolution of radiation-induced genomic instability. *PLoS One* 9:e108234
310. Widel M, Lalik A, Krzywon A, Poleszczuk J, Fujarewicz K, Rzeszowska-Wolny J (2015) The different radiation response and radiation-induced bystander effects in colorectal carcinoma cells differing in p53 status. *Mutat Res* 778:61-70
311. Wu J, Ding J, Yang J, Guo X, Zheng Y (2018) MicroRNA Roles in the Nuclear Factor Kappa B Signaling Pathway in Cancer. *Front Immunol* 9:546
312. Wu K, Chen Z, Peng Q, Chen G, Yan W, Chen X (2019) Ku86 alleviates human umbilical vein endothelial cellular apoptosis and senescence induced by a low dose of ionizing radiation. *J Int Med Res* 47:893-904
313. Wu L, Shao L, An N, Wang J, Pazhanisamy S, Feng W, Hauer-Jensen M, Miyamoto S, Zhou D (2011) IKKbeta regulates the repair of DNA double-strand breaks induced by ionizing radiation in MCF-7 breast cancer cells. *PLoS One* 6:e18447
314. Wu LH, Li P, Zhao QL, Piao JL, Jiao YF, Kadowaki M, Kondo T (2014) Arbutin, an intracellular hydroxyl radical scavenger, protects radiation-induced apoptosis in human lymphoma U937 cells. *Apoptosis* 19:1654-1663
315. Wu Y, Zhang Y, Wang L, Diao Z, Liu W (2015) The Role of Autophagy in Kidney Inflammatory Injury via the NF-kappaB Route Induced by LPS. *Int J Med Sci* 12:655-667
316. Wu ZH, Shi Y, Tibbetts RS, Miyamoto S (2006) Molecular linkage between the kinase ATM and NF-kappaB signaling in response to genotoxic stimuli. *Science* 311:1141-1146
317. Wu ZH, Wong ET, Shi Y, Niu J, Chen Z, Miyamoto S, Tergaonkar V (2010) ATM- and NEMO-dependent ELKS ubiquitination coordinates TAK1-mediated IKK activation in response to genotoxic stress. *Mol Cell* 40:75-86
318. Xiong Z, Jiang R, Li X, Liu Y, Guo F (2015) Different Roles of GRP78 on Cell Proliferation and Apoptosis in Cartilage Development. *Int J Mol Sci* 16:21153-21176

319. Xu D, Tahara H (2013) The role of exosomes and microRNAs in senescence and aging. *Adv Drug Deliv Rev* 65:368-375
320. Xu S, Wang J, Ding N, Hu W, Zhang X, Wang B, Hua J, Wei W, Zhu Q (2015) Exosome-mediated microRNA transfer plays a role in radiation-induced bystander effect. *RNA Biol* 12:1355-1363
321. Yang H, Asaad N, Held KD (2005) Medium-mediated intercellular communication is involved in bystander responses of X-ray-irradiated normal human fibroblasts. *Oncogene* 24:2096-2103
322. Yang H, Wang H, Ren J, Chen Q, Chen ZJ (2017a) cGAS is essential for cellular senescence. *Proc Natl Acad Sci U S A* 114:E4612-E4620
323. Yang J, Amiri KI, Burke JR, Schmid JA, Richmond A (2006) BMS-345541 targets inhibitor of kappaB kinase and induces apoptosis in melanoma: involvement of nuclear factor kappaB and mitochondria pathways. *Clin Cancer Res* 12:950-960
324. Yang S, Xu J, Shao W, Geng C, Li J, Guo F, Miao H, Shen W, Ye T, Liu Y, Xu H, Zhang X (2015) Radiation-Induced Bystander Effects in A549 Cells Exposed to 6 MV X-rays. *Cell Biochem Biophys* 72:877-882
325. Yang Y, Xia F, Hermance N, Mabb A, Simonson S, Morrissey S, Gandhi P, Munson M, Miyamoto S, Kelliher MA (2011) A cytosolic ATM/NEMO/RIP1 complex recruits TAK1 to mediate the NF-kappaB and p38 mitogen-activated protein kinase (MAPK)/MAPK-activated protein 2 responses to DNA damage. *Mol Cell Biol* 31:2774-2786
326. Yang Y, Wang JK (2016) The functional analysis of MicroRNAs involved in NF-kappaB signaling. *Eur Rev Med Pharmacol Sci* 20:1764-1774
327. Yang YM, Fang F, Li X, Yu L, Wang ZC (2017b) TRAIL overexpression co-regulated by Egr1 and HRE enhances radiosensitivity of hypoxic A549 cells depending on its apoptosis inducing role. *Oncol Rep* 37:533-539
328. Ye W, Tang X, Yang Z, Liu C, Zhang X, Jin J, Lyu J (2017) Plasma-derived exosomes contribute to inflammation via the TLR9-NF-kappaB pathway in chronic heart failure patients. *Mol Immunol* 87:114-121
329. Yemelyanov A, Gasparian A, Lindholm P, Dang L, Pierce JW, Kisseljov F, Karseladze A, Budunova I (2006) Effects of IKK inhibitor PS1145 on NF-kappaB function, proliferation, apoptosis and invasion activity in prostate carcinoma cells. *Oncogene* 25:387-398
330. Yokota Y, Funayama T, Mutou-Yoshihara Y, Ikeda H, Kobayashi Y (2015) The bystander cell-killing effect mediated by nitric oxide in normal human fibroblasts varies with irradiation dose but not with radiation quality. *Int J Radiat Biol* 91:383-388
331. You Y, Wen R, Pathak R, Li A, Li W, St Clair D, Hauer-Jensen M, Zhou D, Liang Y (2014) Latexin sensitizes leukemogenic cells to gamma-irradiation-induced cell-cycle arrest and cell death through Rps3 pathway. *Cell Death Dis* 5:e1493
332. Yu H, Aravindan N, Xu J, Natarajan M (2017) Inter- and intra-cellular mechanism of NF-kB-dependent survival advantage and clonal expansion of radio-resistant cancer cells. *Cell Signal* 31:105-111
333. Yu KN (2019) Radiation-induced rescue effect. *J Radiat Res* 60:163-170
334. Yu T, Xiong Z, Chen S, Tu G (2005) The use of models in "target" theory to evaluate the survival curves of human ovarian carcinoma cell line exposure to adriamycin combined with ultrasound. *Ultrason Sonochem* 12:345-348
335. Yuan D, Xu J, Wang J, Pan Y, Fu J, Bai Y, Zhang J, Shao C (2016) Extracellular miR-1246 promotes lung cancer cell proliferation and enhances radioresistance by directly targeting DR5. *Oncotarget* 7:32707-32722
336. Yuan GJ, Deng JJ, Cao DD, Shi L, Chen X, Lei JJ, Xu XM (2017) Autophagic cell death induced by reactive oxygen species is involved in hyperthermic sensitization to ionizing radiation in human hepatocellular carcinoma cells. *World J Gastroenterol* 23:5530-5537
337. Zhang JZ, Liu Z, Liu J, Ren JX, Sun TS (2014) Mitochondrial DNA induces inflammation and increases TLR9/NF-kappaB expression in lung tissue. *Int J Mol Med* 33:817-824

338. Zhang X, Ye C, Sun F, Wei W, Hu B, Wang J (2016) Both Complexity and Location of DNA Damage Contribute to Cellular Senescence Induced by Ionizing Radiation. *PLoS One* 11:e0155725
339. Zhao Y, Ma X, Wang J, Chen S, Yuan H, Xu A, Hang H, Wu L (2015) The Roles of p21(Waf1/CIP1) and Hus1 in Generation and Transmission of Damage Signals Stimulated by Low-Dose Alpha-Particle Irradiation. *Radiat Res* 184:578-585
340. Zhong Z, Umemura A, Sanchez-Lopez E, Liang S, Shalapour S, Wong J, He F, Boassa D, Perkins G, Ali SR, McGeough MD, Ellisman MH, Seki E, Gustafsson AB, Hoffman HM, Diaz-Meco MT, Moscat J, Karin M (2016) NF-kappaB Restricts Inflammasome Activation via Elimination of Damaged Mitochondria. *Cell* 164:896-910
341. Zhou H, Ivanov VN, Gillespie J, Geard CR, Amundson SA, Brenner DJ, Yu Z, Lieberman HB, Hei TK (2005) Mechanism of radiation-induced bystander effect: role of the cyclooxygenase-2 signaling pathway. *Proc Natl Acad Sci U S A* 102:14641-14646
342. Zhou H, Ivanov VN, Lien YC, Davidson M, Hei TK (2008) Mitochondrial function and nuclear factor-kappaB-mediated signaling in radiation-induced bystander effects. *Cancer Res* 68:2233-2240
343. Zhou Y, Lee JH, Jiang W, Crowe JL, Zha S, Paull TT (2017) Regulation of the DNA Damage Response by DNA-PKcs Inhibitory Phosphorylation of ATM. *Mol Cell* 65:91-104
344. Zhu J, Cynader MS, Jia W (2015) TDP-43 Inhibits NF-kappaB Activity by Blocking p65 Nuclear Translocation. *PLoS One* 10:e0142296
345. Zorov DB, Juhaszova M, Sollott SJ (2014) Mitochondrial reactive oxygen species (ROS) and ROS-induced ROS release. *Physiol Rev* 94:909-950

11. Acknowledgements

First of all, I would like to thank Dr. Günther Reitz, Dr. Christa Baumstark and Dr. Christine E. Hellweg for making my research possible. Thank you for believing in me and my ideas, for taking the time to help me work through my problems and encourage me endlessly. I have learned so much from you. Your guidance and support will never be forgotten.

In these last few years, you helped me towards incredible opportunities. From research at the heavy ion accelerator in Japan to participation in the NASA Space Radiation Summer School in Brookhaven, USA, you did everything you could to provide unique ways for me to grow.

I would also like to thank Dr. Jutta Engel and Dr. Yvonne Dzierma for the supervision of my thesis. Your patience and encouragement gave me strength and security. I am glad for your counsel and thankful for all the fruitful discussions. Yvonne, it means a lot to me that you took the time to show me the radiation therapy facilities of the university clinic and explain physics to me.

A tremendously big thank you goes to my colleagues of the radiation biology department of the German Aerospace Center. You made coming to work a pleasure and I am really lucky to have met all of you. Especially I would like to thank Sebastian Feles, Claudia Schmitz and Felix Fuchs. You are one of a kind. Your help in all regards of life, your tips and tricks in the lab, the amazing work-atmosphere you created and just the way you are make me happy to call you friends. Thank you!

Lastly I would like to thank my family and friends. You always had my back, you never questioned my eventual success and you always – in good times and bad – stood by me. You are awesome.

12. Curriculum Vitae

Aus datenschutzrechtlichen Gründen wird der Lebenslauf
in der elektronischen Fassung der Dissertation nicht veröffentlicht

Aus datenschutzrechtlichen Gründen wird der Lebenslauf
in der elektronischen Fassung der Dissertation nicht veröffentlicht

Aus datenschutzrechtlichen Gründen wird der Lebenslauf
in der elektronischen Fassung der Dissertation nicht veröffentlicht

Aus datenschutzrechtlichen Gründen wird der Lebenslauf
in der elektronischen Fassung der Dissertation nicht veröffentlicht

Aus datenschutzrechtlichen Gründen wird der Lebenslauf
in der elektronischen Fassung der Dissertation nicht veröffentlicht

